

Role of STIL Overexpression in Supernumerary
Centriole Formation, Chromosomal Instability and
Cancer Development in Mice

von

M.V.Sc. Amira-Talaat Moussa

Inaugural-Dissertation zur Erlangung der Doktorwürde
der Tierärztlichen Fakultät der Ludwig-Maximilians-Universität
München

Role of STIL Overexpression in Supernumerary Centriole
Formation, Chromosomal Instability and Cancer Development in
Mice

von

M.V.Sc. Amira-Talaat Moussa
aus Zagazig-Sharkia, Ägypten

München 2022

Aus dem Veterinärwissenschaftlichen Department
der Tierärztlichen Fakultät
der Ludwig-Maximilians-Universität München

Lehrstuhl für Molekulare Tierzucht und Biotechnologie

Arbeit angefertigt unter der Leitung von Univ.-Prof. Dr. Bernhard Aigner

Angefertigt in der Klinischen Kooperationseinheit
Molekulare Hämatologie/Onkologie
Deutsches Krebsforschungszentrum (DKFZ) und
Medizinische Klinik V, Universität Heidelberg
Mentor: Prof. Dr. Alwin Krämer

**Gedruckt mit Genehmigung der Tierärztlichen Fakultät
der Ludwig-Maximilians-Universität München**

Dekan: Univ.-Prof. Dr. Reinhard K. Straubinger, Ph.D.

Berichterstatter: Univ.-Prof. Dr. Bernhard Aigner

Korreferent: Univ.-Prof. Dr. Laurent Frantz

Tag der Promotion: 12. Februar 2022

To my family

LIST OF CONTENTS

I. INTRODUCTION	1
1. Centrosome	1
1.1. Centrosome structure.....	1
1.1.1. The mother centriole	2
1.1.2. The daughter centriole.....	2
1.1.3. Wall structure of centrioles	2
1.1.4. Microtubules.....	2
1.1.5. Pericentriolar material (PCM).....	3
1.2. Centrosome function	3
2. Stem cell leukemia (SCL)/T-cell acute leukemia (TAL1) Interrupting Locus (STIL).....	4
2.1. STIL protein structure	5
2.2. STIL protein role in centrosome duplication in cell cycle	6
2.3. Function of the STIL protein.....	8
2.4. Abnormalities in <i>STIL</i> gene and protein	8
2.4.1. Mutations.....	9
2.4.2. Deletions.....	9
2.4.3. STIL protein downregulation	9
2.4.4. STIL protein upregulation.....	10
3. Centrosome abnormalities.....	10
3.1. Centrosome amplification	10
3.2. Cancer and centrosome abnormalities.....	11
4. Can centrosome amplification drive tumorigenesis <i>in vivo</i>?.....	12
5. Aim of the thesis	15
II. MATERIALS UND METHODS	16
1. Materials	16
1.1. <i>In vivo</i> experiments	16
1.1.1. Genetically engineered mice	16
1.1.2. Pharmaceutical preparations for skin carcinogenesis.....	17
1.1.3. Materials for genotyping and polymerase chain reaction analysis	17
1.1.4. Primers for genotyping.....	17

1.2.	<i>In vitro</i> experiments	18
1.2.1.	Cell culture	18
1.2.1.1.	Cell lines.....	18
1.2.1.2.	Cell culture supplements	18
1.2.1.3.	siRNA transfection (<i>in vitro Stil</i> knockdown) materials.....	18
1.2.1.4.	ON-TARGETplus Mouse <i>Stil</i> (20460) siRNA sequences	19
1.2.1.5.	Plasmid transfection (<i>in vitro Stil</i> overexpression) materials.....	19
1.3.	Materials for real-time RT-PCR, qPCR	20
1.3.1.	Primers for qPCR	20
1.4.	Materials for immunoblotting	20
1.5.	Materials for immunofluorescence staining	21
1.6.	Antibodies for immunoblotting and immunofluorescence staining.....	22
1.7.	Materials for metaphase spreads for M-FISH analysis	22
1.8.	Materials for proliferation assay	22
1.9.	Materials for FACS analysis (apoptosis assay and cell cycle analysis)....	23
1.10.	Materials for senescence-associated beta-galactosidase assay.....	23
1.11.	Materials for Hematoxylin and Eosin (H&E) staining.....	23
1.12.	Utilities and consumables.....	23
2.	Methods	24
2.1.	Mice.....	24
2.1.1.	Husbandry and maintenance of mice	24
2.1.2.	B6-STIL (STIL ^{fl/fl}) mice.....	24
2.1.3.	STIL ^{OE} transgenic mice.....	26
2.1.3.1.	STIL ^{OE} MEFs	27
2.1.4.	Epithelium-specific STIL ^{OE} transgenic mice (K14 ^(CreERT2) ;STIL ^{OE})	28
2.1.5.	Epithelium-specific STIL ^{OE} and TP53 inactivation transgenic mice (K14 ^(CreERT2) ;STIL ^{OE} ;P53 ^{dn})	30
2.2.	Skin carcinogenesis assay, Two-stage chemically induced cancer model.	31
2.2.1.	Skin carcinogenesis assay of tamoxifen-inducible epithelium-specific STIL ^{OE} mice with and without TP53 inactivation assay.....	33
2.2.2.	Genotyping and polymerase chain reaction analysis (PCR)	35
2.2.3.	RNA isolation and qPCR analysis	37
2.2.3.1.	MEF qPCR analysis	37
2.2.3.2.	Mice tissues qPCR analysis	37
2.2.4.	Copy Number Variation (CNV) by Whole Genome Sequencing	37

2.3.	<i>In vitro</i> cell culture	38
2.3.1.	Immunoblotting	38
2.3.1.1.	Validation of anti-STIL antibody in Immunoblotting	39
2.3.1.1.1.	Human osteosarcoma cell line (U2OS-eGFP- <i>STIL</i>)	39
2.3.1.1.2.	STIL protein knockdown by siRNA transfection in MEFs	39
2.3.1.1.3.	In vitro STIL protein overexpression by CMV-Flag- <i>Stil</i> plasmid transfection in WT MEF	39
2.3.2.	Immunofluorescence staining (IF)	42
2.3.2.1.	MEF IF staining	42
2.3.2.2.	Mice tissues IF staining	42
2.3.3.	Metaphase spreads and Multiplex fluorescence in situ hybridization (M- FISH) analysis	43
2.3.4.	Proliferation assay	43
2.3.5.	Cell cycle analysis	43
2.3.6.	Apoptosis assay	44
2.3.7.	Senescence-associated beta-galactosidase assay	44
2.3.8.	Histopathology staining	44
3.	Statistical analysis	45
III.	RESULTS	46
1.	Generation of STIL^{OE} transgenic mice	46
1.1.	STIL overexpression reduces the incidence of spontaneous tumors in STIL ^{OE} mice	48
1.2.	STIL ^{OE} is downregulated in the tumor tissues	50
1.3.	STIL ^{OE} is associated with an increased rate of newly born deaths	52
2.	Generation of STIL^{OE} MEFs	54
2.1.	Characterization of STIL ^{OE} MEFs	54
2.1.1.	Genotyping	54
2.1.2.	STIL ^{OE} MEFs show increased <i>Stil</i> mRNA expression levels	54
2.1.3.	Validation of anti-STIL antibody in Western blotting	55
2.1.4.	STIL ^{OE} MEFs show increased STIL protein level	56
2.2.	STIL overexpression leads to centriole rosettes formation and centrosome amplification	57
2.3.	STIL ^{OE} MEFs have an abnormal phenotype with marked aneuploidy	59

2.4.	STIL overexpression impairs proliferation	62
2.5.	STIL overexpression induces cellular deaths.....	63
3.	Generation of transgenic mice with epithelium-specific STIL overexpression and with or without TP53 inactivation	64
3.1.	Generation of STIL ^{OE} transgenic mouse lines (K14 ^(CreERT2) ;STIL ^{OE}) and (K14 ^(CreERT2) ;STIL ^{OE} ;P53 ^{dn})	64
3.2.	Characterization of K14 ^(CreERT2) ;STIL ^{OE} mice with epithelium-specific STIL overexpression	64
3.3.	STIL overexpression decreases the incidence and multiplicity of chemically induced skin tumors.....	65
3.4.	Skin carcinogenesis assay in K14 ^(CreERT2) ;STIL ^{OE} ;P53 ^{dn} mice with epithelium-specific STIL overexpression and TP53 inactivation.....	68
4.	Centrosome amplification inhibits tumor formation.....	70
IV.	DISCUSSION.....	71
1.	STIL overexpression induces centrosome amplification that causes aneuploidy and impairs proliferation with increased cellular deaths.	72
2.	STIL-induced centrosome amplification inhibits tumor formation	73
2.1.	STIL-induced centrosome amplification inhibits spontaneous tumor formation in aging mice	73
2.2.	STIL-induced centrosome amplification inhibits chemically induced skin tumor formation.....	74
3.	Negative selection against STIL overexpression and centrosome amplification	75
4.	Conclusion: STIL-induced centrosome amplification causes a dose-dependent reduction in tumor formation.....	76
V.	SUMMARY.....	77
VI.	ZUSAMMENFASSUNG	79
VII.	REFERENCES.....	81
VIII.	APPENDIX.....	97

IX. ACKNOWLEDGEMENT98

ABBREVIATIONS

aa	Amino acid
APC/C	Anaphase-promoting complex / cyclosome
B6	Black 6 mice (C57BL/6)
CENPJ/CPAP	Centromere protein J/centrosomal P4.1-associated protein
CIN	Chromosomal instability
CNV	Copy number variations
com	Complete recombinant
E	Embryonic development day
ER	Estrogen receptor
ERT	Modified ER ligand binding domain sensitized for Tamoxifen
ES cells	Embryonic stem cells
FELASA	Federation of European Laboratory Animals Science Associations
fwd	Forward
GCPs	Gamma-tubulin complex proteins
GLI1	Glioma-associated oncogene 1
h	hour
H&E	Hematoxylin and Eosin
Hm	Homozygous
Ht	Heterozygous
IF	Immunofluorescence staining
inc	Partial/incomplete recombinant
IVC	Individually ventilated cage
kDa	Kilodalton
LMF	Light microscopy facility
LN	Lymph node
LSL	LoxP - STOP cassette - loxP

MCPH	Autosomal recessive primary microcephaly
MEFs	Mouse embryonic fibroblasts
mLBD-ER	Mutant ligand binding domain estrogen receptor
Mt	Mutant
MTs	Microtubules
P3	Passage 3
PCM	Pericentriolar material
PCR	Polymerase chain reaction analysis
PLK1	Polo-like Kinase 1
PLK4	Polo-like Kinase 4
PLK4 ^{OE}	PLK4 protein overexpression
Rec	Recombinant
rev	Reverse
Rpm	Round per minute
RT	Room temperature
SAS6	Spindle assembly abnormal protein 6 homolog
SCC	Squamous cell carcinomas
SCL/TAL1	Stem cell leukemia/T-cell acute leukemia 1
Shh	Sonic hedgehog
STIL	SCL/TAL1 interrupting locus
STIL ^{OE}	STIL protein overexpression
SUFU	Suppressor-of-fused homolog
Tam	Tamoxifen
Tm	Tumor
WGS	Whole genome sequencing
ZPF	Zentrum für Präklinische Forschung
γ -TRC	γ -tubulin ring complex

I. INTRODUCTION

1. Centrosome

Centrosomes have been first described in 1887 by two scientists, E. Van Beneden from Belgium and T. Boveri from Germany. The former mentioned it as *corpuscule central*, and the term *centrosome* was proposed by the latter. They observed that it is a self-duplicating cell organelle that is inherited from mother cells to daughter cells after organizing the cell division by dynamic formation of a mitotic spindle. It has a crucial role in the progression of cell division. Boveri thoroughly described the centrosome as an organelle with a dense dot inside. After another decade of detailed research on the centrosomes in cleaving eggs of the sea urchin and *Ascaris*, he described the duplication cycle of this dot and named it centriole (Scheer, 2014).

Boveri recognized also that amplified centrosomes caused abnormal multipolar mitoses with random chromosome segregation leading to aneuploidy, which led to abnormal developed sea urchin embryos with absence of cell-to-cell adhesion, cell death and unlimited overgrowth of some cells (Boveri, 1902; Sander, 1993). Therefore, he proposed a connection between centrosome amplification, abnormal mitosis, abnormal chromosome segregation and cancer (Boveri, 2008; Ribbert, 1914). Knowledge on the role of centrosomes in disease is continually increasing, as abnormal centrosomes have been found in microcephaly and undeveloped brains (Kaindl et al., 2010), and centrosome amplification was detected in cancer (Nigg, 2002).

1.1. Centrosome structure

Centrosomes are evolutionary conserved among eukaryotic cells with little variation; however, some eukaryotes do not contain centrosomes, e.g. most fungi and plants (Patwardhan et al., 2018). The centrosome is a cytoplasmic organelle located close to the nucleus, composed of two core centrioles, the mother and daughter centrioles, perpendicular to each other and embedded into a proteinaceous lattice termed pericentriolar material (Fig. 1). Each centriole is cylinder-shaped, consists of repeated nine-fold microtubule triplets, has a variable size with a diameter of about 250 nm and a length up to 500 nm (Carvalho-Santos et al., 2011).

1.1.1. The mother centriole

The mother centriole is the more mature centriole, characterized by the presence of proteinaceous appendages: nine distal appendages and variable numbers, ranging from 3 to 12 of the subdistal appendages, depending on cell type, proliferation activity, and cellular age. They are involved in cell membrane attachment, cilium formation and microtubule nucleation, respectively (Uzbekov and Alieva, 2018).

1.1.2. The daughter centriole

The daughter centriole is the less mature centriole, attached to the proximal end of the mother centriole. It originates from the cartwheel structure and has ribs (electronically thick plates) instead of appendages at its distal end. The STIL protein is a part of the cartwheel structure, which is the nidus for microtubule triplet elongation that built up in anticlockwise direction forming the centriole wall (Fig. 1) (Hirono, 2014). The cartwheel consists of stalk attached perpendicularly to the original centriole. This stalk is the hub for different number of stacks formed centrally from nine SAS6 dimer and STIL, where CPAP and CEP135 connects them to the microtubules. Each stack from the cross section composed of central hub surrounded by nine spokes of these proteins that terminated with a pin head structure anchoring the microtubule (A) and stabilized by γ -tubulin ring complex, the microtubule minus end (Guichard et al., 2010; Gupta et al., 2020). The cartwheel is present only in the procentriole and disappears from the full-length centriole in metaphase in mammals (Hirono, 2014; Nievergelt et al., 2018; Uzbekov and Alieva, 2018).

1.1.3. Wall structure of centrioles

The wall of both centrioles is composed of nine microtubule (MT) triplets, arranged from inside to outside as (A,B,C), with a linker protein between A and C microtubules, which is important for centriole stability (Wang et al., 2017). MTs are forming the full length of the centriole except for the C microtubule that ends earlier at the origin of the subdistal appendage (Firat-Karalar and Stearns, 2014; Schmidt et al., 2009; Uzbekov and Alieva, 2018).

1.1.4. Microtubules

MTs arrays consist of repeated units of α - and β -tubulin heterodimers. MTs are essential for organizing the eukaryotic cell cytoskeleton, signaling, kinetics, transport, matrix to localize organelles, motility, and spindle fiber formation in

mitosis. They dynamically elongate and depolymerize. MT nucleation starts with α - and β -tubulin dimer assembly at the γ -tubulin ring complex (γ -TRC) in the pericentriolar material. By electron microscopy the γ -TRC appears as ring like arrangement of γ -tubulin complexed with additional γ -tubulin complex proteins (GCPs no. 2,3,4,5,6) and NEDD1 that caps the minus end forming a stable binding site for α - and β -tubulin dimers to elongate at its plus end (Kollman et al., 2011).

1.1.5. Pericentriolar material (PCM)

The PCM surrounds the mother centriole proximally and consists of more than 100 different proteins that have prominent roles in MT nucleation, centrosome duplication during the cell cycle and spindle fiber assembly in mitosis. The best known proteins are the scaffold components pericentrin, CEP192, CPAP, and CEP152, the kinases Plk1 and Aurora A, as well as the effectors as γ -tubulin and TACC2 (Lüders and Stearns, 2007; O'Connell and Khodjakov, 2007; Woodruff et al., 2014).

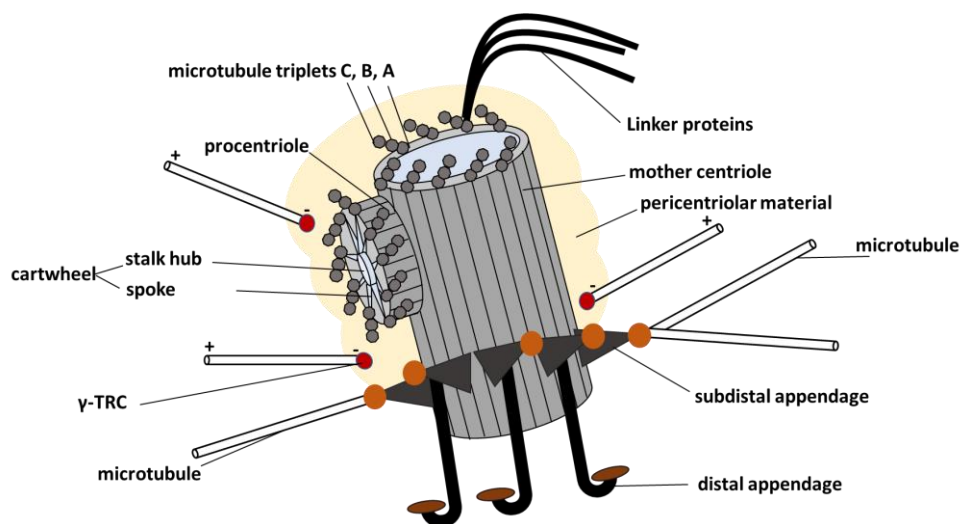


Figure 1 – A replicating mother centriole in S phase. The scheme represents a parent mother centriole connected proximally to a newly formed daughter pro-centriole, surrounded by pericentriolar material. The mother centriole is characterized by distal and subdistal appendages. The daughter pro-centriole is characterized by a cartwheel structure with the STIL protein constituting its formation. The wall of both centrioles is composed of nine MT triplets, arranged from inside to outside as (A,B,C).

1.2. Centrosome function

Centrosomes have multiple functions depending on cell cycle phase and cell type. In interphase, they organize MT formation needed for the cytoskeleton system giving each cell its shape that suits its function, e.g. they assist in shape modification for phagolysosome formation in phagocytes (Gordon, 2016; Mogilner and Keren,

2009; Schatten, 2008; Wakida et al., 2010). During mitosis, they control proper chromosome segregation by establishing a bipolar spindle fiber array (Chavali et al., 2014; Pihan, 2013). Therefore, centrosomes are the main microtubule-organizing center (MTOC) in the mammalian cell.

The centrosome has variable functions in different cell types; in all cells, the mother centriole can adhere to the plasma membrane to form the basal body, from where the non-motile primary cilium arises, which is important for cell signaling and communication with the extracellular environment. In ciliated cells it forms the basal body with beating cilia extending from deuterosome, which is formed of duplicating daughter centrioles (Arquint et al., 2014; Vertii et al., 2016; Werner et al., 2017). In flagellated cells as sperm, the flagellum arises from a single basal body which becomes the centrosome after ova fertilization to allow for spindle formation for the first cell division of the zygote, since ova do not contain centrosomes (Carvalho-Santos et al., 2011; Gibbons and Grimstone, 1960; Gruss, 2018; Jin et al., 2012). So, it has a role in cell signaling, ciliogenesis and cell migration (Schliwa et al., 1999; Wakida et al., 2010).

Centrosomes also have a role in brain development and differentiation of neurons. It has been found that in male *Drosophila* germline cells and mouse glial cells the daughter cell that receives the mother centriole becomes a progenitor stem cell, while the daughter cell that receives the daughter centriole differentiates into a neuron (Chavali et al., 2014; Wang et al., 2009). The centrosome also controls spindle orientation to keep symmetric and asymmetric cell divisions in balance (Florio and Huttner, 2014; LaMonica et al., 2013; Lancaster and Knoblich, 2012). Disturbance of the balance between symmetric and asymmetric cell divisions due to low or high levels of centrosomal proteins leads to microcephaly (Kaindl et al., 2010; Marthiens et al., 2013).

2. Stem cell leukemia (SCL)/T-cell acute leukemia (TAL1) Interrupting Locus (*STIL*)

The *STIL* gene is located on chromosome 1 (1p33-chr1) in humans and chromosome 4 in mice. The naming is due to its initial finding in a common chromosomal rearrangement in pediatric acute lymphoblastic leukemia cell, resulting in interrupting the SCL/TAL1 gene locus due to an interstitial deletion of

260 kb between *STIL* and the 5-prime UTR of *SCL* leading to a fusion of both loci, so that the *SCL* expression is controlled by the *STIL* promoter (Aplan et al., 1990, 1992). The human *STIL* protein has five isoforms, the active isoform contains 1287 amino acids in humans, and 1262 in mice, with more than 70% identity between the human and mouse amino acid sequence (Collazo-Garcia et al., 1995; Karkera et al., 2002). Also, the *STIL* gene promoter in humans and mice shows a high degree of conserved sequences (Colaizzo-Anas and Aplan, 2003).

2.1. STIL protein structure

STIL has conserved regions among species that interact with several centrosomal proteins within the course of centrosome duplication (Fig. 2). The *STIL* N-terminal domain (amino acids 15-364) interacts with CEP85 to ensure efficient PLK4 stimulation for assembly of daughter centrioles. The *STIL* conserved region 2 domain (amino acids 385-499) interacts with CPAP, promoting MT growth to build up a full-length centriole. The *STIL* coiled-coil domain (amino acids 715-758) is important for *STIL* protein oligomerization and interacts with PLK4 to initiate cartwheel formation. In addition, it interacts with CDK1/Cyclin B to transfer the *STIL* protein from centrosomes to cytoplasm. The *STIL* STAN domain (amino acids 1015-1148) binds to SAS6 to build up the cartwheel. The *STIL* KEN box domain (amino acids 1233-1287) binds to APC/C, stimulating *STIL* degradation. The *STIL* C-terminus reacts with SUFU, a *Sonic hedgehog* (*Shh*) pathway negative regulator, inhibiting its suppressing function of GLI1. This pathway is needed for proliferation and development of neural stem cells (Choudhry et al., 2014). So, *STIL* promotes the expression of the *Shh*-targeted genes (Arquint and Nigg, 2014, 2016; Cottee et al., 2015; David et al., 2016; Izraeli et al., 2001; Kasai et al., 2008; Liu et al., 2018; Nievergelt et al., 2018; Patwardhan et al., 2018; Sun et al., 2014; Zhang et al., 2009; Zitouni et al., 2016).

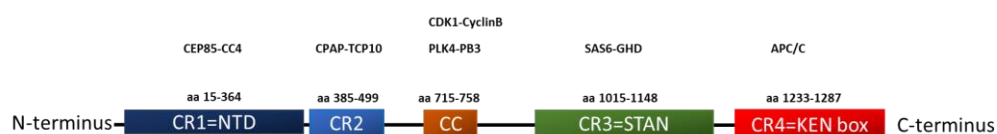


Figure 2 – Schematic of the known *STIL* protein domains and the specific binding domains of interacting proteins. CR = conserved regions, NTD = N-terminal domain, CC = coiled-coil, TCP = Trichoplax domain, PB3 = polo box 3, GHD = globular head domain.

2.2. STIL protein role in centrosome duplication in cell cycle

Centrosomal duplication takes place in interphase, where each centriole acts as a template for procentriole formation. This process is controlled by a set of centrosomal proteins including STIL. In G₁ phase of cell cycle, the mother and daughter centrioles get separated but stay connected by a proximal linker (Fig. 3), which consists of thick filaments of rootletin, CCDC102B, LRRC45, Cep68 and C-Nap1 (Xia et al., 2018).

During G₁/S, the level of cytoplasmic STIL is increasing (Vulprecht et al., 2012). CEP63 localizes proximally at the mother centriole and interacts with CEP152, which in turn binds to CEP192 to stimulate PLK4 to accumulate at the proximal mother centriole, thereby inducing the assembly of the cartwheel (Fig. 1), the nidus of procentriole formation, by phosphorylating NEDD1 and STIL. Both proteins, in turn, recruits SAS6 to the cartwheel (Chi et al., 2020; Moyer et al., 2015; Nievergelt et al., 2018). The STIL CR2 motif then interacts with CPAP, triggering MT growth and controlling centriole length (Arquint and Nigg, 2016; Arquint et al., 2012; Brown et al., 2013; Cottee et al., 2013; Sonnen et al., 2013; Tang et al., 2011; Vulprecht et al., 2012).

In S phase, the MT triplets elongate from the microtubule plus end of each daughter centriole until the full centriole is reached, with centriole length being controlled by CPAP (Sullenberger et al., 2020). During G₂ phase, the CP110/CEP97 proteins cap the plus end of the elongated daughter centriole (Spektor et al., 2007).

In G₂/M and just before mitosis, centrosome maturation takes place. This process starts with linker protein dissociation due to Nek2A phosphorylation, leading to complete separation of the two centrosomes (Xia et al., 2018). Also, the distal and subdistal appendages get formed on the mother centriole (Kong et al., 2014; Wang et al., 2011). In addition, PCM accumulates around the proximal end of the mother centriole of the two newly formed centrosomes by the control of Aurora A and PLK1 (Hoyer-Fender, 2010; Joukov et al., 2014) so that by the end of mitosis, each daughter cell gets one centrosome (Guichard et al., 2010).

In metaphase of mitosis, the CDK1 binds to the centrosomal STIL protein and transfers it to the cytoplasm. So, the STIL protein disappears from the centrosome and the cartwheel disassemble then completely disappears (Vulprecht et al., 2012).

In anaphase, the active APC/C binds to cytoplasmic STIL protein licensing it for degradation (Patwardhan et al., 2018). The capability of the centrosome to replicate and proceed to the separation step in G₁ phase of the next cell cycle is stimulated in anaphase by the effect of PLK1 (Kong et al., 2014; Tsou et al., 2009).

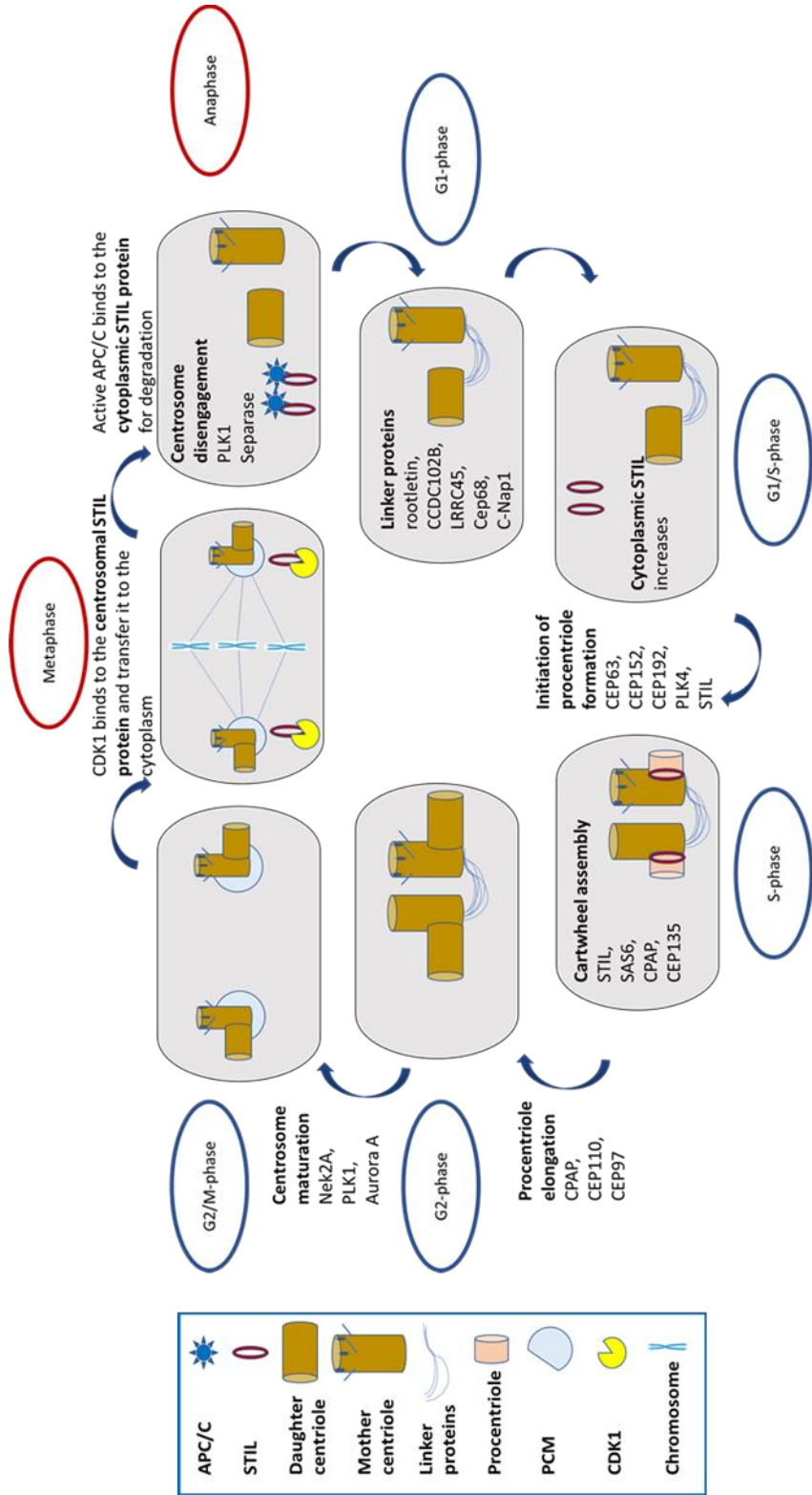


Figure 3 – Functions of STIL in centrosome duplication during cell cycle. Cytoplasmic STIL protein levels increase in G1/S phase and STIL is degraded near the end of mitosis in anaphase.

2.3. Function of the STIL protein

STIL is mainly a structural protein of the centriole, where it is required for centriole duplication and stability. It is a main component of the cartwheel during procentriole formation (Tang et al., 2011). Vulprecht et al. (2012) found that centrosomes and primary cilia were absent in *Stil*^(-/-) mouse embryonic fibroblasts (MEFs). When STIL expression was induced in these *Stil*^(-/-) MEFs, centrosomes and primary cilia re-appeared. On the other hand, STIL overexpression in the U2OS cell line leads to centrosome amplification and centriole rosette formation (Arquint et al., 2012; Cosenza et al., 2017).

STIL has both direct and indirect roles in *Shh* signaling. Directly, it suppresses SUFU function, deleting its inhibiting action on GLI1. Izraeli et al. (1999) confirmed this in *Stil*^(-/-) mouse embryos that showed reduced GLI1 expression. Indirect role due to its function in centrosome biogenesis, where *Stil*^(-/-) mutant cells, which lack centrosomes and primary cilia, are also depleted of *Shh* receptors, as they localize to cilia membranes (David et al., 2014; Scholey and Anderson, 2006). So, *STIL* deletion leads to interruption of *Shh* signaling, which is important for proper nervous system development.

Kumar et al. (2009) suggested that the STIL protein has a role in proliferation of neural cells as the gene is expressed in the embryonic human brain. Li et al. (2013) detected that STIL is expressed in all tissues of zebrafish and that its expression in general was higher in embryos compared to adults. They applied in situ hybridization and detected that the spinal cord and the brain specifically in the ventricular zone showed higher *stil* mRNA levels in embryos compared to other tissues, which suggests that *stil* is important in giving rise of subventricular progenitor cells, possibly by directing spindle orientation (LaMonica et al., 2013).

In addition, *Stil* knockout mouse embryos show holoprosencephaly that is defined as asymmetric development of the right and left prosencephalon with marked cell death and defects of the neural folds, plus random heart looping and impaired *Shh* signaling (Izraeli et al., 1999, 2001). So, STIL plays an important role in embryogenesis, cellular proliferation, and correct development of the neural system.

2.4. Abnormalities in *STIL* gene and protein

STIL protein abnormalities lead to impaired centrosome function, abnormal

mitosis, chromosomal instability, abnormal proliferation, aneuploidy, and cell death. Also, abnormal STIL protein levels affect the activity of all the proteins interacting with it (Fig. 2) (Arquint and Nigg, 2016; Patwardhan et al., 2018).

2.4.1. Mutations

Patients with homozygous mutations in *STIL* show autosomal recessive primary microcephaly 7 (MCPH7), which is a rare brain developmental disorder in which the head circumference is reduced during pregnancy and at birth with greater than or equal to four standard deviations and variable degrees of mental retardation and impaired intellectual skills. This is due to the presence of dysfunctional STIL protein, causing aberrant centrosome numbers, either less than normal or amplified, which lead to abnormal spindle positioning in neurogenic progenitor cells, thereby causing aberrant differentiation and cell death (Cristofoli et al., 2017; Kaindl et al., 2010; Kakar et al., 2015; Kumar et al., 2009; Papari et al., 2013; Patwardhan et al., 2018; Pfaff et al., 2007; Siskos et al., 2021).

2.4.2. Deletions

It has been found that a chromosomal deletion between *STIL* and *SCL* results in fused *STIL/SCL* mRNA, which occurs in 11-27% of children diagnosed with T-cell acute lymphoblastic leukemia. These cases showed better prognosis than children with unfused SCL protein (Aplan et al., 1991; Cave et al., 2004; Curry and Smith, 2003; Gustafsson et al., 2018). A deletion of the KEN box of the STIL protein results in an undegradable STIL protein and thereby leads to centrosome amplification (Arquint and Nigg, 2014).

2.4.3. STIL protein downregulation

STIL loss results in the absence of centrosomes and primary cilia, and abnormal mitosis (Castiel et al., 2011; David et al., 2014). It is lethal during embryogenesis, where dead embryos at midgestation show abnormal development of the neural system (Izraeli et al., 1999). Moreover, *Stil* knockdown has an effect on Chfr, a protein that blocks mitosis when cells are stressed by reducing activated CDK1/Cyclin B (Castiel et al., 2011). In addition, STIL depletion has been found to affect PLK4 activity and is accompanied with increased E-cadherin expression and subsequently decreased metastatic and invasive ability of cancer cells (Kazazian et al., 2017; Moyer et al., 2015).

2.4.4. STIL protein upregulation

STIL overexpression results in centriole rosette formations and centrosome amplification, which in turn leads to abnormal mitosis and chromosomal instability with abnormal spindle orientation (Arquint et al., 2012; Cosenza et al., 2017). STIL overexpression was found in cancers of colon, lung, ovary and prostate, in which the cells showed high mitotic index and metastatic features (Erez et al., 2004; Kitagawa et al., 2011; Rabinowicz et al., 2017; Ramaswamy et al., 2003).

3. Centrosome abnormalities

Centrosome abnormalities are classified into numerical and structural aberrations. Numerical aberrations defined as presence of centrioles or centrosomes in extra copies than normal (centrosome amplification, supernumerary centrosomes), while structural aberrations are centrosomes with abnormal size (ranging from small flecks to large focal aggregates), shape (corkscrew, string or filaments or elongated arrays and ring-like), position (focal, diffuse, clustered and scattered) and composition (abnormal protein levels, few or no centrioles and atypical phosphorylation) (Chan, 2011; Chng et al., 2006; Cosenza and Krämer, 2016; D'Assoro et al., 2002; Ghadimi et al., 2000; Godinho and Pellman, 2014; Nigg, 2002, 2006; Pihan et al., 1998).

Down regulation of the proteins involved in centriole duplication, foremost PLK4, STIL and SAS6, leads to no or few centrioles with structural defects and loss of normal spindle formation (Pihan, 2013), while overexpression of these proteins causes centriole amplification (Arquint and Nigg, 2014; Arquint et al., 2012; Peel et al., 2007; Serçin et al., 2016; Shinmura et al., 2015).

3.1. Centrosome amplification

Centrosome amplification is defined as the formation of supernumerary centrosomes, leading to the presence of more than two centrosomes per cell or the presence of centriole rosettes, which consist of multiple daughter centrioles surrounding a central mother centriole forming a rosette shape (Cosenza et al., 2017). Centrosome amplification originates from many causes, e.g. overexpression of centriole replication proteins PLK4, STIL and SAS6 (Anderhub et al., 2012; Erez et al., 2004; Macmillan et al., 2001), loss of the tumor suppressor protein TP53 (Fukasawa et al., 1996; Tarapore and Fukasawa, 2002), and absence of cytokinesis

and mitotic slippage, which lead to accumulation of centrosomes within one cell (Sinha et al., 2019; Trachana et al., 2007; Wu et al., 2020).

Supernumerary centrosomes can lead to multipolar spindles in mitosis, associated with multipolar divisions and subsequent cell death. To avoid this, many tumor cells can cluster supernumerary centrosomes into a pseudo-bipolar mitotic spindle, leading to successful bipolar division with an increased but tolerable rate of chromosome mis-segregation (Basto et al., 2008; Chan, 2011; Godinho and Pellman, 2014; Pihan, 2013; Quintyne et al., 2005).

3.2. Cancer and centrosome abnormalities

Cancer is listed as the major cause of death among humans in 70% of countries according to the World Health Organization (WHO) in 2019. In 2020, worldwide, the number of new cancer patients was estimated as 19.3 million, with 10.0 million cancer deaths. The universal cancer load is predicted to reach 28.4 million cases by 2040, with a 47% increased rate from 2020. Breast, lung, colorectal, prostate and stomach cancer are most diagnosed. Recent and previous studies implicated centrosome aberrations in cancer pathogenesis, where they show altered centrosome functions such as enhanced MT nucleation (Gustafson et al., 2000; Krämer et al., 2005; Lingle et al., 1998; Mittal et al., 2021; Miyoshi et al., 2001).

Early studies found pronounced centrosome amplification in malignant tumors of advanced stages as well as in animal xenograft models of human tumors (D'Assoro et al., 2002; Gustafson et al., 2000; Kuo et al., 2000; Miyoshi et al., 2001). Various studies of early and late stages of almost all types of malignancies revealed the presence of abnormal numerical centrosomes (Friedländer, 1982; Kaneko et al., 1980; Seifert, 1978). Moreover, analysis of breast and prostate cancer tissue in a mouse model displayed structural centrosome aberrations, characterized by enlarged pericentriolar material, abnormal centrosome positioning and multipolar mitoses, which have been suggested to be the origin of normal tissue architecture loss, chromosome mis-segregation, chromosome instability and aneuploidy (Anderhub et al., 2012; D'Assoro et al., 2002; Ganem et al., 2009; Lingle and Salisbury, 1999; Schatten et al., 2000). Lingle et al. (2002) proposed a significant correlation between chromosome instability and centrosome amplification.

Collectively, centrosome amplification is correlated with chromosome instability,

aneuploidy, and tumor aggressiveness.

On the other hand, Duensing et al. (2001) and Ganem et al. (2009) detected that cells with high-level centrosome amplification were unable to survive due to either mitotic catastrophe and apoptosis or senescence proposing that high levels of chromosome instability induces cell death (Janssen et al., 2009; Silk et al., 2013; Zasadil et al., 2016). This is usually due to TP53 effect, it has role in tetraploidy checkpoint to arrest the cell cycle of amplified centrosomes cells (Andreassen et al., 2001). Also, it induces senescence in aneuploid cells, screens for damaged DNA, chromosome mis-segregation, abnormal spindles during cell cycle and lengthy mitosis (Bazzi and Anderson, 2014; Giam et al., 2020; Lambrus et al., 2015; Uetake and Sluder, 2004; Wong and Stearns, 2005).

However, Funk et al., (2021) recently reported that pronounced chromosome instability suppresses tumor formation and induces cell death even in the absence of TP53.

In contrast, low-level centrosome amplification seems to allow for positive selection of viable cell clones with little chromosome instability in the process of tumorigenesis (Duensing et al., 2001; Duijf et al., 2013; Ganem et al., 2009; McGranahan et al., 2012; Silk et al., 2013; Zasadil et al., 2013).

Also, tetraploid cells seem to better tolerate chromosomal instability as the loss of genetic material is not as detrimental in a 4N DNA background (Nigg, 2002, 2006).

4. Can centrosome amplification drive tumorigenesis *in vivo*?

Normal centrosome numbers are needed to establish a bipolar mitotic spindle, resulting in normal chromosome segregation (Cosenza et al., 2017). Disruption of centrosome number or structure leads to chromosome mis-segregation, abnormal mitosis, chromosomal instability, and subsequent aneuploidy, which is a hallmark of cancer. Virtually, all types of cancer show either numerical or structural centrosome abnormalities, which are frequently correlated with karyotype abnormalities, clinical aggressiveness, drug-resistance and poor prognosis in several primary human malignancies (Anderhub et al., 2012; Chan, 2011; Cosenza and Krämer, 2016; Ghadimi et al., 2000; Godinho and Pellman, 2014; Greaves and Maley, 2012; Lee et al., 2011; Lengauer et al., 1997; Lingle et al., 2002; Nigg,

2002). Despite the correlative evidence of centrosomes involvement in tumorigenesis, a direct causative role of centrosome amplification in tumorigenesis is still unclear and debated (Anderhub et al., 2012; Boveri, 2008; Nigg, 2006; Zyss and Gergely, 2009). Therefore, establishing *in vivo* centrosome abnormalities in flies and animal models was advisable to test the fate of centrosome amplification and its role in tumorigenesis (Nigg, 2006).

PLK4, SAS6 and STIL overexpression have been found to lead to supernumerary centrosomes *in vitro*. Previous *in vivo* studies have focused on overexpression of PLK4 in *Drosophila* and mice, but the results regarding the induction of tumor formation in mice have been conflicting. Already in 2013 it has been found that PLK4 overexpression in mouse brains *in vivo* led to microcephaly instead of tumor formation (Marthiens et al., 2013). This was a consequence of multipolar divisions with subsequent aneuploidy leading to inefficient proliferation, premature differentiation, and cell death due to centrosome amplification in cells without the ability of centrosomal clustering. Cells showed apoptosis with tissue degeneration rather than malignant transformation. Notably, mutations in *PLK4* and other genes encoding centrosomal proteins can lead to microcephaly in humans (Chavali et al., 2014; Martin et al., 2014).

In 2015, Vitre and coworkers found that in PLK4-overexpressing transgenic mice with functional *Tp53*, increasing PLK4 levels led to centrosome amplification in liver and skin. However, this did not promote spontaneous tumor development in these tissues or enhance the growth of chemically induced skin tumors. In the absence of *Tp53*, PLK4 overexpression generated widespread centrosome amplification, but did not drive tumor development either. Therefore, the authors concluded that PLK4-induced supernumerary centrosomes are not sufficient to drive tumor formation (Vitre et al., 2015).

In contrast, Serçin and coworkers in 2016 found that PLK4 overexpression does enhance tumor formation in *Tp53*^{-/-} mice (Serçin et al., 2016). Earlier studies in *Drosophila* had already suggested that PLK4 overexpression is sufficient to promote tumorigenesis. Extra centrosomes due to overexpression of SAK, the PLK4 fly homolog, led to tumor formation in a neuroblast transplantation assay, which occurred via compromised spindle orientation and asymmetric stem cell division leading to neural stem cell pool expansion (Basto et al., 2008). In 2017,

Levine et al. described that in another mouse model of conditional PLK4 overexpression, chronic low level PLK4 overexpression led to low level centrosome amplification. By nine months of age, these mice exhibited increased spontaneous formation of lymphomas, squamous cell carcinomas and sarcomas irrespective of their *Tp53* status. It was shown that aneuploidy and chromosomal instability levels of these tumors were similar to those of many human cancers. It was also found that centrosome amplification by PLK4 overexpression promoted the initiation, but not progression of adenomatous intestinal tumors in an APC^{Min} mouse model (Levine et al., 2017).

As a serine/threonine kinase, PLK4 has additional functions besides the regulation of centriole duplication (Rosario et al., 2015). On the other hand, STIL is a structural protein without enzymatic activity and - up to now - no known roles outside the centrosome. STIL overexpression is found in several human malignancies and previous studies on STIL overexpression in cell lines revealed that it induces supernumerary centrosomes similar to PLK4 (Arquint et al., 2012; Erez et al., 2004). The role of STIL in centriole replication has been initially described both by our laboratory and by others (Arquint et al., 2012; David et al., 2014; Kitagawa et al., 2011; Tang et al., 2011; Vulprecht et al., 2012). In cell line models, STIL overexpression leads to supernumerary centrosomes and centriole rosette formation with subsequent induction of chromosomal instability by generation of two asymmetric spindle poles with unbalanced numbers of microtubules emanating from the two mitotic half-spindles (Cosenza et al., 2017). Taken together, STIL overexpression is suitable for testing the contribution of extra centrosomes to the development of chromosomal instability and tumor formation *in vivo* and investigating its role in tumor initiation, promotion and progression in a mouse model and will add important information to the conflicting data generated by PLK4 overexpressing mice.

5. Aim of the thesis

Using spontaneous and chemically induced tumor models in *STIL* overexpressing transgenic mice, which has been generated by our laboratory, we aim to investigate whether *STIL*-induced centrosome amplification causes abnormal mitoses, chromosomal instability, aneuploidy, and subsequent tumor development *in vivo* (Fig. 4).

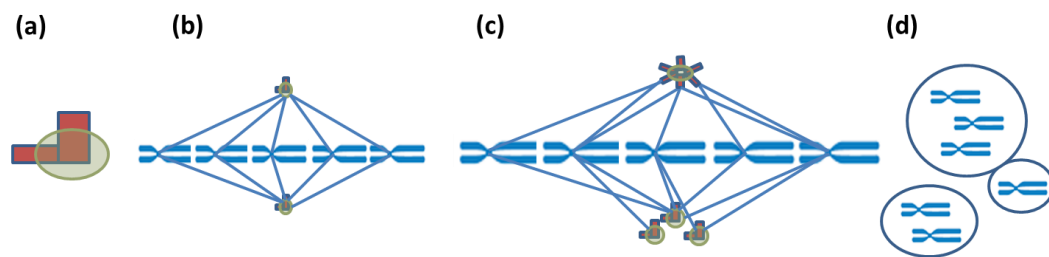


Figure 4: Centrosome amplification, aberrant mitosis, and aneuploidy. Diagram showing a normal centrosome (a) that duplicates in interphase before mitosis to ensure a normal chromosome segregation in metaphase (b). Centrosome overduplication results in centrosome amplification, causing clustered, pseudo-bipolar (c) or multipolar mitoses with subsequent chromosome mis-segregation and aneuploidy, expressed as daughter cells with abnormal chromosome numbers and micronucleus formation (d), which is described as a hall mark of cancer.

II. MATERIALS AND METHODS

1. Materials

Materials for *in vivo* and *in vitro* experiments are summarized in the following tables.

1.1. *In vivo* experiments

1.1.1. Genetically engineered mice

Table 1: Genetically engineered mice

Name	Specification	Source
B6-STIL (STIL ^{fl/fl}) mice	The strain carries the Gt(ROSA)26Sor ^{tm1} (Stil-IRES-mCherry) ^{Pg} transgene within Rosa 26 Locus in chromosome no. 6, on a B6 background. STIL overexpressing (STIL ^{OE}) transgenic mice, overexpress murine STIL under the transcriptional control of the ubiquitously expressed Rosa26 promoter when bred with Cre-deleter lines, where Cre mediates the excision of an upstream STOP cassette.	Polygene Transgenetics AG, Switzerland on behalf of Clinical cooperation unit of molecular hematology/oncology (DKFZ-Heidelberg)
CMV-Cre mice	This strain carries the Tg(CMV-cre)1Cgn transgene, on a B6 background. Cre recombinase is under the control of the human cytomegalovirus promoter (CMV). In this X-linked transgenic strain, deletion of loxP-flanked genes occurs in all tissues, including germ cells (Schwenk et al., 1995).	Kindly provided by animal facility (DKFZ-Heidelberg)
K14 ^{creERT2} mice	The strain carries the Krt14 ^{tm1.1} (Cre/ERT2) ^{Hjg} mutation on a B6;129P2 background. Cre is expressed under the control of a Keratin 14 promoter upon treatment with tamoxifen (Amen et al., 2013).	Kindly provided by cellular and molecular Pathology division (DKFZ-Heidelberg)
P53 ^{dn} mice	The strain carries the heterozygous LSL-Trp53 ^{tm1Tyj} conditional point mutation on the (R172H) position in exon 5 of Trp53 locus, on a B6 background. Upon Cre activation and STOP cassette excision, a TP53 dominant negative version is expressed showing higher affinity for binding to the <i>Trp53</i> target genes promoters leading to inactivation of the wild-type <i>Trp53</i> allele (Olive et al., 2004; Willis et al., 2004).	Kindly provided by applied functional genomics and molecular oncology of gastrointestinal tumors divisions (DKFZ-Heidelberg)

1.1.2. Pharmaceutical preparations for skin carcinogenesis

Table 2: Pharmaceutical preparations

Name	Source
Tamoxifen free base	Sigma-Aldrich, Cat. No. T5648-1g
Sunflower Seed Oil	Sigma-Aldrich, Cat. No. S5007-250ml
DMBA (Dimethylbenzanthracene)	Sigma-Aldrich, Cat. No. D3254-100MG
TPA (Tetradecanoylphorbol acetate)	Sigma-Aldrich, Cat. No. P8139-25MG

1.1.3. Materials for genotyping and polymerase chain reaction analysis

Table 3: Materials for genotyping

Name	Components, Source
SampleIN™ Direct PCR Kit (highQu)	Th.Geyer, Cat. No. 11784200
ALLin™ HS Red Taq Mastermix (highQu)	Th.Geyer, Cat. No. 11784624
NFW (nuclease-free water)	Qiagen, Cat. No. 129115
10x TAE (Tris-acetate-EDTA) buffer	400 mM Tris/HCl pH 8.0, 200 mM Acetic acid, 10 mM EDTA
1x TAE buffer	100 ml 10x TAE buffer, 900 ml ddH ₂ O
Agarose gel	1% agarose in 1x TAE buffer dissolved in microwave, 0.1 µL/mL ethidiumbromide.

1.1.4. Primers for genotyping

Table 4: Primers for genotyping

Name	Forward primer (5' - 3')	Reverse primer (5' - 3')	Band size (bp)
Rosa	AAAGTCGCTCTGAGTTGT TAT	GGAGCGGGAGAAATGG ATATG	546
Stop cassette	TAATATGCGAAGTGGAC CTGG	GTGGCAGCTTCTTTAGC AAC	427
CMV-Cre	GGCGCGGCAACACCATT TT	CCGGGCTGCCACGACCA A	420
STIL-rec	AAAGTCGCTCTGAGTTGT TAT	CATCGTCGTCCTTGTAG TCAG	410
K14	CGCCAATTAACCCTCACT AAAGG(Mt)	ATCCATCAAATCGACCA CCA(WT)	357
P53-unrec	AGCCTTAGACATAACAC ACGAACT(WT) GCCACCATGGCTTGAGTA A(Mt)	CTTGGAGACATAGCCAC ACTG(WT)	565WT 270Mt
P53-rec	AGCCTGCCTAGCTTCCTC AGG	CTTGGAGACATAGCCAC ACTG	290WT 330Mt

1.2. *In vitro* experiments

1.2.1. Cell culture

1.2.1.1. Cell lines

Table 5: Cell lines

Name	Specification	Source
U2OS-eGFP- <i>STIL</i>	Tetracycline inducible eGFP- <i>STIL</i> human osteosarcoma cell line	Clinical cooperation unit of molecular hematology/oncology (DKFZ-Heidelberg)
NIH-3T3	Mouse embryonic fibroblast	Kindly provided by molecular genome analysis division (DKFZ-Heidelberg)
MEF	Mouse embryonic fibroblast (primary cell line)	Derived from mice embryos' body at embryonic age of 12-13 days

1.2.1.2. Cell culture supplements

Table 6: Cell culture supplements

Name	Source
DMEM (Dulbecco's Modified Eagle's Medium)	Life Technologies, Cat. No. 31966047
Opti-MEM I Reduced Serum Medium	Life Technologies, Cat. No. 31985047
DMSO (Dimethylsulfoxid)	Serva Electrophoresis, Cat. No. 20385.01-250ML
DPBS (Dulbecco's Phosphate Buffered Saline)	Life Technologies, Cat. No. 14200083
FBS (Fetal Bovine Serum)	Clontech, Cat. No. 631106
MEM Non-Essential Amino Acids Solution (100X)	Thermofisher scientific, Cat. No. 11140050
Tetracycline hydrochloride cell culture tested	Sigma-Aldrich, Cat. No. T7660-5G
Penicillin-Streptomycin (10,000 U/mL)	Life Technologies, Cat. No. 15140122
Hygromycin B	Life Technologies, Cat. No. 10687010
Puromycin	Life Technologies, Cat. No. A11138-02
Trypsin	Life Technologies, Cat. No. 15090046

1.2.1.3. siRNA transfection (*in vitro Stil* knockdown) materials

Table 7: siRNA transfection supplements

Name	Source
5x siRNA Buffer	GE-Healthcare Life Sciences (Dharmacon), Cat. No. B-002000-UB-100
ON-TARGETplus Mouse <i>Stil</i> (20460)	Dharmacon, Cat. No. L-063476-01-0005,

siRNA – SMARTpool (a pool of four different <i>Stil</i> siRNA)	5nmol
Luciferase siRNA	Eurofins, Cat. No. 6274233
Lipofectamin RNAiMAX	Life Technologies, Cat. No. 13778075

1.2.1.4. ON-TARGETplus Mouse *Stil* (20460) siRNA sequences

Table 8: Oligoribonucleotides (siRNA) target sequences

Name	Target sequence (antisense 5' - 3')
ON-TARGETplus SMARTpool siRNA – J-063476-09, <i>Stil</i>	GCACAGAUCCAGCGCUUUAU
ON-TARGETplus SMARTpool siRNA – J-063476-10, <i>Stil</i>	CAAGAAACCUAAGUAGUAA
ON-TARGETplus SMARTpool siRNA – J-063476-11, <i>Stil</i>	CAUGGAAGACACCGUGAAA
ON-TARGETplus SMARTpool siRNA – J-063476-12, <i>Stil</i>	GGGCCCAACAAAUCAGUUA
Luciferase	UCGAAGUACUCAGCGUAAG

1.2.1.5. Plasmid transfection (*in vitro Stil* overexpression) materials

Table 9: Plasmid transfection supplements

Name	Components, Source
pcDNA3.1(-) plasmid	Kindly provided by Division of Redox Regulation (DKFZ-Heidelberg)
SOC medium	20 mM Glucose, 0.5% Yeast extract, 2% Trypton, 2.5 mM KCl, 0.05% NaCl, 10 mM MgCl ₂ , pH 7.0
LB medium	Roth, Cat. No. X968.2
LB Agar	Roth, Cat. No. X969.2
Carbenicillin	Sigma-Aldrich, Cat. No. 69101-3 5g
QIAprep Spin Miniprep Kit (250)	Qiagen, Cat. No. 27106
Bam HI	New England Biolabs, Cat. No. R0136
Eco RI	New England Biolabs, Cat. No. R0101
Phusion® High-Fidelity DNA Polymerase	New England Biolabs, Cat. No. M0530S
6x DNA loading dye	30% Glycerol, 100 mM Tris/HCl pH 7.5, 0.01% Xylencyanol, 0.01% Bromophenol blue, 200 mM EDTA
FullRanger 100 bp DNA Ladder	BioCat, Cat. No. 11815-NB
HighRanger 1 kb DNA Ladder	BioCat, Cat. No. 11915-NB
LowRanger 100 bp DNA Ladder	BioCat, Cat. No. 11515-NB
High Pure PCR Product Purification Kit	Roche, Cat. No. 11732676001
Shrimp Alkaline Phosphatase (SAP)	VWR, Cat. No. E70092Y
NxGen T4 DNA-Ligase	BioCat, Cat. No. 30241-1-LU
QIAGEN Plasmid Maxi Kit (25)	Qiagen, Cat. No. 12163
Lipofectamin 2000	Life Technologies, Cat. No. 11668027

1.3. Materials for real-time RT-PCR, qPCR

Table 10: Materials for qPCR

Name	Source
Stainless Steel Beads, 5 mm (200)	Qiagen, Cat. No. 69989
Rneasy Mini Kit (50)	Qiagen 74106, Cat. No. 217004
AllPrep DNA/RNA/Protein Mini Kit (50)	Qiagen, Cat. No. 80004
QuantiTect Rev. Transcription Kit (50)	Qiagen, Cat. No. 205311
QuantiTect SYBR Green PCR Kit (40)	Qiagen, Cat. No. 204141

1.3.1. Primers for qPCR

Table 11: Primers for qPCR

Name	Forward primer (5' - 3')	Reverse primer (5' - 3')	Band size (bp)
<i>Hprt</i>	TGATCAGTCAACGGGGGAC A	TTCGAGAGGTCCTTTTCAC CA	191
<i>Pbib</i>	TCGTCTTTGGACTCTTTGG AA	AGCGCTCACCATAGATGCT C	189
<i>Stila</i>	GACACAATTCAGGACTGGT AGAC	GGCATGATCCACTTTCTGT TCA	128
<i>Stilc</i>	TCCTTGTGAGAGTAGGACG C	TCAAGGTCAGTGTCATGCT T	249

1.4. Materials for immunoblotting

Table 12: Materials for immunoblotting

Name	Components, Source
cOmplete™ tablets EASYpack	Roche, Cat. No. 05892970001
PhosStop™ EASYpack	Roche, Cat. No. 04906837001
CEB (Cellular fractionation buffer)	10 mM HEPES, 10 mM KCL, 0.1 mM EDTA, 0.5 mM DTT, plus freshly added 0.05% NP40, 20% cOmplete™ and 10% PhosStop™
RIPA (Radioimmunoprecipitation assay) buffer	1 mM NaCl, 50 mM Tris/HCl pH 7.4, 1 mM EDTA, 0.25% Sodium deoxycholate, plus freshly added 1% NP40, 20% cOmplete™ and 10% PhosStop™
Quick Start™ Bradford 1x Dye Reagent	Bio-Rad Laboratories, Cat. No. 500-0205
5x Laemmli sample buffer	5% SDS, 50% Glycerol, 1% bromophenol blue, 1M Tris-HCl/pH 6.8, 5% β-Mercaptoethanol
Precision Plus Protein™ Dual Color Standards	Bio-Rad Laboratories, Cat. No. 161-0394
Acrylamide	Sigma, Cat. No. A3553

Bisacrylamide	Promega, Cat. No. V3143
Kornberg Solution A	0.15% Bis-Acrylamide, 30% Acrylamide
Kornberg Solution B	0.4% SDS, 3 M Tris-Base pH 8.8
Kornberg Solution C	0.4% SDS, 0.75 M Tris-Base pH 6.8
Kornberg running buffer	0.1% SDS, 0.6% Tris-Base, 2.87% Glycine
Rotiphorese® Gel 30	Roth, Cat. No. 3029.1
APS (ammonium peroxodisulfate)	Roth, Cat. No. 9592.2
TEMED (Tetramethylethylenediamine)	Serva Electrophoresis, Cat. No. 35925.01
Separating gel (10%)	Kornberg Solution A (33%) and B (25%), ddH ₂ O (42%)
Stacking gel	Kornberg Solution C (24%), Rotiphorese® Gel 30 (12.6%), ddH ₂ O (63.4%)
Trans-Blot Turbo RTA Transfer Kit, nitrocellulose	Bio-Rad Laboratories, Cat. No. 170-4271
Blocking buffer	5% Skim milk in 0.1% TBST
Skim Milk Powder	Gerbu, Cat. No. 1602.05
1x TBST (Tris-Buffered Saline and Tween 20)	150 mM NaCl, 10 mM Tris, 0.1% Tween 20
Clarity™ Western Blotting ECL Substrate	Bio-Rad Laboratories, Cat. No. 170-5061

1.5. Materials for immunofluorescence staining

Table 13: Materials for immunofluorescence staining

Name	Components, Source
1x PBS (Phosphate Buffered Saline)	NaCl 137 mM, KCl 2.7 mM, Na ₂ HPO ₄ 10 mM, KH ₂ PO ₄ 1.8 mM, PH 7.4
1x PHEM buffer	60 mM PIPES, 25 mM HEPES, 8 mM EGTA, 2mM MgCl ₂ , pH 6.9
TritonX-100	Thermofisher scientific, Cat. No. 28313
Fixative solution	Methanol: Acetone (1:1) for 10 minutes Or 4 %PFA for 15 minutes
Methanol	Sigma-Aldrich, Cat. No. 32213-1L-M
Acetone	Sigma-Aldrich, Cat. No. 179973-2.5L
Paraformaldehyd (PFA)	Sigma-Aldrich, Cat. No. 158127-500G
Permeabilizing solution	1x PBS, 0,2% Triton-X-100
Blocking buffer	10% goat serum in 1x PBS
Goat serum	Life Technologies, Cat. No. 16210064
Hoechst 33342	Becton Dickinson, Cat. No. 561908
Vectashield mounting medium	Linaris, Cat. No. H-1000
Vector® TrueVIEW™ Autofluorescence Quenching Kit	Linaris, Cat. No. SP-8400
MemBrite Fix 543/560 Cell Surface Staining Kit	Hölzel Diagnostika, Cat. No. B-30094-T

1.6. Antibodies for immunoblotting and immunofluorescence staining

Table 14: Antibodies for immunoblotting and immunofluorescence staining

Name/Clone/Fluorochrome	Species	Dilution	Source
Primary antibodies			
Anti-centrin / 20H5	Mouse (monoclonal)	1:1000	Millipore, Cat. No. 04-1624
Anti-centrin-2 / W16110A	Rat (monoclonal)	1:50	Biolegend, Cat. No. 698602
Anti-pericentrin	Rabbit (polyclonal)	1:1000	Abcam, Cat. No. ab4448
Anti-STIL	Rabbit (polyclonal)	1:1000	Biomol, Cat. No. A302-442A
Anti- β -Actin / C4-HRP	Mouse (monoclonal)	1:5000	Santa Cruz/TEBU Bio, Cat. No. sc-47778 HRP
Anti- α -tubulin / DM1A	Mouse (monoclonal)	1:5000	Sigma, Cat. No. T6199-200 μ l
Secondary antibodies			
Anti-Mouse IgG-Alexa Fluor488	Goat (polyclonal)	1:1000	Life Technologies, Cat. No. A11029
Anti-Rat IgG-Alexa Fluor 488	Donkey (polyclonal)	1:1000	Thermo Scientific, Cat. No. A-21208
Anti-Rabbit IgG-Alexa Fluor 568	Goat (polyclonal)	1:1000	Life Technologies, Cat. No. A11036
Anti-mouse IgG (H+L)-HRPO	Goat (polyclonal)	1:10000	Dianova, Cat. No. 115-035-003
Anti-rabbit IgG (H+L)-HRPO	Goat (polyclonal)	1:10000	Dianova, Cat. No. 111-035-003

1.7. Materials for metaphase spreads for M-FISH analysis

Table 15: Materials for metaphase spreads

Name	Components, Source
Colcemid	Biochrom, Cat. No. L 6221
Hypotonic solution	KCl 0.55%: Na Citrate 1% (1:1)
Glacial acetic acid	Fisher Scientific, Cat. No. 10171460
Fixative solution	Methanol: Glacial acetic acid (3:1)

1.8. Materials for proliferation assay

Table 16: Materials for proliferation assay

Name	Source
TC10 Trypan Blue Dye 0,4%	Bio-Rad Laboratories, Cat. No. 145-0013
PrestoBlue® Cell Viability Reagent	Life Technologies, Cat. No. A-13261

1.9. Materials for FACS analysis (apoptosis assay and cell cycle analysis)**Table 17: Materials for FACS analysis**

Name	Source
Apotracker™ Green (20 tests)	BioLegend, Cat. No. 427401
Cell Staining Buffer (500 ml)	BioLegend, Cat. No. 420201
7-AAD Staining solution	Becton Dickinson, Cat. No. 559925
RNase A - 10 mg/ml	Life Technologies, Cat. No. EN0531
Propidium iodide - 1.0 mg/mL solution in water	Life Technologies, Cat. No. P3566

1.10. Materials for senescence-associated beta-galactosidase assay**Table 18: Materials for senescence-associated beta-galactosidase assay**

Name	Source
Paclitaxel	Biomol, Cat. No. AG-CN2-0045-M005
Senescence β -Galactosidase Staining Kit	Cell Signaling, Cat. No. 9860S
DMF (Dimethylformamid)	Biotrend, Cat. No. 40470000-2

1.11. Materials for Hematoxylin and Eosin (H&E) staining**Table 19: Materials for H&E staining**

Name	Components, Source
Tissue-Tek® O.C.T.™ Compound	SAKURA, Cat. No. 4583
PFA (Paraformaldehyde) pure	Serva Electrophoresis, Cat. No. 31628.01
Hematoxylin solution according to Gill II	Roth, Cat. No. 472301-500ML
Ethanol absolute	Sigma-Aldrich, Cat. No. 1024282500
Eosin Y	Appllichem, Cat. No. A0822,0025
Eosin Y stock solution	1 g eosin Y, 20 ml ddH ₂ O, 80 ml of absolute ethanol
Eosin Y working solution	25 ml of eosin Y stock solution, 75 ml of 70% ethanol, 4 ml glacial acetic acid
Aqueous Hydrochloric acid 0.1%	2 ml of 25% HCL in 100 ml 70% ethanol
Xylenes	Sigma-Aldrich, Cat. No. 534056-4L
Neo-Mount	Sigma-Aldrich, Cat. No. 1090160500

1.12. Utilities and consumables

Falcons, tubes, Whatman filter paper, etc. were from Starlab, Eppendorf (Germany), GE Healthcare, Whatman (UK), Thermo Fisher Scientific and Millipore (USA).

2. Methods

2.1. Mice

2.1.1. Husbandry and maintenance of mice

The mice were kept in the DKFZ experimental animal facility / ZPF in ATV, room 1.109. The skin carcinogenesis mouse groups were held in the husbandry of Dr. Karin Müller-Decker's department in room S2.102 at DKFZ. They were maintained under controlled specified pathogen-free (SPF) measures according to the FELASA regulations (FELASA working group on revision of guidelines for health monitoring of rodents and rabbits et al., 2014; Gyger et al., 2019) and their health status was monitored daily. The husbandry rooms were air-conditioned to ensure 22°C +/- 2°C room temperature and 55% +/- 10% relative humidity with light system cycle to set twelve hours light and dark. The IVC cages (GM500, Tecniplast) had two to four mice from the same age, genotype, and sex except for the separated males after mating, which were housed individually to avoid male domination fights. Mice were ear-marked, and ear punches were genotyped at three weeks of age. The dirty cages were weekly exchanged with a clean one supplied with environmental enrichments. Autoclaved partly decalcified water and standard diet were provided ad libitum. Mice after weaning had holding diet (KLIBA, Cat. No. 3437) and in breeding had breeding diet (KLIBA, Cat. No. 3307). For the skin carcinogenesis assay, four weeks old mice were transferred from ATV-1.109 to S2.102. They had one week to accommodate the new housing and were fed Altromin diet (Altromin, Cat. No. 1324 FF). All mouse experiments were carried out in accordance with the German animal protection legislation and were approved by Baden-Württemberg government.

2.1.2. B6-STIL (STIL^{f/f}) mice

We have generated B6-STIL mice, Gt(ROSA)26Sor^{tm1(Stil-IRES-mCherry)Pg}, by the help of Polygene Transgenetics AG, Switzerland, which cloned the Flag-tagged *Stil* cDNA construct into a Rosa26 targeting vector that contained loxP - STOP cassette - loxP and IRES-mCherry sequences (Fig. 5 and 6). This vector was then inserted in C57BL/6 ES cells by electroporation. Neomycin-resistant cells were selected by PCR screening, karyotype analysis and morphological clone characteristics. After that, a vector positive C57BL/6 ES cell clone was injected into C57BL/6 blastocysts, which were transferred into a Black 6 (B6) foster mouse. The resulting

chimeric offspring was mated to verify germ-line transmission and bred for another three rounds (Capecchi, 1989; Smithies et al., 1985). No signs of a harmful phenotype could be detected at Polygene Transgenetics AG. Then, these mice were sent to the Clinical Cooperation Unit Molecular Hematology/Oncology (DKFZ-Heidelberg) and kept as homozygous inbred line, loxP - STOP cassette - loxP - Rosa^{Flag-Stil-IRES-mCherry} (STIL^{fl/fl}) in ATV, room 1.109.



Figure 5: Stil construct cloned into B6-STIL mice. The stop cassette prevents the translation of Flag-tagged STIL. Lox = loxp sites, Tk-neo-pA = bacterial neomycin phosphotransferase (*neo*) gene, FRT = FRT sites for flippase recombination flanking the IRES-RFP = red fluorescent protein (mCherry)-containing IRES that allow coexpression of Flag-STIL and mCherry proteins simultaneously.

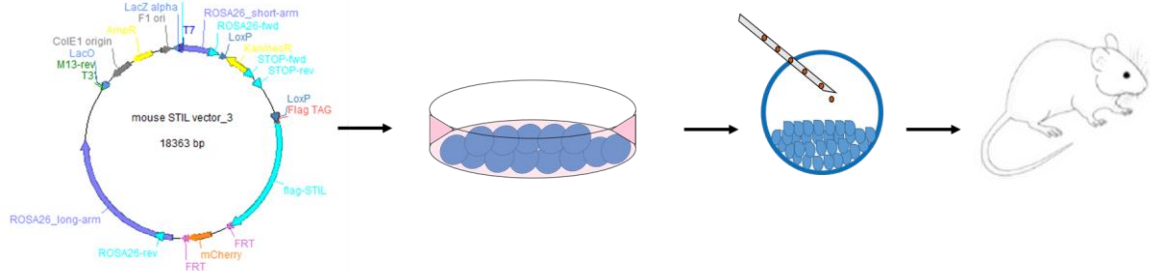


Figure 6: Generation of transgenic B6-STIL mice. The Flag-*Stil* construct vector was inserted into C57BL/6 ES cells by electroporation. Then, neomycin-resistant cells were selected and injected into C57BL/6 blastocysts, which were transferred into a B6 foster mouse.

B6-STIL mice were used to:

- (A) generate and characterize STIL-overexpressing (STIL^{OE}) mice with ubiquitous STIL overexpression by crossing B6-STIL (STIL^{fl/fl}) mice with a CMV-Cre-deleter line. These mice were used to assess for potential spontaneous tumor formation due to STIL-overexpression over a period of 23 months. Table 20 indicates the mice used.

Table 20: Mouse groups used for spontaneous tumor development assessment.

Group	Transgenic Mice	Mouse no.
Control	STIL ^{fl/fl} mice	28
	CMV-Cre; STIL ^{fl/wt}	9
Heterozygous STIL ^{OE}	CMV-Cre;STIL ^{lox/wt}	7
Homozygous STIL ^{OE}	CMV-Cre;STIL ^{lox/lox}	11

(B) generate and characterize mouse embryonic fibroblasts (MEFs) derived from STIL^{OE} mice. These primary cells were used to determine centrosome amplification, chromosomal aberrations, and abnormal mitoses *in vitro*.

Table 21: MEF groups for *in vitro* experiments.

Group	Transgenic Mice	Mouse no.
Control MEFs	C57BL/6	3
	STIL ^{fl/fl}	1
	CMV-Cre	1
Heterozygous STIL ^{OE} MEFs	CMV-Cre;STIL ^{lox/wt}	3
Homozygous STIL ^{OE} MEFs	CMV-Cre;STIL ^{lox/lox}	3

(C) generate and characterize tamoxifen-inducible epithelium-specific STIL^{OE} mice (K14^(CreERT2);STIL^{OE}) with conditional STIL overexpression in K14-expressing epithelial cells, by crossing B6-STIL mice with K14^{CreERT2} mice.

(D) generate and characterize tamoxifen-inducible epithelium-specific STIL^{OE} and p53 inactivation mice (K14^(CreERT2);STIL^{OE};P53^{dn}) with conditional STIL overexpression and TP53 inactivation in K14-expressing epithelial cells, by crossing K14^(CreERT2);STIL^{fl/wt} mice with P53^{R172H/wt} mice. Mice from subprojects (C) and (D) were used to assess the role of STIL overexpression and TP53 inactivation in skin carcinogenesis.

Table 22: Skin carcinogenesis mice groups.

Group	Cre-Induction	Initiation	Promotion	Mouse no.
K14 ^(CreERT2) ;STIL ^{fl/wt} mice	Oil	DMBA	TPA	15
K14 ^(CreERT2) ;STIL ^{OE} mice	Tam	DMBA	TPA	30
K14 ^(CreERT2) ;STIL ^{fl/wt} ;P53 ^{R172H/wt} mice	Oil	DMBA	TPA	6
K14 ^(CreERT2) ;STIL ^{OE} ;P53 ^{dn} mice	Tam	DMBA	TPA	21

2.1.3. STIL^{OE} transgenic mice

The transgenic STIL^{fl/fl} B6-STIL mouse line was crossed with the CMV-Cre mouse line (human cytomegalovirus promoter Cre-deleter line) to generate hemizygous;heterozygous CMV-Cre;STIL^{lox/wt} mice that overexpress murine STIL (STIL^{OE}) under the transcriptional control of the ubiquitous Rosa26 promoter after Cre-recombinase-mediated excision of an upstream STOP cassette (Fig. 7). CMV-

Cre;STIL^{lox/wt} mice were subsequently back-crossed to STIL^{fl/fl} mice to obtain hemizygous;homozygous CMV-Cre;STIL^{lox/lox} mice. These mice were continuously examined and monitored for apparent developmental defects and spontaneous tumor growth over a period of 23 months. They were also under official burden assessment as our lab is the first to establish this genetically altered mouse without previously published data for it. In the burden assessment, the mice were examined at birth for body color, activity, weight, and size. At weaning, at two months of age, and then every three months mice were examined for the following points: nutritional status, body posture, behavior and motor skills, fur and body openings, reaction to handling, and weight.

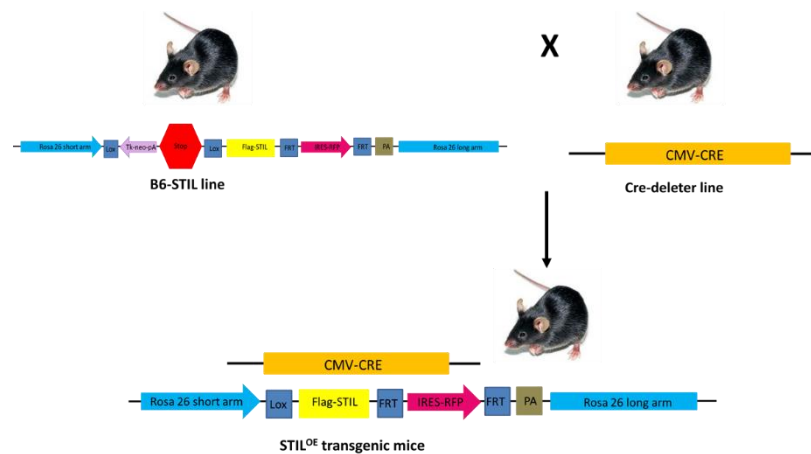


Figure 7: Generation of STIL^{OE} mice. STIL^{OE} transgenic mice overexpress murine STIL under the transcriptional control of the ubiquitously expressed Rosa26 promoter upon Cre-mediated excision of an upstream STOP cassette.

2.1.3.1. STIL^{OE} MEFs

The same breeding strategy as described for STIL^{OE} mice was used to generate primary heterozygous and homozygous STIL^{OE} MEFs (CMV-Cre;STIL^{lox/wt} and CMV-Cre;STIL^{lox/lox}). The males and females were bred for three days. Vaginal plug control was carried out daily. In positive animals, this is considered E0.5 (embryonic developmental day). At E12.5, the pregnant females were sacrificed, and the embryos were isolated. Embryo heads were used for genotyping, while the MEFs were prepared from the body (Fig. 8). The body was trypsinized at 4°C overnight with shaking. At the next day, the resulting suspension was plated in DMEM supplied with fetal calf serum (FCS) 10%, Pen/Strep 1% and 1% MEM Non-Essential Amino Acids Solution (100x). The cells were passaged once reaching 70-80% confluence. Early passages (p1-p6) were used for qPCR analysis

and immunoblotting to determine the level of STIL overexpression at both mRNA and protein levels. In addition, cells were plated on coverslips to be processed for immunofluorescence staining to analyze for centrosome amplification. MEFs were used also for metaphase spread preparation and M-FISH analysis to detect chromosomal aberrations, as well as for live imaging, cell cycle analysis, proliferation, apoptosis, and senescence assays to analyze for abnormal mitoses, viability, and cell cycle distribution. The same procedure was performed with wildtype (WT) B6 mice and STIL^{fl/fl} and CMV-Cre embryos as controls.

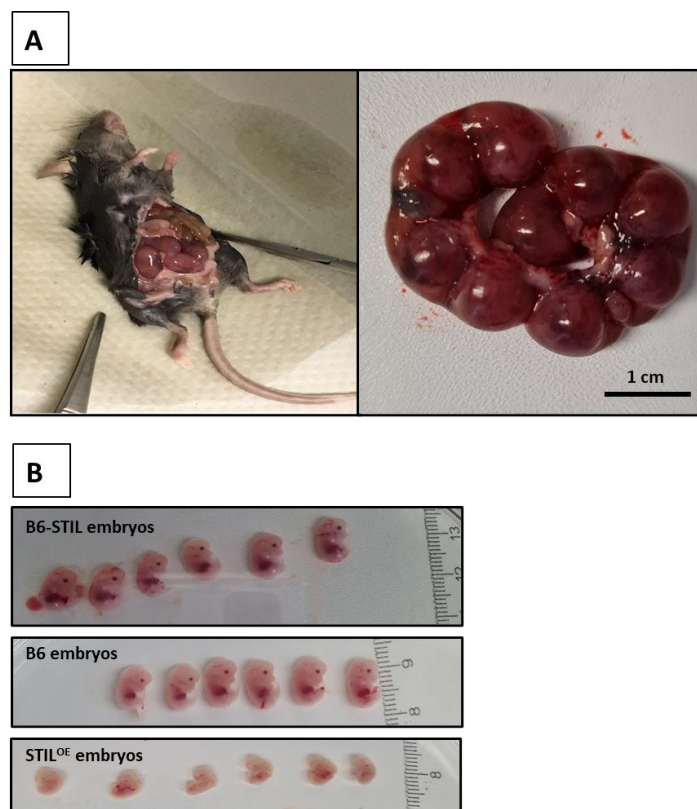


Figure 8: Generation of STIL^{OE} MEFs. (A) Pregnant female mouse at E12.5 showing multiple embryonic sacs in the uterus (left) and extracted uterus with embryonic sacs (right). (B) Embryos were extracted from the uterus under sterile conditions using 1x PBS to proceed to MEF preparation.

2.1.4. Epithelium-specific STIL^{OE} transgenic mice (K14^(CreERT2);STIL^{OE})

To generate mice with conditional STIL overexpression in K14-expressing epithelial cells, STIL^{fl/fl} mice were crossbred with K14^(CreERT2) mice to obtain K14^(CreERT2);STIL^{fl/wt} animals. The K14 promoter is active in stratified epithelia of skin, tongue, esophagus, fore-stomach, urinary bladder and mammary gland (Vassar et al., 1989). The K14^(CreERT2) system allows for the induction of transgene expression at selected times and sites, as CreERT2 encodes a fusion protein

between Cre recombinase and the tamoxifen-responsive hormone-binding domain of the estrogen receptor, leading to Cre activation only after tamoxifen administration, which in turn mediates excision of the STOP cassette, leading to conditional STIL overexpression in tissues with K14 promoter activity ($K14^{(CreERT2)};STIL^{OE}$) (Fig. 9). These mice were subsequently subjected to a skin carcinogenesis assay (Fig. 12) to analyze for the impact of STIL overexpression on chemically induced skin tumorigenesis.

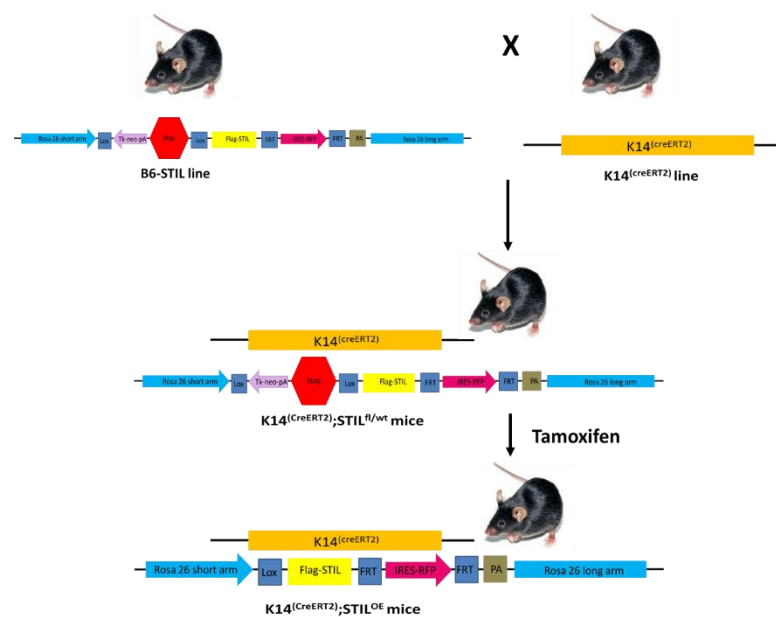


Figure 9: Generation of epithelium-specific STIL^{OE} transgenic mice ($K14^{(CreERT2)};STIL^{OE}$). STIL^{fl/fl} mice were bred with K14^(CreERT2) mice to obtain K14^(CreERT2);STIL^{fl/wt} mice, which overexpress murine STIL in skin epithelium after tamoxifen administration.

2.1.5. Epithelium-specific STIL^{OE} and TP53 inactivation transgenic mice (K14^(CreERT2);STIL^{OE};P53^{dn})

Conditional STIL overexpression with TP53 inactivation in K14-expressing epithelial cells was generated by breeding of K14^(CreERT2);STIL^{fl/wt} mice with P53^{R172H/wt} mice to get K14^(CreERT2);STIL^{fl/wt};P53^{R172H/wt} animals. Upon tamoxifen administration, Cre is activated in K14-expressing tissues leading to STOP cassette excision from both the *Stil* and *Tp53* constructs, leading to conditional STIL overexpression and TP53 inactivation in tissues with K14 promoter activity (K14^(CreERT2);STIL^{OE};P53^{dn}) (Fig. 10). These mice were used in the skin carcinogenesis assay to investigate the effects of STIL overexpression on skin tumor formation in the absence of TP53.

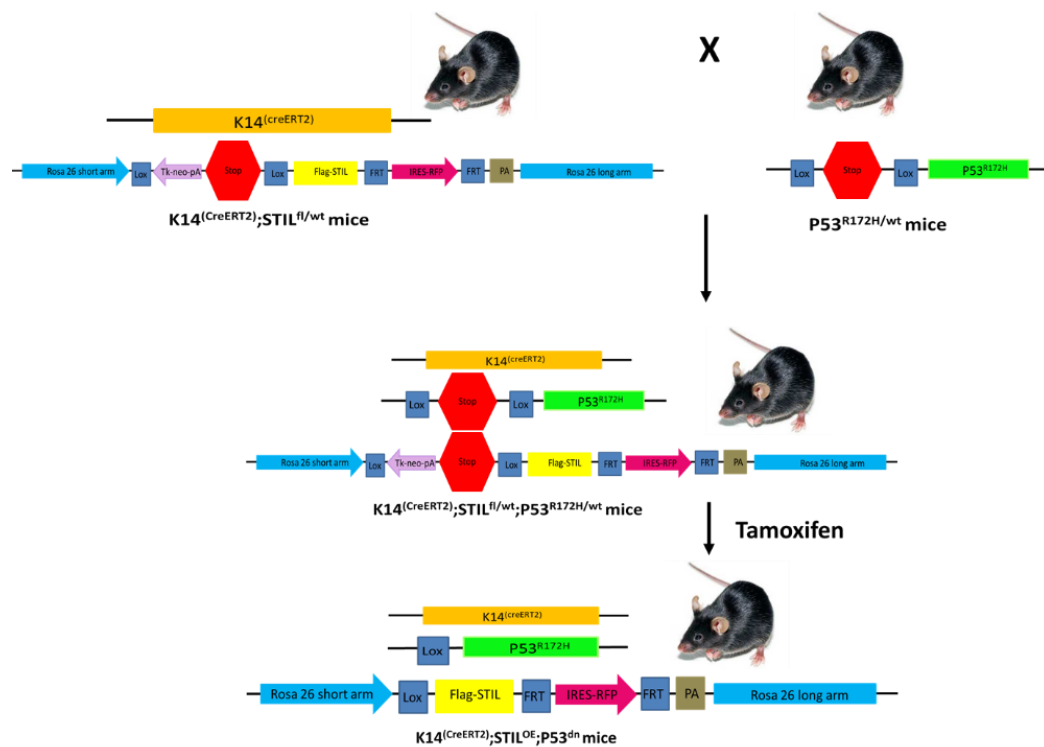


Figure 10: Generation of epithelium-specific STIL^{OE} and p53 inactivation transgenic mice (K14^(CreERT2);STIL^{OE};P53^{dn}). K14^(CreERT2);STIL^{fl/wt} mice were crossed with P53^{R172H/wt} mice to get K14^(CreERT2);STIL^{fl/wt};P53^{R172H/wt} mice, which overexpress STIL with inactivation of p53 in epithelia upon tamoxifen administration.

2.2. Skin carcinogenesis assay, Two-stage chemically induced cancer model

Skin cancer, as well as many cancer forms, develops through a multistage process, starting with induction of Ras mutations, followed by activation of cell proliferation by EGFR, Stat3, Akt and later *TP53* mutations. This occurs due to exposure of cells to a carcinogen/mutagen, an agent that leads to cancer initiation, then to a promoter that leads to cancer promotion (Brabletz et al., 2005; Hanahan and Weinberg, 2000; Kemp, 2005; Pitot and Dragan, 1991).

Many additional environmental and genetic factors may modify skin cancer formation, but their exact effects are not clearly known. The mouse skin carcinogenesis assay allows to *in vivo* analyze the effect of these factors on the course of epithelial carcinogenesis. This is done by (i) applying a standard controlled protocol for induction of skin carcinogenesis and (ii) to analyze the effect of additional factors on the modification of skin cancer initiation, promotion, and progression.

The effects of gene modifications in this assay can be studied in genetically modified mice by using the inducible tamoxifen Cre-ERT-LoxP recombination system (Abel et al., 2009; Chen and Roop, 2008; DiGiovanni, 1992; Feil et al., 1996; Wilker et al., 2005).

The skin carcinogenesis assay consists of two stages, tumor initiation and tumor promotion. Initiation is done by application of a mutagen such as 7,12-Dimethylbenz[a]anthracene (DMBA), one small dose applied topically over the mouse back skin (Sung et al., 2005), which targets the keratinocyte stem cell in the basal cell layer of the interfollicular epidermis and in the hair follicle bulge region. DMBA typically induces mutations in *Hras* and *Kras* by transversion of A to T in *Hras*, codon 61. This mutation can be detected three to four weeks post treatment and later on in most formed papillomas (Abel et al., 2009; Balmain et al., 1984; Brown et al., 1990; DiGiovanni, 1992; Morris, 2004; Nelson et al., 1992).

In the second stage, a tumor promoting drug such as 12-O-Tetradecanoylphorbol-13-acetate (TPA) is frequently topically applied leading to promotion of the mutated stem cells by activating protein kinase C (PKC) signal transduction inducing cell growth, proliferation, differentiation proteins and DNA synthesis

(Blumberg, 1980; Castagna et al., 1982; Fukushima et al., 2016; Fürstenberger et al., 1981; Lii et al., 2016; Rebois and Patel, 1985) to finally form tumors/papillomas, defined as finger-like outward hyperplastic epidermal cell projections covered with thick keratinized layers, starting at about six weeks after initiation of TPA treatment (DiGiovanni, 1992; Hennings et al., 1987; Kangsamaksin et al., 2007; Kemp, 2005; Leedham and Wright, 2008; Trempus et al., 2007; Yuspa et al., 1982). TPA also stimulates reactive oxygen species (ROS) production leading to inflammation with increased production of growth factors, ending with thick skin due to hyperplasia of the epidermis (Abel et al., 2009; DiGiovanni, 1992).

Papillomas can progress to invasive squamous cell carcinomas (SCC) 5-12 months after TPA treatment depending on the genetic background of the mouse; for example, it is more frequent in FVB mice compared to BALB/c mice and also depending on the target gene effect in the transgenic mice (Hennings et al., 1993). SCCs are nests of squamous epidermal cells surrounding a keratinized center infiltrated in dermis. SCC cells harbor *Tp53* mutations, chromosomal abnormalities as trisomy of chromosomes 6 and 7 and aneuploidy (Aldaz and Conti, 1989; Aldaz et al., 1989; Conti et al., 1986; Ruggeri et al., 1991).

Tamoxifen is used in genetically modified experimental animals to induce gene expression conditionally and selectively in specific tissues within the Cre-LoxP recombination system. This is important to investigate the conditional effect of knocking out or knocking in of genes, which cannot be ubiquitously expressed due to the induction of life-threatening abnormalities. Using this methodology, tamoxifen interacts with an estrogen receptor with a mutant ligand binding domain fused to Cre recombinase, which in turn is fused to a tissue-specific promoter. This leads to tissue-specific Cre expression and subsequent recombination of LoxP sites flanking the gene of interest. In our K14^{creERT2} mice (Fig. 11), the Cre recombinase is expressed under the control of a Keratin 14 (K14) promoter upon treatment with tamoxifen in tissues with an active K14 promoter as in stratified epithelium of skin, tongue, esophagus, fore-stomach, urinary bladder, and mammary gland epithelium (Amen et al., 2013; Feil et al., 1996; Vassar et al., 1989).

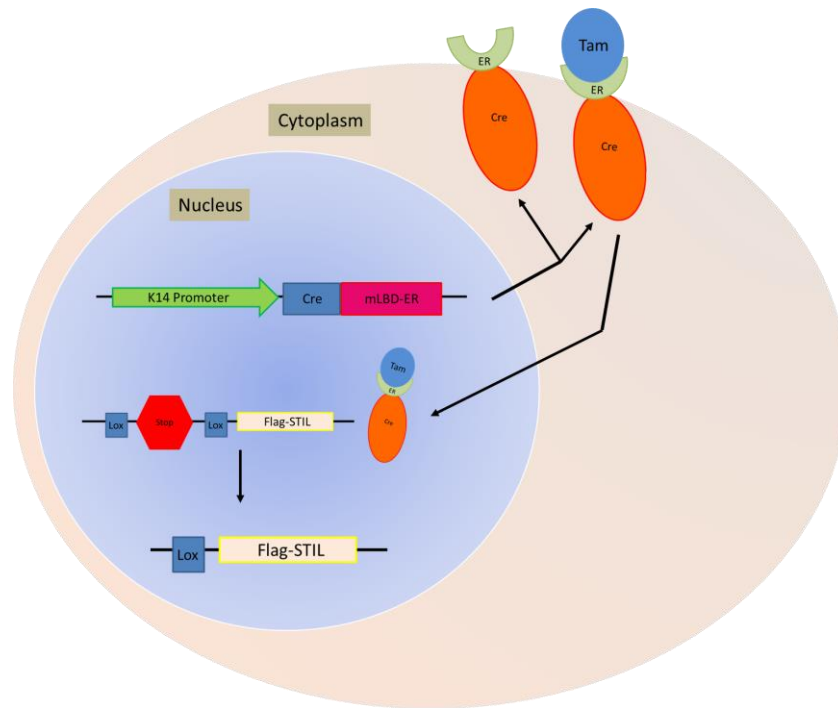


Figure 11: Tamoxifen-K14^(CreERT2)-regulated STIL overexpression system. Tissues with K14 promoter expresses Cre recombinase, which is fused to a mutant ligand binding domain estrogen receptor (mLBD-ER). This protein, CreER, is restricted to the cytoplasm until complexed with tamoxifen. Then tamoxifen-CreER translocates to the nucleus, where Cre recombinase mediates excision of the STOP cassette, leading to conditional STIL overexpression in tissues with K14 promoter activity.

2.2.1. Skin carcinogenesis assay of tamoxifen-inducible epithelium-specific STIL^{OE} mice with and without TP53 inactivation

To examine the effect of STIL overexpression (K14^(CreERT2);STIL^{OE}) and STIL overexpression in combination with TP53 inactivation (K14^(CreERT2);STIL^{OE};P53^{dn}) on skin tumor development, K14^(CreERT2);STIL^{fl/wt} and female K14^(CreERT2);STIL^{fl/wt};P53^{R172H/wt} mice were induced by tamoxifen (Tam). As controls the same genotypic groups treated with vehicle (Oil) were used (Table 23). Tam was freshly prepared and administrated intraperitoneally to five-weeks old mice (Fig. 12 A and B). Four Tam doses were given within two weeks. One dose per mouse was 1 mg Tam/100 μ l 10% ethanol in sunflower seed oil. It was prepared as follows: 1 mg of Tam powder was dissolved in 10 μ l of 100%, highest purity ethanol using an ultrasonic water bath at 37°C for 2 minutes. Then, 90 μ l of sterile sunflower oil was added and completely dissolved by the help of 37°C ultrasonic water bath for 5 minutes. Each of the control mice was injected with 100 μ l of 10% ethanol in sunflower seed oil (Table 23).

Table 23: Dose and frequency of compound application

Compound	Dose per mouse	Frequency	Age of mouse
Oil	100 μ l of 10% ethanol in sunflower seed oil	Twice a week	5th and 6th week
Tam	1 mg Tam/100 μ l 10% of ethanol in sunflower seed oil	Twice a week	5th and 6th week
DMBA	400 nMol DMBA/100 μ l acetone	Once	7th week
TPA	10 nMol TPA/100 μ l acetone	Three times a week	8th - 28th week

At the age of 7 weeks, a single cutaneous DMBA dose was applied to the shaved back skin of the mice by spraying. After one week, TPA was administered three times weekly by spraying for 20 weeks to promote tumor development. TPA induces irritation (chronic epidermal hyperplasia) that, in combination with mutations induced by DMBA, results in the development of papillomas, which start in control mice by 6-8 weeks of promotion, eventually converted to SCC starting by 20 weeks from promotion in control animals. Mice weight and tumors were scored weekly by counting those that reached a diameter of 1 mm or greater and are constantly present. Two weeks after the end of TPA administration, mice were photographed and sacrificed by cervical dislocation. Samples from papillomas, skin, tongue, esophagus, fore-stomach, kidney, liver, and urinary bladder were collected for qPCR, genotyping, immunofluorescence staining, Western blotting, and histological examination. Each organ was sampled in three portions to be used for the mentioned experiments. One portion was directly frozen in liquid nitrogen and stored in -80°C , another one was fixed in paraformaldehyde for preparing Formalin-fixed paraffin embedded (FFPE) blocks, and the third one was cryopreserved in Tissue-Tek® O.C.T.™ Compound for tissue cryosectioning. This experiment was performed in collaboration with the Dr. Karin Müller-Decker group at DKFZ.

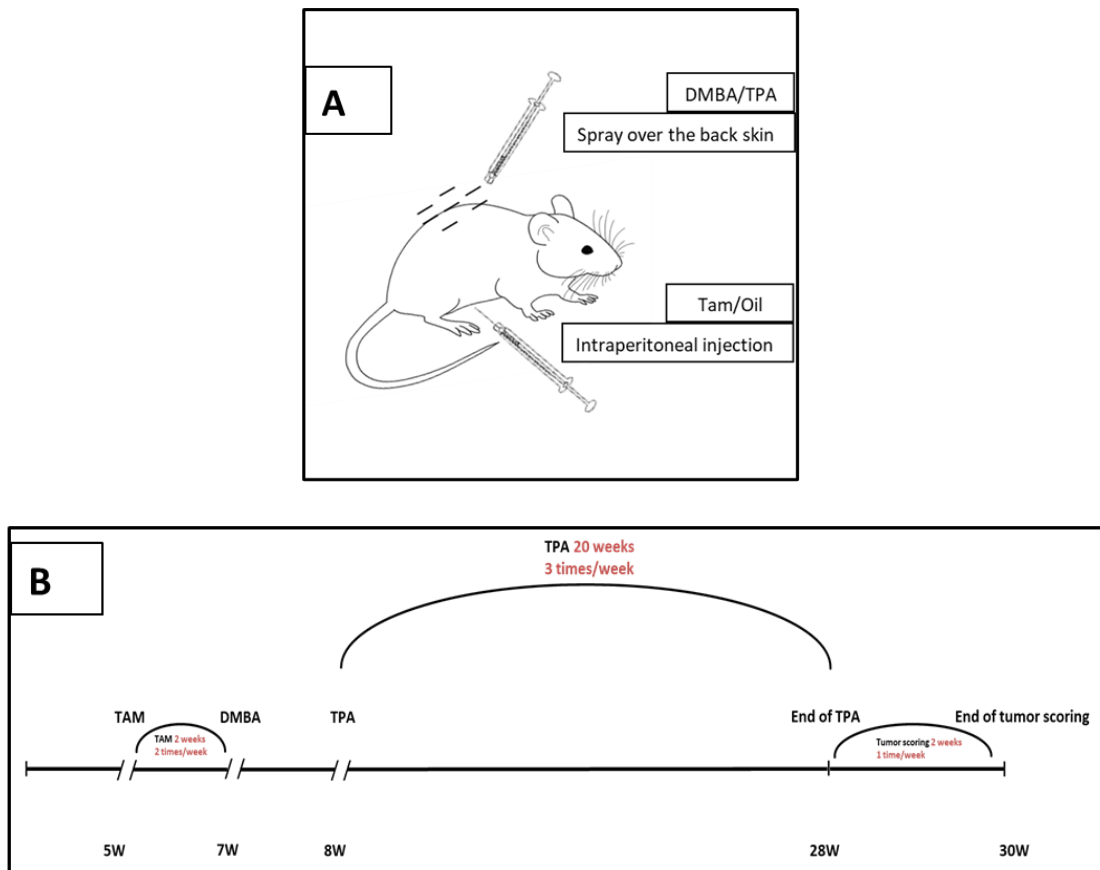


Figure 12: Tam/Oil, DMBA and TPA route of administration and timeline. A) Routes of administration for the different compounds. B) Diagram showing the timeline of DMBA and TPA administration.

2.2.2. Genotyping and polymerase chain reaction analysis (PCR)

DNA was isolated using the SampleIN™ Direct PCR Kit and AllPrep DNA/RNA/Protein Mini Kit from ear punches (EP), the head of the embryos, and MEFs of the corresponding embryos, tumors, papillomas and different mouse tissues. ALLin™ HS Red Taq Mastermix was used according to the manufacturer's protocol. CMV-Cre, STOP cassette, Rosa, K14, P53 nonrec, Rosa-STIL (STIL-rec) and P53-rec primers were used as indicated (Fig. 13). Katharina Sack and Jana Schairer helped in genotyping.

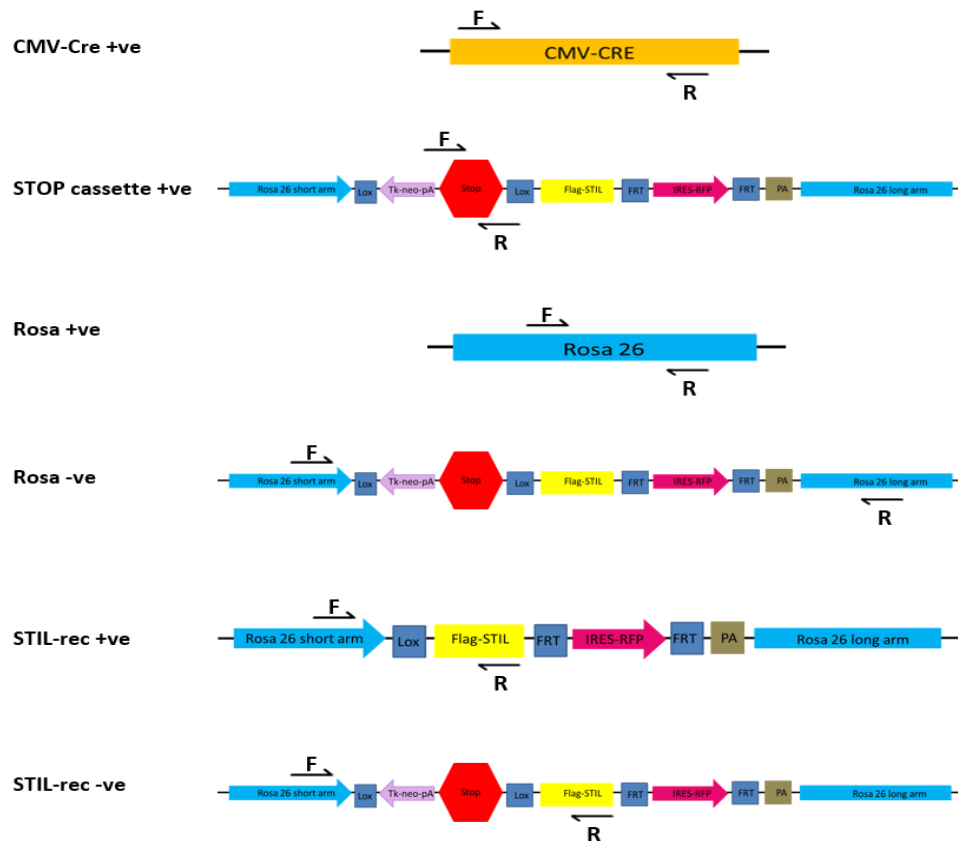


Figure 13: Primer binding sites for genotyping showing forward (F) and reverse (R) primers binding sites, +ve = indicates successful presence of PCR product represented by a band, -ve = indicates unsuccessful presence of PCR product (no band).

The amplification conditions used for each primer in a FlexCycler2 PCR Thermal Cycler (Analytik Jena AG, Germany) were:

<p>STIL-STOP-ROSA</p> <ul style="list-style-type: none"> • 95 °C 03 min • 95 °C 30 sec • 58 °C 30 sec x30 • 72 °C 01 min • 72 °C 05 min • 04 °C Pause 	<p>CMV-Cre</p> <ul style="list-style-type: none"> • 95 °C 03 min • 95 °C 30 sec • 63 °C 45 sec x30 • 72 °C 01 min • 72 °C 05 min • 04 °C Pause 	<p>STIL-rec</p> <ul style="list-style-type: none"> • 95 °C 03 min • 95 °C 30 sec • 53 °C 30 sec x30 • 72 °C 01 min • 72 °C 05 min • 04 °C Pause
<p>K14</p> <ul style="list-style-type: none"> • 95 °C 03 min • 95 °C 45 sec x35 • 58 °C 30 sec • 72 °C 01 min • 72 °C 05 min • 04 °C Pause 	<p>P53-nonrec</p> <ul style="list-style-type: none"> • 95 °C 03 min • 95 °C 15 sec x35 • 61 °C 15 sec • 72 °C 20 sec • 72 °C 05 min • 04 °C Pause 	<p>P53-rec</p> <ul style="list-style-type: none"> • 94 °C 03 min • 94 °C 01 min x30 • 60 °C 02 min • 72 °C 02 min • 72 °C 05 min • 04 °C Pause

2.2.3. RNA isolation and qPCR analysis

2.2.3.1. MEF qPCR analysis

RNA was isolated using the RNeasy Mini Kit. The RNA concentration was measured using the NanoDrop™ 2000 Spectrophotometer (PeqLab Biotechnologie Erlangen), 500 or 1000 or 2000 ng of RNA was reverse transcribed using the QuantiTect Rev. Transcription Kit according to the manufacturer's protocol. Real-time RT-PCR was performed using the Quantitect SYBR Green PCR kit. *Stila* primers were used for amplification of the target gene, and HPRT and PIPB were used as reference genes, respectively. RT-PCR was performed in a LightCycler® 480 Instrument with the settings given in Table 24. Relative quantification has been done by compensating the values of reference genes and target gene in the double delta cycle threshold equation ($2^{-\Delta\Delta CT}$ method).

2.2.3.2. Mouse tissue qPCR analysis

Different tissues were homogenized using TissueLyser II (Qiagen, Cat. No. 85300) and Stainless-Steel Beads, 5 mm (Qiagen, Cat. No. 69989). RNA was isolated using the AllPrep DNA/RNA/Protein Mini Kit according to the manufacturer's protocol. *Stilc* primers were used for amplification of the target gene, and HPRT and PIPB were used as reference genes, respectively.

Table 24: LightCycler® 480 Instrument settings for *Stil* qPCR.

Programme name	Cycles	Hold (hh:mm:ss)	Target (°C)	Acquisition mode
Preincubation	1	00:15:00	95	None
Programme name	Cycles	Hold (hh:mm:ss)	Target (°C)	Acquisition mode
Amplification	45	00:00:15	94	None
		00:00:30	55	None
		00:00:30	72	Quantifications-Single
Programme name	Cycles	Hold (hh:mm:ss)	Target (°C)	Acquisition mode
Melting Curve	1	00:00:05	95	None
		00:01:00	65	None
		00:00:00	97	Continuous
Programme name	Cycles	Hold (hh:mm:ss)	Target (°C)	Acquisition mode
Cooling	1	00:00:30	40	None

2.2.4. Copy number variation (CNV) analysis by whole genome sequencing

Genomic DNA from healthy spleen and lymph node tumors of control and STIL^{OE} mice was extracted using the All Prep DNA/RNA/Protein Mini Kit according to the manufacturer's protocol. Prior to that a homogenization step using TissueLyser II (Qiagen, Cat. No. 85300) and Stainless-Steel Beads, 5 mm (Qiagen, Cat. No.

69989) was performed. Low coverage whole genome sequencing (WGS) was then performed by the DKFZ - High Throughput Sequencing core facility, where sample libraries were prepared, and sample quality was controlled. WGS was done using HiSeq 4000 Paired-End 100bp / Nano DNA (Illumina). The resulting raw sequences were in FASTQ format, which then were transferred to the DKFZ - ODCF (Omics IT and Data Management Core Facility) to be processed and aligned to the mouse reference genome as .bam files, followed by further analysis for copy number variations (CNV) with the help of Agnes Hotz-Wagenblatt, Dennis Friedel, Daniel Schrimpf, Damian Stichel and Timothy Wohlfromm, all at DKFZ.

2.3. *In vitro* cell culture

Cell lines were cultured in cell culture dishes or flasks with appropriate growth medium and incubated with 5% CO₂ at 37°C. Cell lines were periodically tested for mycoplasma infection.

2.3.1. Immunoblotting

Protein lysates were prepared as follows: DMEM medium was removed and cells in the cell culture plate were washed twice with cold 1x PBS. 200-400 µl of RIPA buffer or CEB buffer freshly supplied with PhosStop™ and cOmplete™ (phosphatase and protease inhibitors) was added on the plate on ice. Cells in RIPA or CEB buffer were scrapped and incubated for 20 minutes on ice with frequent gentle tapping on the tube. Samples were centrifuged for 20 minutes at 10000 rpm at 4°C. The supernatant was transferred into precooled tubes. Protein concentration in the lysates was measured using the Bradford assay by mixing 1 µl of lysate in 1 ml Quick Start™ Bradford dye and measuring by spectrophotometry at 595 nm absorbance. Lysates were mixed with 5x Laemmli sample loading buffer and incubated at 95°C for 10 minutes. Equal amounts of protein (100-200 µg) were loaded into a 10% acrylamide gel according to the protocol by Thomas and Kornberg (Thomas and Kornberg, 1975) to perform protein electrophoresis separation at 120 V for 90 minutes. Semidry transfer of protein from the 10% acrylamide gel to a nitrocellulose membrane was done using a Trans-Blot Turbo Transfer™ device according to the manufacturer's protocol. The membrane was blocked with blocking buffer for one hour at room temperature with gentle shaking. Then, a primary antibody in blocking buffer was added and incubated with gentle shaking at 4°C overnight, followed by three times 1x TBST washing (five minutes

each). HRP-linked IgG secondary antibody in blocking buffer was added and incubated for one hour at room temperature followed by three times 1x TBST washing (five minutes each). Then, the membrane was developed by five minutes incubation with Clarity™ ECL Western Blotting Substrate. The ChemiDoc™ Touch Imaging device was used for signal detection. Image processing was done using Image Lab software.

2.3.1.1. Validation of anti-STIL antibody in immunoblotting

2.3.1.1.1. Human osteosarcoma cell line (U2OS-eGFP-STIL)

U2OS-eGFP-STIL cells contain a T-Rex-inducible system (Cosenza, 2015). Addition of 4 µg/ml tetracycline to the culture medium (DMEM supplied with FCS 10%, Pen/Strep 1%, 1.5 µg/mL Puromycin and 100 µg/mL Hygromycin B) for 72h leads to eGFP-STIL expression. Protein lysates from tetracycline-induced-eGFP-STIL^{OE}-U2OS cell was prepared as described above.

2.3.1.1.2. STIL protein knockdown by siRNA transfection in MEFs

3 x 10⁵ STIL^{OE} MEFs were plated in 6-well plates and transfected with 25 or 50 nM ON-TARGETplus Mouse *Stil* siRNA–SMARTpool in Opti-Mem medium and Lipofectamine RNAiMAX according to the manufacturer's protocol for 24h. At the next day, the transfected medium was replaced with DMEM supplied with FCS 10%, Pen/Strep 1%, 1% MEM Non-Essential Amino Acids Solution (100X) and incubated for another 24h. After that, the cells were collected and analyzed for the knockdown efficiency with immunoblotting.

2.3.1.1.3. *In vitro* STIL protein overexpression by CMV-Flag-*Stil* plasmid transfection in wildtype MEFs

- a) Cloning of amplified Flag-*Stil* construct from D059.1 TV vector into pcDNA3.1(-) plasmid (CMV plasmid) (Fig. 14)

Flag-*Stil* construct vector was amplified by cloning in *E. Coli* DH5α through heat shock transformation. This is done by adding 5 µl of the vector to 100 µl of competent *E. Coli* DH5α bacteria on ice then incubated for 30 minutes. Followed by heat shock at 42°C for 45 seconds, quickly replacing it again on ice for 2 minutes. Then, incubating it in 900 µl of SOC medium at 37°C with shaking for 1h. Then, the SOC medium with bacteria is plated on LB-agar supplied with carbenicillin to allow the transformed resistant colonies to grow by overnight incubation at 37°C.

After that the colonies were transferred to LB-medium supplied with carbenicillin and incubated at 37°C with shaking overnight. The same was done to the empty pcDNA3.1(-) plasmid. Plasmid DNA was extracted using QIAGEN Plasmid Mini Kit according to the manufacturer's protocol. Its concentration was measured by NanoDrop™ 2000 Spectrophotometer.

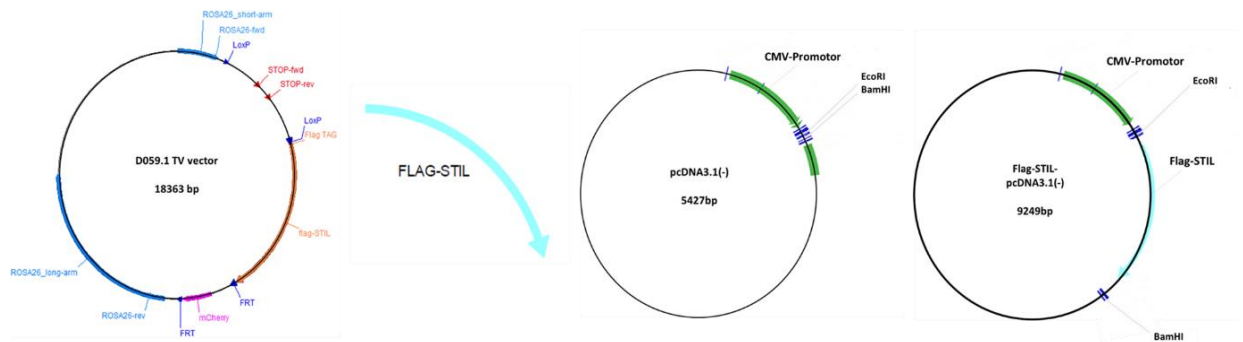


Figure 14: Cloning of amplified Flag-*Stil* construct. The Flag-*Stil* construct was amplified from the D059.1 vector and ligated into the pcDNA3.1(-) plasmid.

Flag-*Stil* construct was amplified from the Flag-*Stil* vector in PCR using Phusion® High-Fidelity DNA Polymerase according to the manufacturer's protocol and the target primers were designed to have EcoRI and BamHI (restriction enzymes) on the peripheries of the primers EcoRI_Flag_*Stil*_fwd (CATGAATTCATGGGGGGTTCTGACTACAA) and BamHI_*Stil*_rev (ATCGGATCCTTAAAATAACTTAGGTA ACT). Amplified PCR product were analysed by 1% agarose gel electrophoresis and visualized using UV light.

Empty pcDNA3.1(-) plasmid and EcoRI_Flag_*Stil*_BamHI PCR product were digested with BamHI and EcoRI restriction enzymes according to manufacturer's protocol. To prepare for ligation a dephosphorylation step is needed, using SAP for 30 minutes at 37°C. Then loaded on 1% agarose gel electrophoresis to detect the digestion product size then purified using High Pure PCR Product Purification Kit according to the manufacturer's protocol. Ligation was done using different ratios of digested, phosphorylated pcDNA3.1 (-) plasmid and Flag-*Stil* PCR products in addition of NxGen T4 DNA Ligase according to the manufacturer's protocol (Fig. 14). Followed by amplification of the ligated plasmid by cloning in *E. Coli* DH5 α through heat shock transformation as described above. Plasmid purification then was done using both of QIAprep Spin Miniprep Kit and QIAGEN Plasmid Maxi

Kit according to manufacturer's protocol. A sample of the ligated plasmid was screened by loading the cleaved Flag-*Stil*-pcDNA3.1(-) with restriction enzyme on 1% agarose gel electrophoresis to detect the product size of the cleaved plasmid. Then, samples of the purified plasmid were sent to Eurofins Genomics - GATC services for Sanger sequencing for precise sequence confirmation of Flag-*Stil* using the designed primers in Table 25.

Table 25: Primers for Flag-*Stil* Sanger sequencing

Name	Sequence (5' - 3')
1_fwd	GTGAAGCCTATCCCCATTA
2_fwd	TGATTAAGCCATCCCAGCC
3_fwd	TCAAGTAGCCCTGTTAGCA
4_fwd	CCAACAGCTCTTCAGAGCA
5_fwd	AGTGAAAACCAGCTGTCAC
6_fwd	GACGGATCGGGAGATCTCC
7_fwd	CCCATTGACGCAAATGGGC
8_fwd	GGATCCGAGCTCGGTACCA
9_fwd	ATGTGTGTCAGTTAGGGTG
10_fwd	CCAGGCTCAAGGCGCGCAT
11_fwd	CTCAAAGGCGGTAATACGG
12_fwd	TCTATTTTCGTTTCATCCATA
13_fwd	GCATAATTCTCTTACTGTC
14_fwd	CAAATAGGGGTTCCGCGCA
15_fwd	ACCATGGTGATGCGGTTTT

b) Transfection of the CMV-Flag-*Stil* plasmid in wildtype MEFs

2×10^5 wildtype MEF cells were plated in 6-well plates and, after reaching 60% confluency, transfected using the following medium: 2 μ g or 4 μ g of Flag-*Stil*-pcDNA3.1(-) DNA was mixed in 50 μ l Opti-Mem at room temperature for five minutes. Lipofectamine 2000 was mixed by vortexing in 50 μ l Opti-Mem for 5 minutes and then mixed with DNA/Opti-Mem for 20 minutes at room temperature. Finally, the mixture was added to 1900 μ l DMEM supplied with FCS 10%, without antibiotics. Each well received 2 ml of the transfecting medium and was incubated for 24h. At the next day, the transfection medium was replaced with DMEM supplied with FCS 10%, Pen/Strep 1%, 1% MEM Non-Essential Amino Acids Solution (100X) and incubated for another 24h. After that the cells were collected by cell scrapping and protein lysates were prepared for immunoblotting.

2.3.2. Immunofluorescence staining (IF)

2.3.2.1. MEF IF staining

10^5 MEF cells were plated in 35 mm cell culture dishes with four cover slips and cultured for 24h. To preserve cell structure and MTs during immunostaining 1x PHEM with 0,5% Triton-X-100 buffer for five minutes applied to the cover slides were used followed by -20°C cold (Methanol and Acetone) fixative solution for seven minutes. Permeabilizing solution was added for five minutes. Then, the cover slips were washed twice with 1x PBS and blocked in blocking buffer for 30 minutes. Incubation of primary antibody in blocking buffer for one hour was followed by three times 1x PBS washing (five minutes each). Then, the secondary antibody and Hoechst 33342 to stain the DNA (1:1000) in 1x PBS were added for 30 minutes followed by three times 1 x PBS washing (five minutes each), five minutes distilled water washing , 30 seconds absolute ethanol incubation and air drying. Vectashield mounting medium was used to mount the cover slides. Nail polish was used to fix the cover slip on the slide.

Slides were examined using an oil 63x objective and a Zeiss Cell Observer Z1 fluorescence microscope supplied with an AxioCam MRm camera (Carl Zeiss, Germany). 45 Z-stacks at each position with $2.4\ \mu\text{M}$ intervals were acquired. The ZEN 3.2 (Blue edition) and ImageJ (Fiji) softwares were used for image analysis.

2.3.2.2. Mouse tissue IF staining

8-10 μm cryo-sections were IF stained as follows: thawing the -80°C stored frozen slide by incubation at room temperature for at least one hour was followed by five minutes washing in 1x PBS, addition of 1x PHEM with 0,5 % Triton-X-100 buffer for five minutes, followed by washing twice in PHEM buffer without Triton and then fixation by -20°C cold (Methanol and Acetone) fixative solution for seven minutes or 4% PFA fixation for 15 minutes. Then, the slides were air dried and circle drawn around each tissue section by Pappen, washed for two minutes in 1x PBS followed by permeabilizing solution incubation. The IF staining procedure and microscopy procedure was performed as described for MEFS above in addition to final step using Vector® TrueVIEWWT Autofluorescence Quenching Kit according to the manufacturer's protocol to eliminate tissue autofluorescence. The Zeiss Cell Observer Z1 fluorescence microscopy with ZEISS Apotome 2 was used for slide examination.

2.3.3. Metaphase spreads and multiplex fluorescence in situ hybridization (M-FISH) analysis

Metaphase spreads were prepared when MEFs reached 70-80% confluency. 10 µg/ml colcemid were added and incubated for five hours at 37°C. Cells were collected and treated with 37°C pre-warmed hypotonic solution for 20 minutes, centrifuged for 10 minutes at 1200 rpm, followed by fixation using ice cold fixative solution. This step was repeated three times. Fixed MEF cells were stored at -20°C until preparation for M-FISH, in collaboration with Brigitte Schoell and Prof. Dr. Anna Jauch (Human Genetics Institute, Heidelberg University Hospital). 20 metaphase spreads were examined from three different embryos of both STIL^{OE} and wildtype MEFs to detect chromosome aberrations.

2.3.4. Proliferation assay

Proliferation was evaluated daily for five consecutive days using passage 3 WT and STIL^{OE} MEFs by 2 methods: (i) Trypan blue staining with automated cell counting using a TC20™ counter that was done with Katharina Sack's help, and (ii) PrestoBlue™ Cell Viability Reagent staining using a Spark microplate reader (Tecan). For the trypan blue staining, 10⁴ cells were plated per 1 cm² growth area of cell culture plate, each MEF line in triplicate. Every 24h, the cells in each well were trypsinized and counted. For the PrestoBlue™ method, 3 x 10² cells per well were seeded in a 96 well plate, each MEF line in triplicate, and supplemented with 99 µl culture medium and 1 µl PrestoBlue™. The plate was incubated at 37°C and 5% CO₂.

2.3.5. Cell cycle analysis

2 x 10⁵ MEF cells in 250 µl 1x PBS with 1% FCS were fixed with 700 µl cold methanol added dropwise with slow vortexing and then incubated for one hour at 4°C. Next, cells were washed with 1x PBS with 1% FCS followed by incubation with 200 µl 1x PBS with 30 µg/ml RNase A for 30 minutes at 37°C. Then, 1 µg/ml propidium iodide (PI) was added for 10 minutes followed by flowcytometry analysis using an Accuri C6 (BD Biosciences) device. 15000 events were counted by FSC/SSC-area with no exclusion of debris and apoptotic cells. Doublets were excluded on the PI plot (width vs area). Cell cycle analysis was done using FlowJo software.

2.3.6. Apoptosis assay

10^5 cells in 20 ml medium per T75 flask of WT and STIL^{OE} MEF lines were plated, one flask for each line, then incubated for seven days and one day before analysis fresh 10 ml of DMEM supplied with fetal calf serum (FCS) 10%, Pen/Strep 1% and 1% MEM Non-Essential Amino Acids Solution (100x) were added to the existing medium. As positive control one WT MEF was trypsinized and treated with 4% PFA for 60 minutes on ice directly before analysis. Then each MEF line was trypsinized and stained with ApotrackerTM Green (Apo-15 peptide) and 7-AAD according to the manufacturer's protocol to detect apoptotic cells. Flowcytometry analysis was done using an Accuri C6 device.

2.3.7. Senescence-associated beta-galactosidase assay

10^5 cells of WT (n=2) and STIL^{OE} (n=3) MEFs were plated in each well of a 24 well plate, 3 wells for each. As positive and mock controls WT MEFs were treated with 100 nM paclitaxel and DMSO, respectively for 48h. After 48h, WT and STIL^{OE} MEFs were stained using the Senescence β -Galactosidase Staining Kit according to the manufacturer's protocol and eosin was used as a counter cytoplasmic staining to detect senescent cells. Images from each well were taken with a Zeiss Cell Observer Z1 fluorescence microscope using 10x objective magnification and a AxioCam MRc 5 color CCD camera. ZEN 3.2 (Blue edition) and ImageJ (Fiji) softwares were used for image analysis. Katharina Sack helped with the assay.

2.3.8. Histopathology staining

Mice were sacrificed by cervical dislocation. Tissues were collected and processed in two portions; one was cryopreserved using Tissue-Tek[®] O.C.T.TM Compound in a methylbutane bath over a liquid nitrogen container. The blocks were stored in -80°C until cryo-sectioning using a Leica CM1950 cryo-microtome (DKFZ- LMF (Light microscopy facility)). 8-10 μ m sections on superfrost slides were haematoxylin/eosin (H&E) stained as follows: fixation in 1% PFA for 10 minutes followed by washing in H₂O for two minutes. Haematoxylin staining was done for five minutes, followed by washing for one minute in tap water and rinsing in aqueous 0.1% hydrochloric acid for 15 seconds, 10 minutes washing under running tap water to remove the excess haematoxylin and then eosin staining for three minutes. Next, slides were dipped in H₂O three times followed by dehydration in

different ethanol dilutions: 75%, 95% and 100%, respectively, each for four minutes followed by 10 minutes incubation in Xylol and mounting of slides using Neo-Mount and cover sliding. Katharina Sack helped with staining and processing.

The second tissue portion was fixed for 24 h in paraformaldehyde, dehydrated in different concentrations of ethanol (70%, 85% and 100%), and incubated in Xylol. Each step lasted for 24 h. The tissues were then embedded in paraffin blocks. Five μm sections of paraffin blocks were prepared using a HM 355 S microtome and H&E staining were processed by Dr. Karin Müller-Decker's group.

H&E-stained slides were examined by a widefield Zeiss Axiophot microscope supplied with a AxioCam MRc 5 colour camera (DKFZ- LMF). ZEN 2011 lite (Blue edition), AxioVision and ImageJ (Fiji) softwares were used for image analysis.

3. Statistical analysis

Data were analysed with GraphPad Prism 8 Software using unpaired t-tests, additional tests are given in the figure legends. The data are presented as mean \pm standard deviation (SD). Experiments were performed in technical triplicates. Statistically significant differences are marked with asterisks, where (****) indicate a P value of less than 0.0001, (***) indicate $P < 0.001$; (**) indicate $P < 0.01$ and (*) indicates $P < 0.05$.

III. RESULTS

1. Generation of STIL^{OE} transgenic mice

To determine whether STIL overexpression causes spontaneous tumor formation *in vivo*, STIL^{OE} mice were generated by crossing B6-STIL line with a CMV-Cre-deleter line as described in 2.1.3. (Fig. 10). Parallely, MEFs were generated from STIL^{OE} mice as described in 2.1.3.1. (Fig. 11) and characterized to examine the STIL overexpression genotypically and phenotypically on the cellular level.

Interestingly, most of the first-generation offspring were B6-STIL (46/71 = 65%) and non-recombinant (non-rec) mice (16/71 = 22.5%), with only 9/71 (12.5%) heterozygous STIL^{OE} mice, which deviates from the expected Mendelian inheritance ratio for first-generation offspring that is 50% B6-STIL mice and 50% recombinant heterozygous STIL^{OE} mice table 27. Non-rec mice have inherited both CMV-Cre allele and one STIL^{fl/wt} construct (CMV-Cre; STIL^{fl/wt}), but without excision of stop cassette in the STIL construct over their whole life time, indicating insufficient Cre recombination as the CMV-Cre line is an X-linked transgenic mice table 1 (Chen et al., 2011). A second generation of mice was then generated by backcrossing of non-rec mice with the parental B6-STIL or CMV-Cre-deleter line (Table 27), which led to successful Cre recombination by excision of the STOP cassette and generation of homozygous (CMV-Cre; STIL^{lox/lox}) and heterozygous (CMV-Cre; STIL^{lox/wt}) STIL^{OE} mice (Fig. 15, A-C).

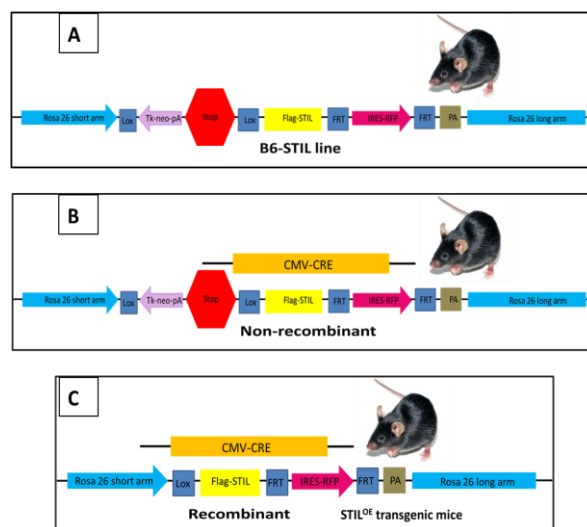


Figure 15: First-generation offspring. (A) B6-STIL mice contain a STOP cassette in front of Flag-*Stil* construct within Rosa locus in B6 mice. (B) In non-rec mice the Cre-recombinase activity was insufficient to delete the upstream STOP cassette leading to

genotypic and phenotypic similarities to B6-STIL mice. (C) In recombinant (Rec) heterozygous STIL^{OE} mice, Cre-recombinase has deleted the upstream STOP cassette leading to STIL overexpression.

Moreover, Cre recombination in heterozygous STIL^{OE} mice was variable. Some mice showed excision of the STOP cassette from all body cells leading to completely recombinant heterozygous STIL^{OE} (Ht_{com}) mice, while others showed only partial excision of STOP cassette from some body cells leading to partially/incompletely recombinant heterozygous STIL^{OE} mice (Ht_{inc}). On the other hand, homozygous STIL^{OE} mice were always only partially/incompletely recombinant (Hm_{inc}). Table 26 indicates the PCR genotyping features of mice using Rosa, STOP, CMV-Cre, and STIL-rec primers (Fig. 16).

Table 26: Mice groups genotyping features.

Mice	Rosa	STOP	CMV-Cre	STIL-rec
B6 (C57BL/6)	+	-	-	-
B6-STIL (STIL ^{fl/fl})	-	+	-	-
CMV-Cre-deleter line	+	-	+	-
Non-rec (CMV-Cre; STIL ^{fl/wt})	+	+	+	-
STIL ^{OE} (Hm _{inc}) (CMV-Cre; STIL ^{lox/lox})	-	+	+	+
STIL ^{OE} (Ht _{com}) (CMV-Cre; STIL ^{lox/wt})	+	-	+	+
STIL ^{OE} (Ht _{inc}) (CMV-Cre; STIL ^{lox/wt})	+	+	+	+

1.1. STIL overexpression reduces the incidence of spontaneous tumors in STIL^{OE} mice

Homozygous and heterozygous, with complete or incomplete STIL-transgene recombination, STIL^{OE} mice from the first- and second-generation offspring as well as control groups of B6-STIL and non-rec mice were monitored and continuously examined for tumor growth and apparent abnormalities over a period of 23 months. Necropsy was done by the age of 23 months. A significant decrease in the spontaneous tumor formation was found in STIL^{OE} mice (Fig. 16, A): A total of 17/37 (45.9%) control (B6-STIL (14/28 (50%) and non-rec mice (3/9 (33.3%)), but only 1/7 (14.3%) heterozygous STIL^{OE} mice and 2/11 (18.2%) homozygous STIL^{OE} mice harbored lymphomas characterized by swollen mesenteric and/or mediastinal lymph nodes (Fig. 16, B-I). Control B6-STIL mice additionally showed enlarged spleens due to malignant lymphoma (5/28 (18%)), which were detected in histopathologic microscopical examinations, and the rest (9/28 (32%)) had swollen lymph nodes. No other tumors than lymphomas were found in any other mice. The control group findings were in agreement with the published tumor incidence levels reported for wildtype B6 mice, for which (Brayton et al., 2012) found a 44.3% lymphoma and a 14.3% histiocytic sarcoma incidence rate.

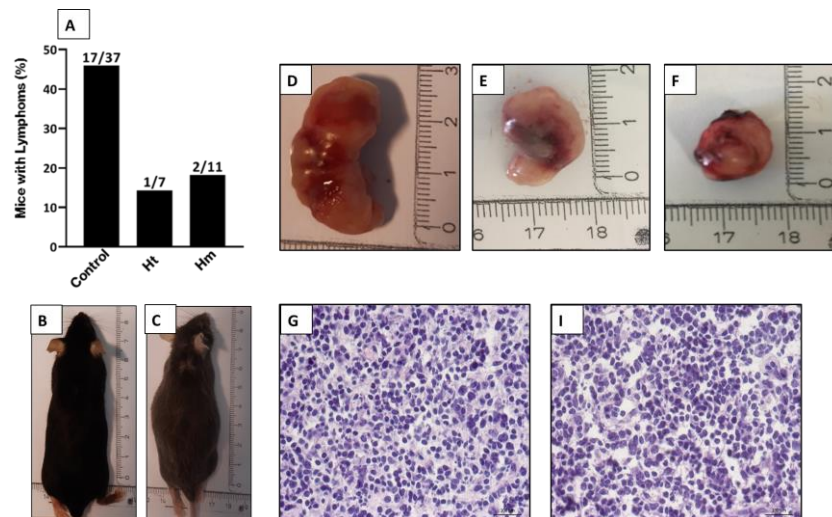


Figure 16: Spontaneous tumor formation. (A) Spontaneous lymphoma incidence in control mice (B6-STIL and non-rec) and STIL^{OE} mice (Ht, Hm) observed at a maximum of 23 months of age. (B) Normal control mouse. (C) Control mouse, showing enlarged belly due to lymphoma sacrificed at 23 months of age. (D-F) Macroscopic images of lymphomas in mesenteric lymph nodes of B6-STIL (D), non-rec (E), STIL^{OE} mice (F), respectively. The latter showed relatively smaller sized lymphomas. (G, I) H&E-stained lymph node sections of non-rec (G) and STIL^{OE} (I) mice, respectively, showing similar histopathological findings of lymphoma characterized by variably sized malignant lymphoblasts, scale bar, 100 μ m.

Tumors and organs were sampled for DNA and RNA extraction and subsequent genotyping and detection of *Stil* mRNA expression levels by qPCR. The genotyping of the tumors and the different tissues were consistent with the ear punch genotyping at 3-weeks of age. However, different tissues showed variable *Stil* mRNA expression levels as depicted in Figure 17, where the kidney, brain and liver displayed the highest values with an up to 90-fold increase in *Stil* mRNA expression. Few outlier liver samples even showed up to 400-fold increased levels. All samples were normalized to the respective tissues of control mice. Furthermore, heterozygous $STIL^{OE}$ mouse tissue samples exhibited proportionally lower expression levels relative to the homozygous ones, confirming the expectations regarding the respective genotypes.

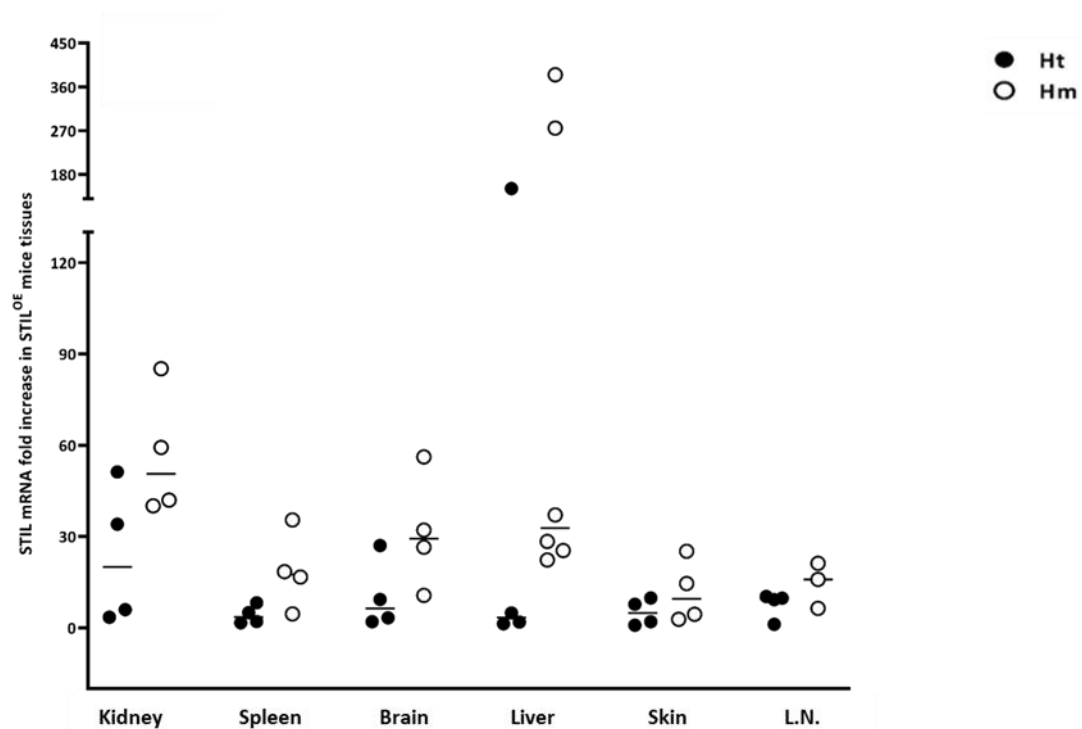


Figure 17: *STIL* mRNA fold increase in different tissues of $STIL^{OE}$ mice. Each data point represents a tissue sample from a mouse. Displayed values were normalized to control mouse tissue using the $2^{-\Delta\Delta CT}$ method; Ht = heterozygous, Hm = homozygous $STIL^{OE}$ mice.

1.2. STIL^{OE} is downregulated in the tumor tissues

Surprisingly, the tumor tissue from lymph node samples of STIL^{OE} mice revealed a marked decrease in *Stil* mRNA expression levels compared to its normal tissue counterpart of the same genotype from healthy mice, suggesting that STIL overexpression has been downregulated within the tumor tissues of control and STIL^{OE} transgenic mice (Fig. 18).

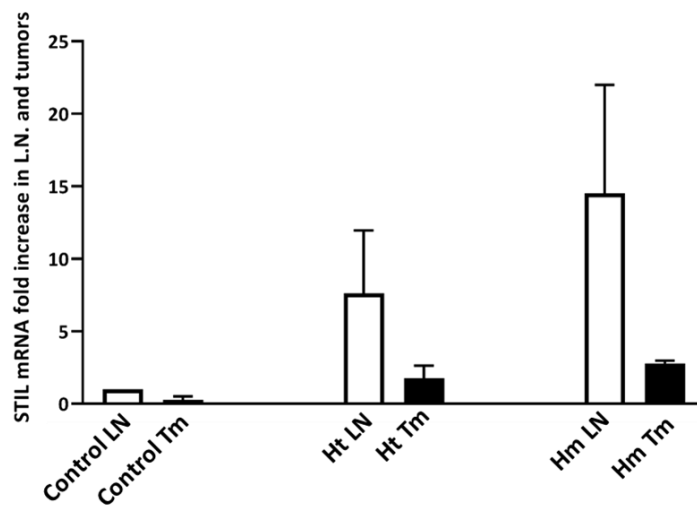


Figure 18: *Stil* mRNA expression levels in healthy and lymphomatous lymph nodes. Each bar represents mean \pm standard deviation (SD) of the described genotype samples (n=3). Displayed values were normalized to control mouse lymph nodes using the $2^{-\Delta\Delta CT}$ method; Mean \pm standard deviation. LN = lymph node, Tm = Tumor/Lymphoma, Ht = heterozygous, Hm = homozygous STIL^{OE} mice.

A comparison between DNA copy number alterations of lymphomatous tissue derived from control versus STIL^{OE} mice showed no significant difference (Fig. 19), suggesting that most of the cellular content of both tumor in both groups originated from non-STIL overexpressing cells.

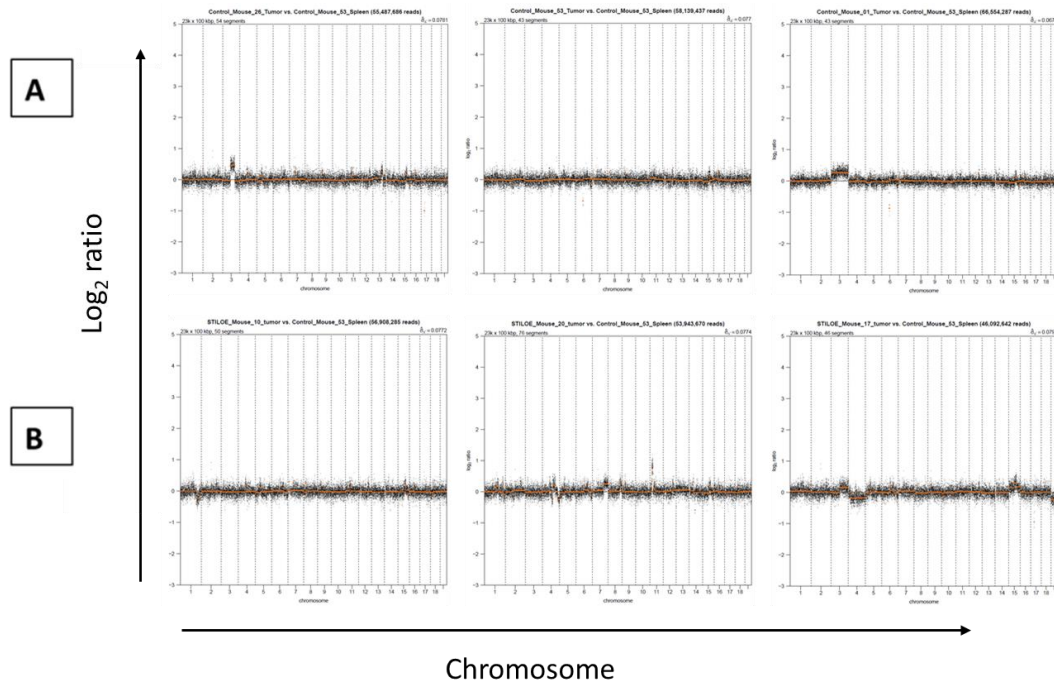


Figure 19: CNV analysis of lymphomatous lymph nodes by low coverage WGS. CNV plots showing genomic aberrations of three control mouse lymphomas (A) and three STIL^{OE} mouse lymphomas (B). All analyses were normalized to healthy control mouse spleen. The sequence read numbers were counted in 23k x 100 kbp windows, each lane represents a chromosome. The horizontal midline represents the normal copy number. The points above and below indicate gains or losses at the respective position.

1.3. $STIL^{OE}$ is associated with an increased rate of newly born deaths.

$STIL^{OE}$ mice became officially designated "unburdened" after, unexpectedly, a reduced spontaneous tumor incidence in comparison to control mice and the tumor incidence levels reported for wildtype B6 mice (Brayton et al., 2012).

To determine Mendelian birth ratios, we proceeded with further breeding of successive generations. The results as shown in table 27 suggest that the frequency of both live homozygous and heterozygous $STIL^{OE}$ mouse offspring was below the expectations, suggesting negative selection against mice with $STIL$ overexpression.

Simultaneously, we found an increased rate of pups that died around birth, with frequencies of 0% in the first generation, 13% in the second generation, 33% in the third generation and 54% in the fourth generation. Genotyping of the dead pups from the fourth generation showed that wildtype and non-recombinant mice constituted 0% of the deaths, while 8% of the deaths belonged to the $STIL^{OE}$ (H_{tinc}) group, and 46% each to the $STIL^{OE}$ (H_{minc}) and $STIL^{OE}$ (H_{tcom}) group. This finding suggests that higher levels of $STIL$ overexpression are not compatible with live. Consequentially, we have applied for burdened breeding approval.

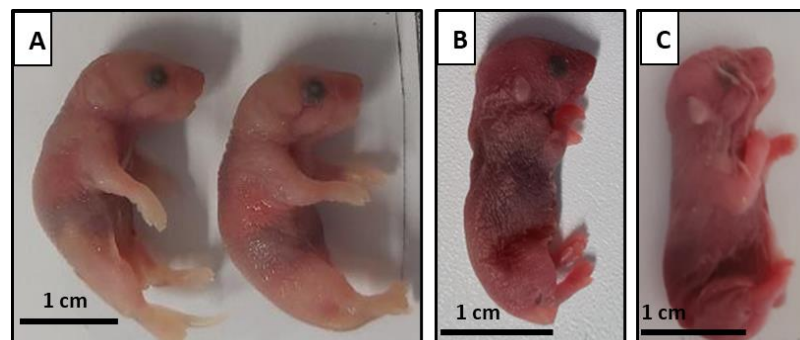


Figure 20: One-day old newly born pups. (A) Control B6 one-day old pups, healthy and alive. (B), (C) $STIL^{OE}$ one-day old dead pups.

Table 27: Breeding generations in STIL^{OE} mice, showing expected and actual STIL^{OE} inheritance ratios.

Gen*	Parents (matings No.)	Total mice	Live mice	Newly born deaths	Newly born deaths	Expected Mendelian inheritance ratio			Actual inheritance ratio					
						WT**	STIL ^{OE} (Ht)	STIL ^{OE} (Hm)	WT**	Non-rec	STIL ^{OE} (Ht _{inc})	STIL ^{OE} (Ht _{com})	STIL ^{OE} (Hm _{inc})	Male : Female
1	B6-STIL x CMV-Cre-deleter line (6)	71	71	0	0%	50%	50%	0%	65%	22.5%	12.5%	0%	0%	40:31
2	STIL ^{OE} (Ht) x B6-STIL (6) / STIL ^{OE} (Ht) x CMV-Cre-deleter line (2)	69	60	9	13%	44% ^m	31% ^m	25% ^m	42%	14.6%	5.8%	7.2%	17.4%	31:29
3	STIL ^{OE} (Ht) x STIL ^{OE} (Ht) (4)	21	14	7	33%	37.5%	37.5%	25%	19%	10%	19%	4.7%	14.3%	5:9
4	STIL ^{OE} (Hm) x STIL ^{OE} (Hm) (2) / STIL ^{OE} (Hm) x STIL ^{OE} (Ht) (3) / STIL ^{OE} (Ht) x STIL ^{OE} (Ht) (2)	37	17	20	54%	21% ^m	25% ^m	54% ^m	19%	5.4%	0%	10.8%	10.8%	9:8

* Gen: Generation, ** WT: Wildtype for STIL recombination, which represents any of the following genotypes: B6 (C57BL/6), B6-STIL (STIL^{Ht}), CMV-Cre-deleter lines. Non-rec = non-recombinant mice, Ht_{inc} = incompletely recombinant heterozygous STIL^{OE} mice, Ht_{com} = completely recombinant heterozygous STIL^{OE} mice, Hm_{inc} = incompletely recombinant homozygous STIL^{OE} mice. ^m = indicating mean values of the expected ratios from breeding of different pairs.

2. Generation of STIL^{OE} MEFs

Primary MEFs were derived from STIL^{OE} and control mice at embryonal day E12.5 - E13 as described in 2.1.3.1. of chapter 2 (Fig. 11), to detect centrosome amplification, mitotic defects, and chromosomal instability.

2.1. Characterization of STIL^{OE} MEFs

2.1.1. Genotyping

STIL^{OE} MEFs were genotyped (Fig. 21) to enable grouping according to Table 26.

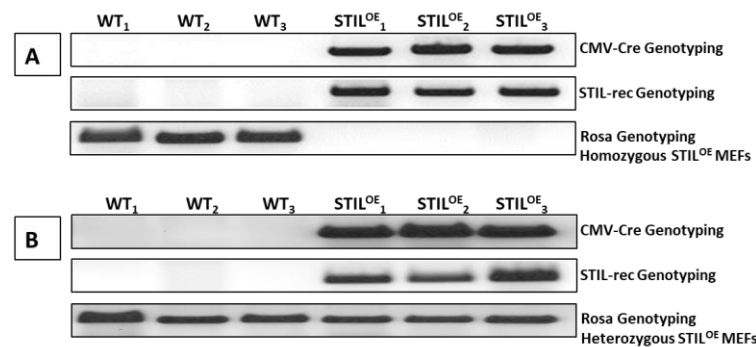


Figure 21: MEF genotyping. PCR results of three independent WT (B6) and STIL^{OE} MEFs each. STIL^{OE} MEFs were positive with CMV-Cre and STIL-rec primers, which were all negative in WT-B6 MEFs. Depending on Rosa primers results, the STIL^{OE} MEFs were classified into (A) homozygous MEFs showing complete absence of the Rosa band and (B) heterozygous MEFs, which were positive with Rosa primers like WT (B6) MEFs due to the absence of the *Stil* construct in one allele of the Rosa26 locus.

2.1.2. STIL^{OE} MEFs show increased *Stil* mRNA expression levels

To explore transcription of the inserted Flag-tagged *Stil* construct, real-time RT-qPCR was carried out using extracted RNA from WT and STIL^{OE} MEFs in passage 3 (P3). Homozygous STIL^{OE} MEFs showed an increase up to 16-fold in *Stil* mRNA expression levels as shown in Figure 22, while heterozygous STIL^{OE} MEFs showed about half of these levels. WT MEFs were used for normalization according to the $2^{-\Delta\Delta CT}$ method.

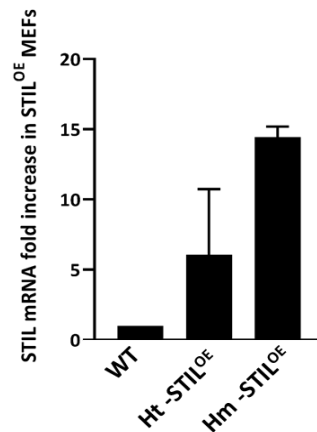


Figure 22: Real-time RT-qPCR of MEFs. Fold increase of *Stil* mRNA in STIL^{OE} MEFs relative to WT MEFs; graph showing the mean \pm standard deviation, n=3.

2.1.3. Validation of anti-STIL antibody in Western blotting

The anti-STIL antibody (A302-442A, Bethyl-Biomol GmbH) was validated for Western blotting using the human osteosarcoma U2OS cell line with tetracycline-inducible GFP-*STIL* (U2OS-GFP-*STIL*) to differentiate between overexpressed and endogenous STIL protein (Fig. 23). The anti-STIL antibody can detect endogenous STIL in the non-induced cell line at band size 170 kDa. After tetracycline addition GFP-*STIL* can be detected at band size 195 kDa, which is in accordance with a GFP protein size of 25 kDa.

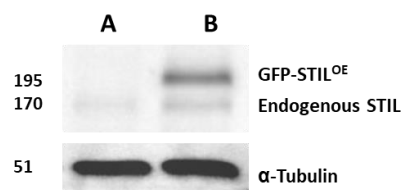


Figure 23: Validation of anti-STIL antibody in U2OS-GFP-STIL cells. (A) Endogenous STIL protein in non-induced U2OS-GFP-STIL cells. (B) Overexpression of GFP-*STIL* protein in U2OS-GFP-*STIL* cells after induction with 4 μ g/ml tetracycline for 72h.

To validate the detection of murine STIL, the anti-STIL antibody was used for immunoblotting of MEF protein lysates, resulting in three bands, one at 170 kDa as expected, plus two bands at 220 and 150 kDa. Therefore, STIL protein knockdown and STIL protein overexpression using siRNA and CMV-Flag-*Stil* plasmid transfection, respectively, in STIL^{OE} and WT MEFs were performed. siRNA

transfection led to loss of the band sized 170 kDa in the STIL^{OE} MEFs, while CMV-Flag-*Stil* plasmid transfection resulted in an enhanced band signal intensity in WT MEFs (Fig. 24, A and B).

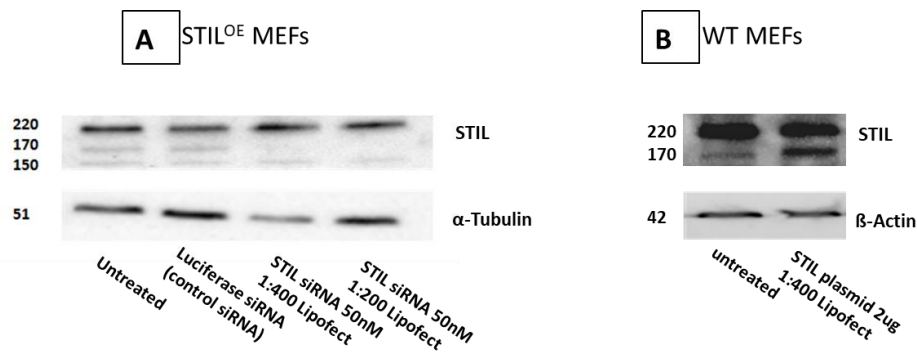


Figure 24: Validation of anti-STIL antibody in MEF protein lysates. (A) Transfection of MEFs with *Stil* siRNA resulting in loss of the band sized 170 kDa. (B) Transfection of MEFs with CMV-Flag-*Stil* plasmid, causing enhanced intensity of the band sized 170 kDa.

2.1.4. STIL^{OE} MEFs show increased STIL protein levels

To demonstrate that STIL is overexpressed at the protein level in STIL^{OE} MEFs as well, STIL^{OE} and WT control MEFs at P3 were used for immunoblotting to determine STIL protein levels. Heterozygous STIL^{OE} (Ht_{inc}) MEFs showed about half the protein expression levels of heterozygous STIL^{OE} (Ht_{com}) cells, which in turn expressed about half the levels of homozygous MEFs, in accordance with their genotypes and *Stil* mRNA expression levels (Fig. 25, A). Intriguingly, levels of overexpressed STIL protein decreased with further passages in heterozygous STIL^{OE} MEFs (Fig. 25, B), suggesting selection against high levels of STIL.

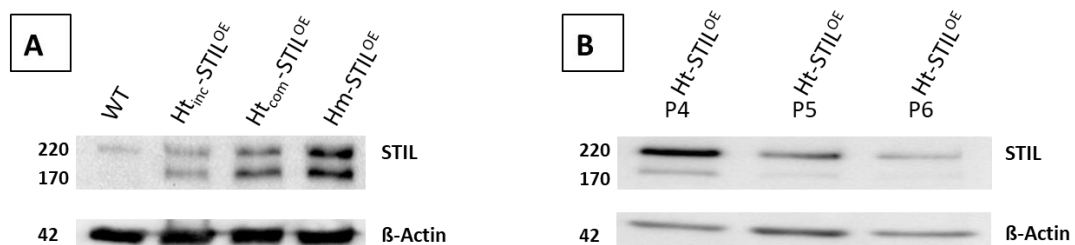


Figure 25: STIL protein levels in STIL^{OE} and WT MEFs. (A) Gradual increase of the 170 kDa band size intensity in STIL^{OE} MEFs depending on the genotype. (B) STIL protein expression levels decrease in heterozygous STIL^{OE} MEFs by passaging the cells from passage 4 to 6.

2.2. STIL overexpression leads to centriole rosette formation and centrosome amplification.

The frequency of supernumerary centrioles was significantly increased in interphase STIL^{OE} MEF cells as compared to the corresponding passage of WT control MEFs. In both Ht and Hm STIL^{OE} MEFs about 48% cells with centriole amplification were found (Fig. 26), as revealed by immunofluorescence microscopy examination of centrosomes using antibodies to centrioles (anti-centrin) and pericentriolar material (anti-pericentrin), while the nuclei were counterstained with Hoechst 33342 (Fig. 27, A and B). Additionally, mitotic STIL^{OE} cells showed an increased frequency of pseudo-bipolar divisions with clustered centrosomes (Fig. 27, C). Quantification of centriole amplification in both of STIL^{OE} and WT MEFs was performed by counting at least 100 interphase cells of corresponding passages in triplicates.

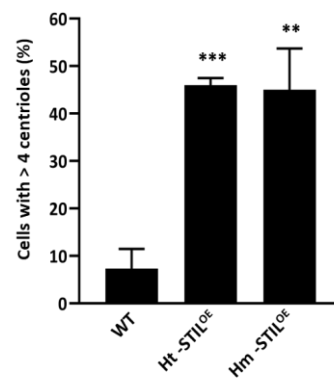


Figure 26: Centriole amplification in STIL^{OE} MEFs in comparison to WT MEFs. Graph showing the mean \pm standard deviation of the percentage of interphase cells with > 4 centrioles, n=3.

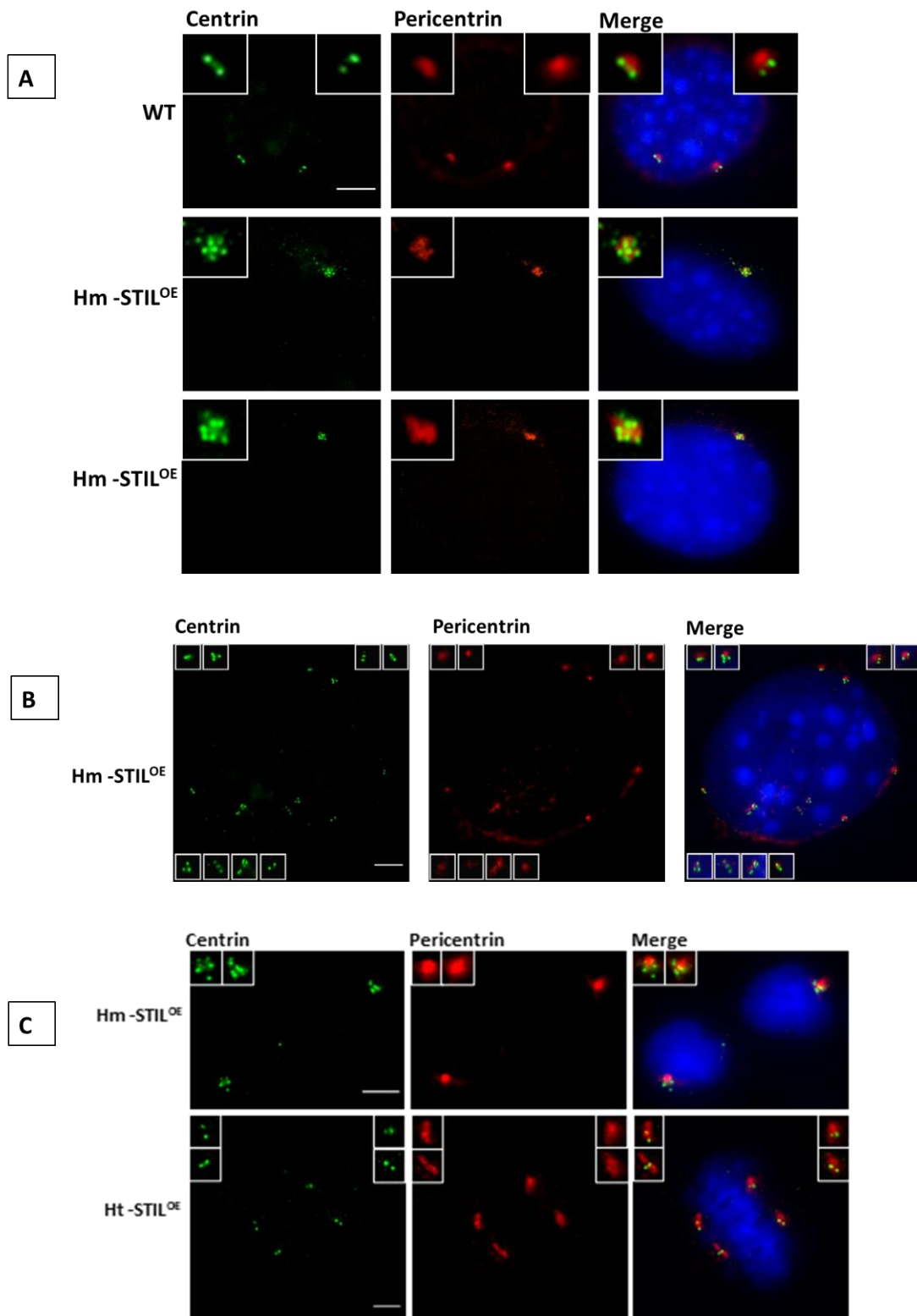


Figure 27: Amplified centrosomes in STIL^{OE} MEFs. (A) STIL^{OE} MEFs containing centriole rosettes, characterized by mother centrioles surrounded by multiple daughter centrioles. (B) STIL^{OE} cell containing nine centrosomes. (C) Clustered bipolar telophase (upper panel) and metaphase (lower panel). Scale bar, 5 μ m.

2.3. STIL^{OE} MEFs have an abnormal phenotype with marked aneuploidy

Interestingly, the Hm STIL^{OE} MEFs were oversized and flattened with enlarged nuclei. In contrast, WT MEFs showed a normal spindle-shaped morphology. Ht STIL^{OE} MEFs revealed an intermediate phenotype (Fig. 28). Notably, some of the STIL^{OE} MEF cells were multinucleated with up to five nuclei, which had not been observed in WT MEFs.

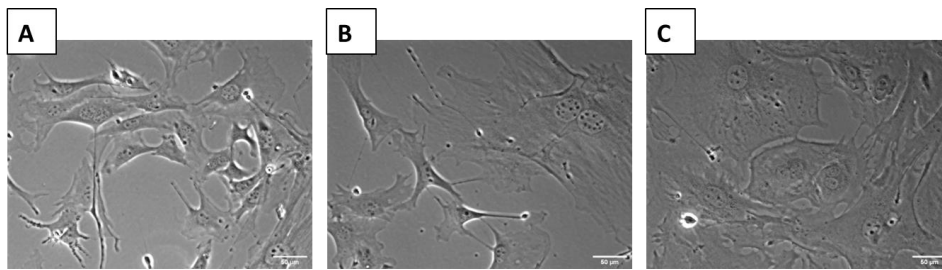


Figure 28: STIL^{OE} MEF phenotype. Phase contrast microscopy images depicting (A) WT MEFs, (B) Ht STIL^{OE} MEFs, and (C) Hm STIL^{OE} MEFs. Scale bar, 50 μ m.

Both, Ht and Hm STIL^{OE} MEFs that were stained with Hoechst 33342 and examined by immunofluorescence microscopy showed an increased frequency of micronucleus formation as an indicator of chromosome missegregation. Micronuclei were identified according to the criteria of Kwon et al., 2020. Micronucleus quantification of STIL^{OE} and WT MEFs was done by counting at least 100 cells of the same passages in triplicates (Fig. 29).

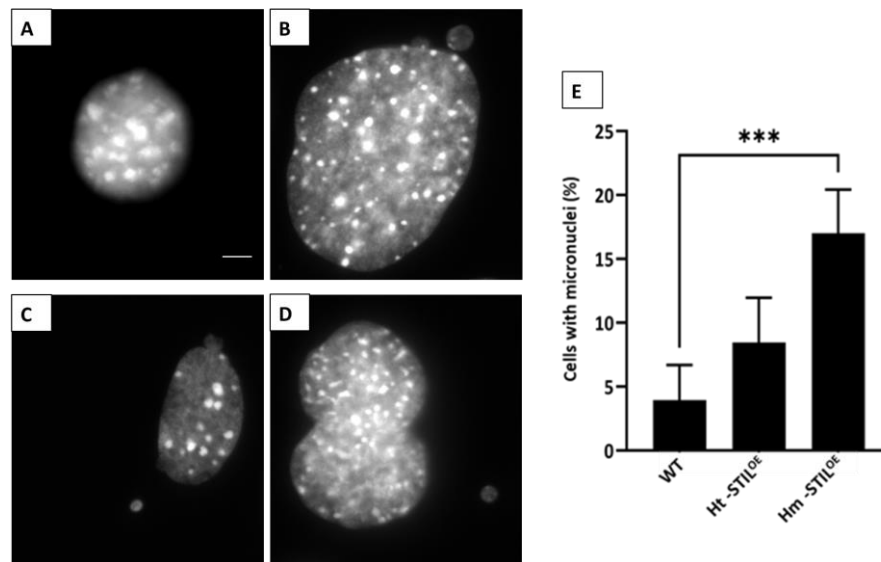


Figure 29: Micronucleus formation in STIL^{OE} MEFs. Hoechst 33342 stained WT MEF cells (A) and STIL^{OE} MEFs with binucleation and micronuclei (B-D). Scale bar, 5 μ m. (E) Graph showing the mean \pm standard deviation of the percentage of cells with micronuclei, n=3.

To determine the level of aneuploidy resulting from chromosome missegregation, WT and STIL^{OE} MEFs were arrested in metaphase using colcemid. Metaphase spreads were prepared and chromosomes were analyzed by M-FISH. 20 metaphase spreads of each MEF line derived from different embryos of both STIL^{OE} and WT MEFs were analyzed and revealed a significant increase in chromosome aberrations, both structural and numerical, in Ht and Hm STIL^{OE} MEFs as compared to WT MEFs (Fig. 30) in addition to increase in tetraploidy incidence in Ht STIL^{OE} MEFs (three fold increase, where mean value of tetraploidy equals to 12%) and Hm STIL^{OE} MEFs (six fold increase, where mean value of tetraploidy equals to 22%) in comparison to the WT MEFs (mean value of tetraploidy = 4%). Tetraploidy is considered as a form of aneuploidy due to centrosome amplification with subsequent failure of cytokinesis (Andreassen et al., 2001; Bayani et al., 2008). Moreover, the STIL^{OE} MEFs showed decomposed nuclei, represented as multiple micronuclei disintegrated in focal spot, each had multiple chromosome paints (Fig. 30, G). Taken together, STIL overexpression in MEFs derived from STIL^{OE} mice induces centrosome amplification with subsequent chromosome missegregation and cellular deaths.

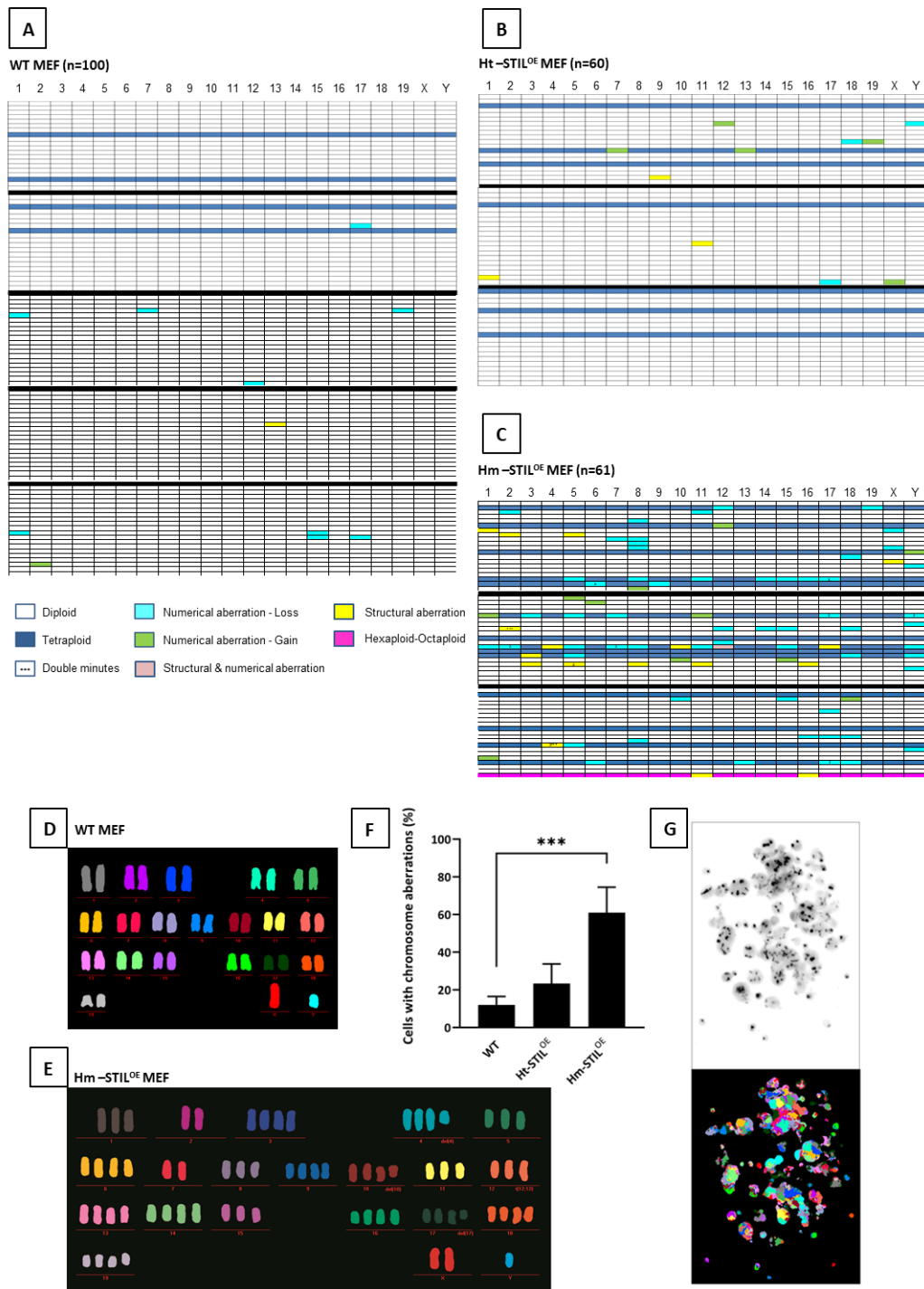


Figure 30: M-FISH staining and analysis of 20 metaphase spreads per MEF line.

Tables represent metaphases, where each row symbolizes one cell of five different WT lines and 3 different lines of each of Ht and Hm, in metaphase in addition to the colored illustrated aberrations (A) WT MEFs (n=100 cell), (B) Ht-STIL^{OE} MEFs (n=60 cell), and (C) Hm-STIL^{OE} MEF (n=61 cell). M-FISH metaphases of a WT MEF cell with a diploid karyotype (38, XY) (D) and a Hm-STIL^{OE} MEF cell with a near tetraploid karyotype (69, XXY,-Y,-1,-2,-2,del(4),-5,-7,-7,-8,del(10),-11,-12,der(12)t(12;12),-15,del(17)) (E). (F) Graph showing the percentage of karyotype aberrations in WT, Ht-STIL^{OE}, Hm-STIL^{OE} calculated from A, B and C. (G) STIL^{OE} MEF cell showing decomposed nucleus, represented by focal multiple disintegrated micronuclei, each had multiple chromosome paints.

2.4. STIL overexpression impairs proliferation

To assess the effect of STIL overexpression on the proliferation of MEFs, a proliferation assay was performed using Ht and Hm STIL^{OE} and WT MEFs in P3 for five consecutive days in cell culture using two independent methods: (i) Trypan blue dye exclusion with automated cell counting using a TC20™ counter, and (ii) PrestoBlue™ Cell Viability Reagent staining evaluation using a Spark microplate reader (Tecan). Both assays demonstrated that STIL^{OE} MEFs proliferate at a slower rate compared to WT MEFs in the following order: WT MEF > Ht STIL^{OE} MEF > Hm STIL^{OE} MEF (Fig. 31, A and B).

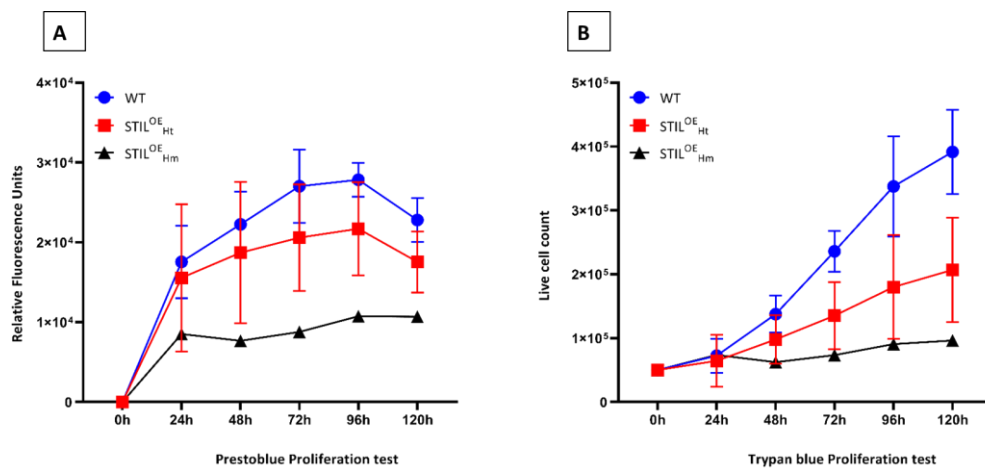


Figure 31: Proliferation assay. (A) Prestoblu-based proliferation assay, WT MEFs (n=4), Ht-STIL^{OE} MEFs (n=8), and Hm-STIL^{OE} MEF (n=1). (B) Trypan blue-based proliferation assay, WT MEFs (n=4), Ht-STIL^{OE} MEFs (n=6), and Hm-STIL^{OE} MEF (n=1). Graphs indicate mean \pm standard deviations of three independent experiments.

2.5. STIL overexpression induces cellular deaths

To understand the low proliferation rate of STIL^{OE} MEFs, apoptosis assays and cell cycle analyses by FACS were performed. The results were correlated to the results of proliferation assay and M-FISH, where STIL^{OE} MEFs showed a STIL-dose-dependent (Hm > Ht), statistically significant increase of apoptosis and cell death rates in comparison to WT MEF (Fig. 35, A and B). Similar results were found by cell cycle analysis, where the Hm STIL^{OE} MEFs showed the highest levels of nonviable cells and cellular debris (< G1) followed by Ht STIL^{OE} MEFs as compared to WT cells (Fig. 32, C and D).

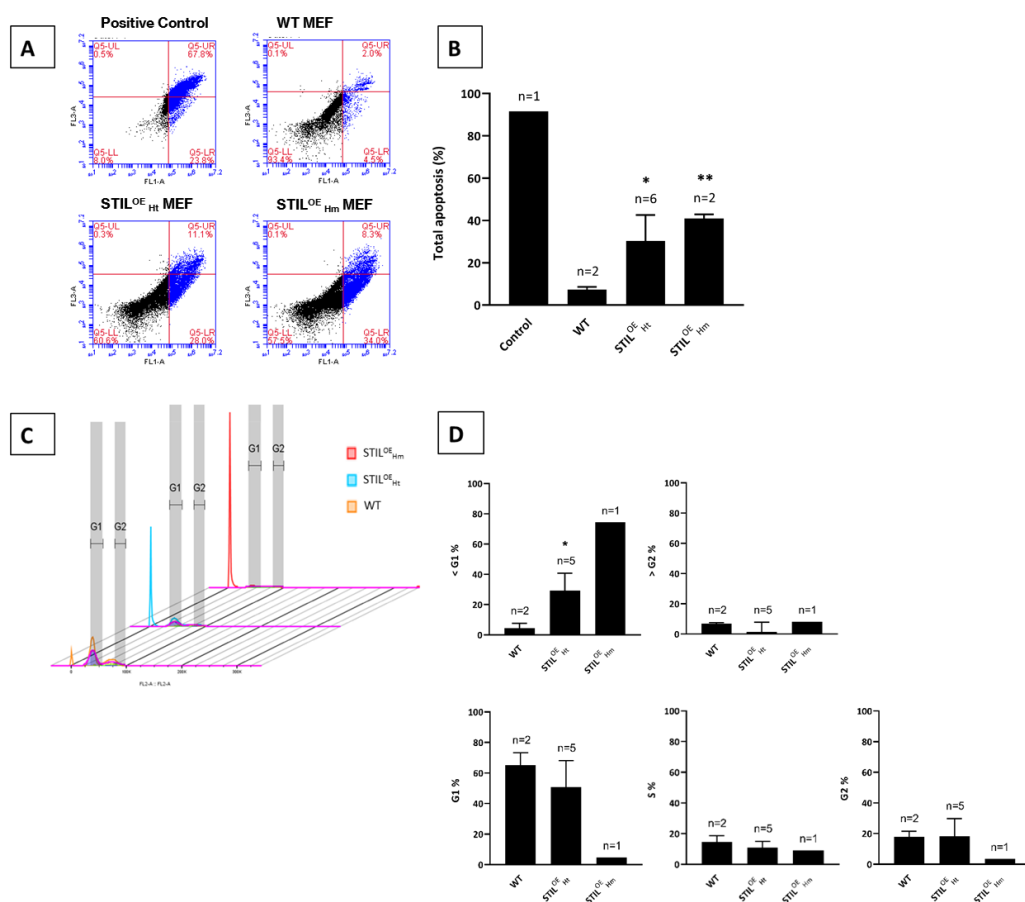


Figure 32: Flow cytometry analysis. (A) Apo-15 peptide/7-AAD - apoptosis assay of 4% PFA-treated WT MEFs (positive control) and untreated WT, Ht STIL^{OE} and Hm STIL^{OE} MEFs. The percentages of apoptotic cells are given in (B); Mean \pm SD of the percentage of Apo-15 peptide/7-AAD-positive MEFs. (C) Cell cycle histogram of WT, Ht STIL^{OE} and Hm STIL^{OE} MEFs showing the increase of the sub-G1 population in STIL^{OE} MEFs. (D) Cell cycle profile of WT, Ht STIL^{OE} and Hm STIL^{OE} MEFs.

3. Generation of transgenic mice with epithelium-specific STIL overexpression and with or without TP53 inactivation

3.1. Generation of STIL^{OE} transgenic mouse lines (K14^(CreERT2);STIL^{OE}) and (K14^(CreERT2);STIL^{OE};P53^{dn})

To generate mice with tamoxifen-inducible epithelium-specific centrosome amplification, B6-STIL mice were crossbred with K14^{CreERT2} mice to obtain K14^(CreERT2);STIL^{fl/wt} animals for epithelium-specific STIL overexpression. K14^(CreERT2);STIL^{fl/wt} mice were bred with P53^{R172H/wt} mice to obtain K14^(CreERT2);STIL^{fl/wt};P53^{R172H/wt} mice for epithelium-specific STIL^{OE} with inactive TP53. Using this system, STIL is conditionally overexpressed in epithelial cells with K14 promoter activity (Vassar et al., 1989). The K14^(CreERT2) system allows for the induction of transgene expression at selected time and site, as CreERT2 encodes a fusion protein between Cre recombinase and the tamoxifen-responsive hormone-binding domain of the estrogen receptor, leading to Cre activation only after intraperitoneal administration of 1 mg of tamoxifen (4 doses given within 2 weeks). Inducible epithelium-specific STIL overexpression was performed to study the role of centrosome amplification during tumorigenesis due to the concerns that generalized STIL overexpression might be embryonically lethal or lead to developmental defects, phenotypes which have been reported for other centrosomal proteins (Chavali et al., 2014). These mice were subsequently subjected to a skin carcinogenesis assay.

3.2. Characterization of K14^(CreERT2);STIL^{OE} mice with epithelium-specific STIL overexpression

Four K14^(CreERT2);STIL^{OE} mice were sacrificed one day after the last dose of tamoxifen treatment and four K14^(CreERT2);STIL^{fl/wt} were sacrificed one day after the last oil dose as a control, to assess recombination and *Stil* expression by genotyping and qPCR in skin and esophageal tissue. The results of genotyping showed band formation by K14 and STOP primers in both groups, while only the tamoxifen-treated group showed positive results with the STIL-rec primers, demonstrating that active Cre recombinase removed the stop cassette in the skin and esophagus epithelia of these mice. qPCR results showed up to 10-fold increased *Stil* mRNA expression levels in both skin and esophagus tissue in the tamoxifen-treated group

(Fig. 33).

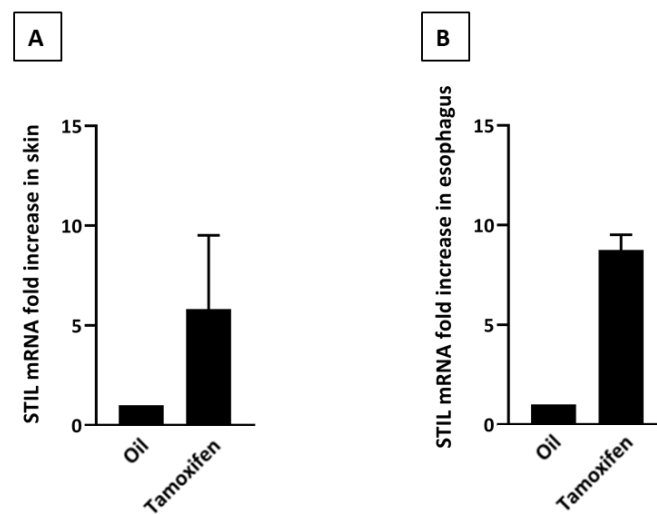


Figure 33: STIL mRNA fold increase in skin (A) and esophagus (B) of $K14^{(CreERT2)};STIL^{OE}$ mice. Fold increase of STIL mRNA in $K14^{(CreERT2)};STIL^{OE}$ mice (tamoxifen-treated) relative to $K14^{(CreERT2)};STIL^{fl/wt}$ mice (oil treated); each graph represents mean \pm standard deviation, $n=4$. Values were normalized to skin and esophagus of oil-treated mice the using $2^{-\Delta\Delta CT}$ method.

3.3. STIL overexpression decreases the incidence and multiplicity of chemically induced skin tumors

Chemical induction of skin tumors in mice is a standardized procedure since decades. It is used to determine the effect of the genes of interest or various other factors on cutaneous tumor initiation, promotion, and progression. It consists of tumor initiation using a chemical mutagen (DMBA) followed by tumor promotion by a proinflammatory chemical (TPA) (Fig. 34). This results in benign papilloma development, which can progress over time to squamous cell carcinoma (SCC) or regress when the treatment is stopped (Coelho et al., 2015; Serçin et al., 2016). This experiment was done in collaboration with Dr. Karin Müller-Decker group at DKFZ.

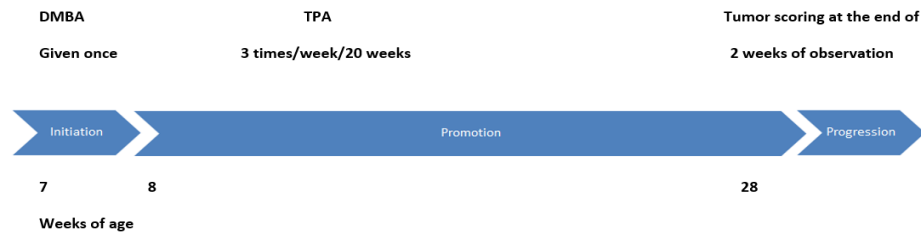


Figure 34: Skin carcinogenesis assay. Diagram showing stages of cutaneous tumorigenesis.

Within the skin carcinogenesis assay, 30 $K14^{(CreERT2)};STIL^{fl/wt}$ mice received tamoxifen for induction of epithelium-specific STIL transgene expression (Tamoxifen group) whereas 15 animals served as a control (Oil group) (table 22 and 23). Remarkably, during the tamoxifen treatment phase, the tamoxifen-treated mice showed transient weight loss, which lasted for up to one week, with recovery afterwards. In week 9 of TPA treatment, papillomas started to appear in mice. Interestingly, the papillomas appeared earlier in the oil group as compared to the tamoxifen-treated mice, which also developed fewer papillomas during the course of the skin carcinogenesis assay.

We found that the tumor incidence, defined as the number of mice bearing papillomas, was significantly lower in tamoxifen-treated versus control mice. Tumor multiplicity, defined as the average number of papillomas per mouse, was significantly lower in tamoxifen-treated versus control mice as well. Also, the time for which mice carried papillomas was significantly longer in control versus tamoxifen-treated mice (Fig. 35). Importantly, after genotyping of the papillomas from both the tamoxifen and oil groups, we found that only about one third (9/30) of the tamoxifen group papillomas was recombinant, i.e., had lost the STOP cassette from the *Stil* expression construct. This indicates that the majority of tamoxifen group papillomas originated from WT epithelial cells as well.

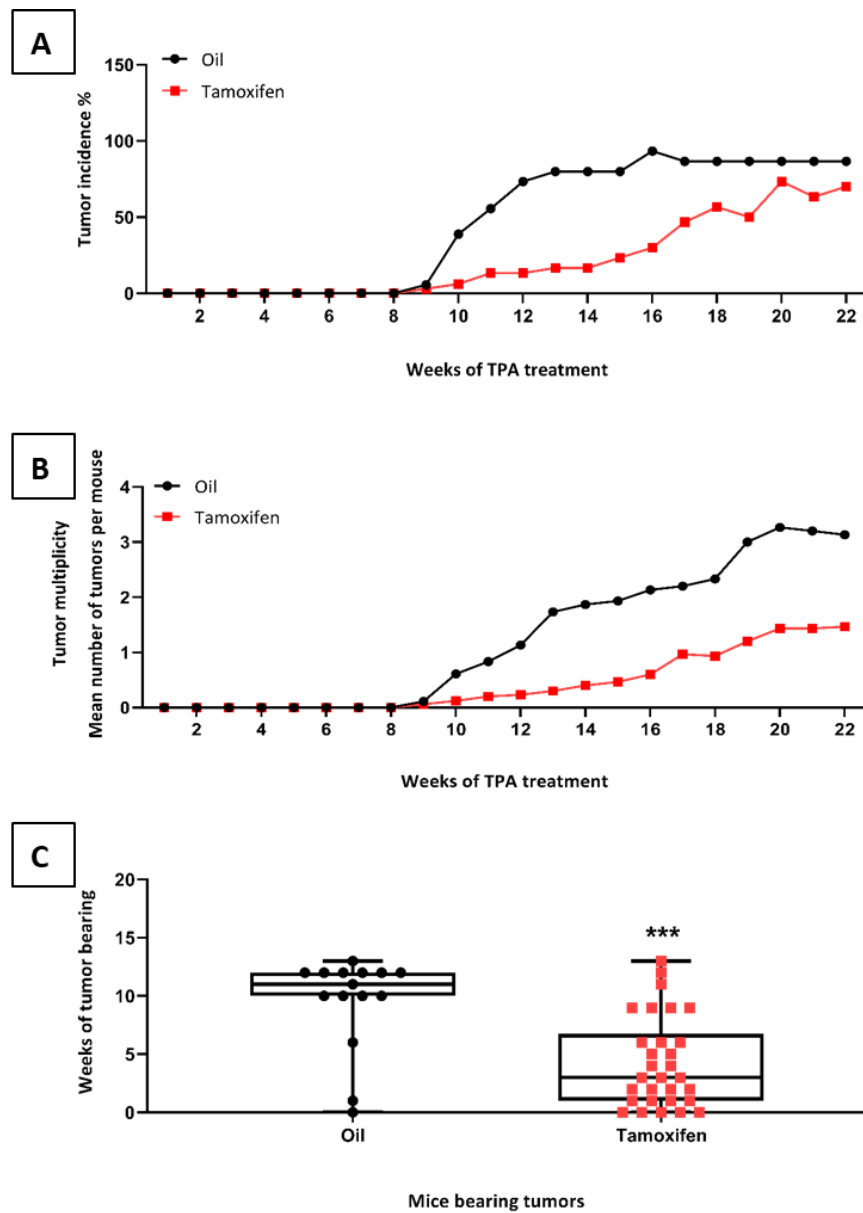


Figure 35: Skin carcinogenesis assay in $K14^{(CreERT2)}$; $STIL^{fl/wt}$ and $K14^{(CreERT2)}$; $STIL^{OE}$ mice. (A) Tumor incidence in $K14^{(CreERT2)}$; $STIL^{OE}$ tamoxifen-treated, versus control oil-treated animals. (B) Tumor multiplicity in tamoxifen-treated $K14^{(CreERT2)}$; $STIL^{OE}$ versus control animals. (C) Weeks during which mice were bearing skin papillomas, during the whole course of tamoxifen-DMBA-TPA treatment. Graph shows mean \pm standard deviation.

3.4. Skin carcinogenesis assay in $K14^{(CreERT2)}$;STIL^{OE};P53^{dn} mice with epithelium-specific STIL overexpression and TP53 inactivation

Analogous to the experiments described in 3.3, a skin carcinogenesis assay was performed using mice with epithelium-specific overexpression of murine STIL and inactivation of TP53 (Table 22) to investigate the effects of centrosome amplification on skin tumor formation in the absence of TP53. For that, a heterozygous loxP Trp53^{tm1Tyj} mouse strain, with a point mutation on the (R172H) position in exon 5 of Trp53 locus, was used in breeding. The mice express mutant TP53 upon Cre-mediated STOP cassette excision, which was confirmed by genotyping via PCR analysis. This mutant TP53 has a higher affinity for binding to TP53 target gene promoters, thereby preventing binding of wildtype TP53, which in turn results in a dominant negative TP53 mutant function (Olive et al., 2004; Willis et al., 2004). Results from the experimental cohort (tamoxifen group (n=21), oil group (n=6)), revealed similar results as shown in 3.3. Both, tumor incidence and tumor multiplicity were still lower in tamoxifen-treated versus control mice (Fig. 36, A-C), however, the tumor incidence and tumor multiplicity in $K14^{(CreERT2)}$;STIL^{OE};P53^{dn} tamoxifen-treated group was slightly higher compared to $K14^{(CreERT2)}$;STIL^{OE} tamoxifen-treated group indicating that TP53 inactivation had a partial rescue effect. Here, all the papillomas of the tamoxifen group were positive for P53-rec primers. However, not all of them were positive for STIL-rec primers (Fig. 36, D).

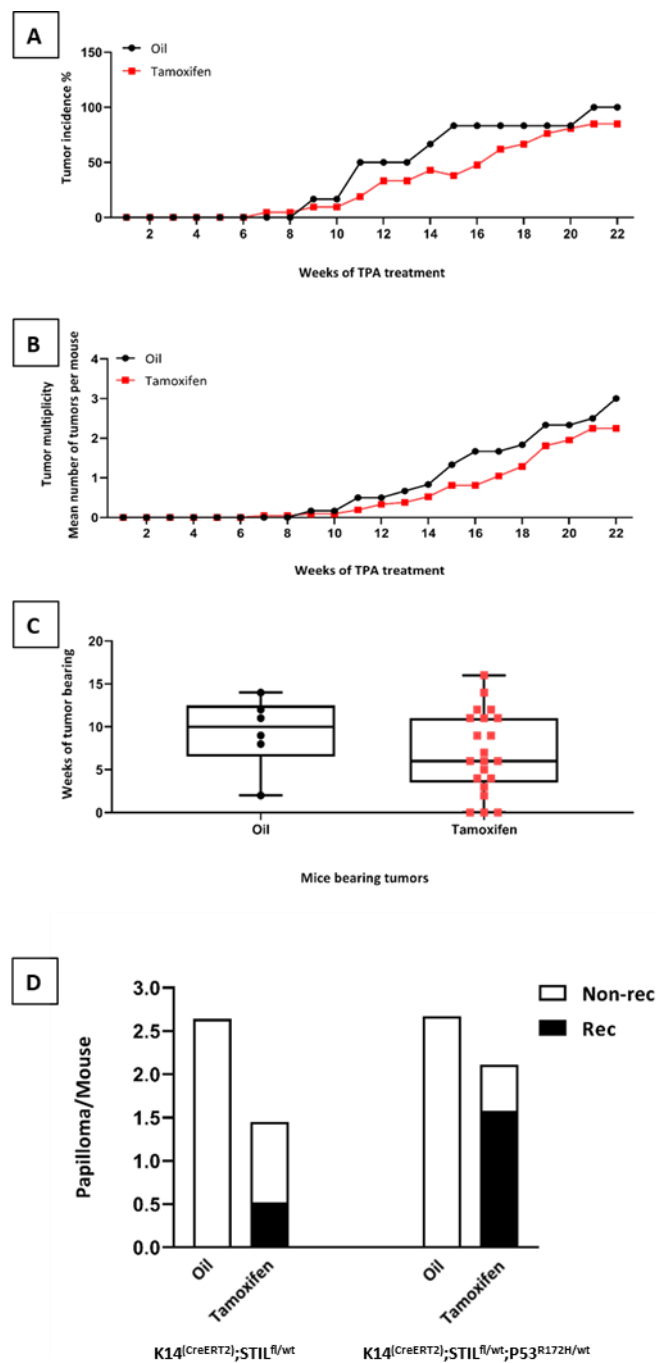


Figure 36: Skin carcinogenesis assay in $K14^{(CreERT2)};STIL^{fl/wt};P53^{R172H/wt}$ and $K14^{(CreERT2)};STIL^{OE};P53^{dn}$ mice: (A) Tumor incidence in skin of $K14^{(CreERT2)};STIL^{OE};P53^{dn}$ mice, tamoxifen-treated, versus control oil-treated animals. (B) Tumor multiplicity in $K14^{(CreERT2)};STIL^{OE};P53^{dn}$ mice versus control mice. (C) Weeks in which mice were bearing skin papillomas, during the whole course of the skin carcinogenesis assay. Graph shows the mean \pm standard deviation. (D) Graph showing the number of STIL-rec (Rec) papillomas per mouse in $K14^{(CreERT2)};STIL^{fl/wt}$ and $K14^{(CreERT2)};STIL^{fl/wt};P53^{R172H/wt}$ mice. Non-rec = indicates the presence of the STOP cassette in the STIL construct (Non-STIL overexpressing papillomas), Rec = indicates successful excision of the STOP cassette in the STIL construct (STIL overexpressing papillomas).

4. Centrosome amplification inhibits tumor formation

In conclusion, rates of both, spontaneous tumor formation in *STIL*^{OE} mice and chemically induced skin papillomas in mice with epithelium-specific *STIL* overexpression and mice with epithelium-specific *STIL* overexpression and *Tp53* inactivation are reduced as compared to WT controls. This suggests that centrosome amplification induced by *STIL* overexpression reduces tumor formation rather than enhancing it in mammals *in vivo*.

IV. DISCUSSION

The centrosome is a vital organelle that controls cell division. Centrosome aberrations gained scientific interest with regard to the development and treatment of cancer as they were observed in almost all types of malignancies (Boveri, 2008; Chan, 2011; Lingle et al., 2002). In addition, centrosome amplification induces aneuploidy both *in vitro* and *in vivo* (Ganem et al., 2009; Marthiens et al., 2013; Sabino et al., 2015; Silkworth et al., 2009). Nevertheless, the question, whether amplified centrosomes can drive tumorigenesis *in vivo* remains unresolved. Previous studies of transgenic mice that overexpress the centrosome replication protein PLK4, which leads to centrosome amplification *in vivo* showed variable outcomes. Some described tumorigenesis induction (Levine et al., 2017), while others stated that amplified centrosomes were not sufficient to drive tumor formation (Coelho et al., 2015; Kulukian et al., 2015; Marthiens et al., 2013; Serçin et al., 2016; Vitre et al., 2015). This may be due to the presence of additional functions of the kinase PLK4 besides being involved in the regulation of centriole duplication (Coelho et al., 2013; Martindill et al., 2007; Rosario et al., 2015).

In this thesis, we analyzed the impact of *in vivo* centrosome amplification on tumorigenesis using a novel transgenic mouse model with overexpression of STIL. STIL is a structural centrosome protein without any other known functions (Arquint et al., 2012; Vulprecht et al., 2012). First, we assessed the ability of STIL-induced centrosome amplification in driving tumorigenesis by generating transgenic STIL^{OE} mice with generalized STIL overexpression and monitoring of spontaneous tumor formation over a period of 23 months. Interestingly, we have found that spontaneous tumor formation was significantly reduced as compared to wildtype control mice. Second, we demonstrated that MEFs derived from STIL^{OE} embryos contained amplified centrosomes and chromosomal aberrations as a consequence of *Stil* mRNA and protein overexpression in a dose-dependent manner. Third, we determined the consequences of conditional epithelium-specific STIL overexpression with regard to skin tumor formation in a skin carcinogenesis assay. The results paralleled those found in the mice with generalized STIL overexpression with epithelium-specific STIL-overexpressing mice showing a significantly decreased rate of skin tumors compared to control animals. To analyze the impact of *Tp53* on *Stil*-induced tumor formation, mice with conditional

epithelium-specific STIL overexpression and TP53 inactivation were generated and subsequently employed in the skin carcinogenesis assay with essentially unchanged results, although the skin tumorigenesis was slightly rescued. We conclude that centrosome amplification due to STIL overexpression unexpectedly reduces tumor formation in mice.

1. STIL overexpression induces centrosome amplification that causes aneuploidy and impairs proliferation with increased cellular deaths

In our study, we used STIL overexpression to induce *in vivo* centrosome amplification in mice. STIL overexpression has been confirmed using MEFs at the mRNA and protein levels. Even further increased *Stil* mRNA and protein levels in homozygous versus heterozygous MEFs did not further boost centrosome amplification, as homozygous and heterozygous MEFs showed comparable values of amplified centrosomes, which suggests saturation effect for centrosome amplification.

Several *in vitro* and *in vivo* studies suggest that amplified centrosome induce errors in chromosome segregation with subsequent aneuploidy (Cosenza and Krämer, 2016; Cosenza et al., 2017; Ganem et al., 2009; Ghadimi et al., 2000; Marthiens et al., 2013; Nigg, 2002; Sabino et al., 2015; Vitre et al., 2015). Aneuploidy defined as cells with numerical or structural aberrant chromosomes, such as gain, loss, deletion, and break. These aneuploid cells are genomically unstable with amplified centrosomes and remarkable in most malignant tumors (D'Assoro et al., 2002; Ghadimi et al., 2000; Li et al., 2000; Lingle et al., 1998, 2002).

Therefore, we analyzed aneuploidy in STIL^{OE} MEFs by M-FISH analysis and found dose-dependent chromosome aberrations with homozygous STIL^{OE} MEFs displaying significantly more severe aneuploidy with increased apoptosis and cell deaths percentage than wildtype MEFs. Importantly and in line with earlier results by others (Daughtry and Chavez, 2016; Funk et al., 2021; Jeganathan et al., 2007; Lepage et al., 2020; Liebelt et al., 2019; Segal and McCoy, 1974; Stingele et al., 2012; Terradas et al., 2012; Torres et al., 2007; Williams et al., 2008), karyotype aberrations and micronucleus formation led to a dose-dependent impairment in

proliferation and detrimental effects on cell viability. Therefore, Williams et al., (2008) proposed that unknown mutations may have the ability to overcome the aneuploidy inhibitory effect on proliferation to derive tumorigenesis in cancer.

2. STIL-induced centrosome amplification inhibits tumor formation

2.1. STIL-induced centrosome amplification inhibits spontaneous tumor formation in aging mice

Aging black 6 mice (C57BL/6) show different types of tumor, where spontaneous lymphoma is the most common with an incidence up to 50% (Brayton et al., 2012). This frequency is in accordance with our control group (B6-STIL and non-rec mice) that showed 45.9% lymphoma incidence. In contrast, heterozygous and homozygous STIL^{OE} mice showed lymphoma rates of only 14.3% and 18.2%, respectively, which is almost two thirds below the expected value. Furthermore, qPCR analyses revealed reduced STIL expression levels in lymphomas compared to control STIL^{OE} lymph node tissue. Also, both STIL^{OE} and control lymphomas harbored similar karyotypes with no specific patterns of CNVs suggesting that the developed aneuploid cells due to centrosome amplification mostly had degenerative changes and that the tumor probably originated from non-STIL-overexpressing cells.

Our results contrast with some studies on transgenic PLK4^{OE} mice, showing that PLK4-induced centrosome amplification induces spontaneous tumor formation (Levine et al., 2017; Shoshani et al., 2021; Wang et al., 2019). However, Coelho et al., (2015) generated heterozygous PLK4^{OE} mice with a construct in one of the ROSA26 locus alleles, without TP53 loss, and kept them for 35 weeks only and not two years to detect tumors. Moreover, the skin and the pancreas derived from these mice showed only hyperplasia without tumor formation.

Another study suggested that chronic PLK4 overexpression does not induce spontaneous tumors in aged mice with active TP53 and centrosome amplification did not exist in these mice. This might be due to TP53 effect as it has role in arresting cell cycle of amplified centrosomes cells (Andreassen et al., 2001), inducing senescence in aneuploid cells with chromosome mis-segregation (Bazzi

and Anderson, 2014; Giam et al., 2020; Lambrus et al., 2015; Uetake and Sluder, 2004; Wong and Stearns, 2005). Furthermore, mice with *Tp53* loss (one allele or both) characterized by spontaneous tumor formation, as lack of TP53 promotes abnormal cell cycle progression and the prepared MEFs from them showed amplified centrosomes (Branca et al., 2020; Donehower et al., 1992, 1995; Fukasawa et al., 1996; Mikule et al., 2007). So, Vitre et al., (2015) generated additionally, *Tp53* knockout mice that overexpress PLK4, which showed no increased frequency of lymphomas or other tumors compared to mice lacking *Tp53*. Therefore, they concluded that centrosome amplification induces genomic instability regardless of *Tp53* status and it is not the primary cause of cancer in mammals.

It is worth mentioning that, in contrast to other tissues, in the liver of some homozygous and heterozygous STIL^{OE} mice very high *Stil* mRNA expression levels without tumor formation were found. This might indicate the ability of liver tissue to withstand the aneuploidy generated by centrosome amplification as liver cells frequently exhibit polyploidy (Duncan et al., 2010), generated by failed cytokinesis. In line, Vitre et al. (2015) found that TP53 limited the accumulation of cells with amplified centrosomes in mouse tissues except for the skin basal cell layer and liver, suggesting that these tissues tolerate centrosome amplification without tumor formation.

2.2. STIL-induced centrosome amplification inhibits chemically induced skin tumor formation

Conditional epithelium-specific STIL overexpression reduced papilloma formation compared to control mice in a standardized skin carcinogenesis assay. In addition, two thirds of the papillomas in the STIL overexpressing mouse group originated from wildtype, non-STIL overexpressing cells. A previous study has found that the number and size of skin papillomas in PLK4-overexpressing mice was not increased as compared to control animals (Vitre et al., 2015). Interestingly and in line with our findings, this study reported an, although statistically insignificant, trend toward lower overall tumor volume in mice with epithelium-specific PLK4 overexpression.

Since it has been reported that centrosome abnormalities, either amplification (Cuomo et al., 2008) or loss (Lambrus et al., 2015) induce cell cycle arrest in active

TP53 cells, we also performed a skin carcinogenesis assay using $K14^{(CreERT2)}$;STIL^{OE};P53^{dn} mice to determine whether TP53 inactivation would enable proliferation aneuploid cells with amplified centrosomes to give rise to more skin papillomas. Although papilloma incidence and multiplicity was still lower than in control animals, TP53 inactivation at least partially rescued papilloma formation in STIL-overexpressing cells, corroborating the earlier findings that TP53 prevents the proliferation of cells with amplified centrosomes (Vitre et al., 2015). However, in contrast data reported by Serçin et al., (2016), we have not found that Tp53 knockout allows for the induction of invasive squamous cell carcinomas by PLK4 overexpression.

3. Negative selection against STIL overexpression and centrosome amplification

The findings reported here demonstrate that homozygous mice with high-level STIL overexpression as well as MEFs derived thereof are selected against. This effect may be due to mitotic cell death as a consequence of the presence of multipolar cell divisions due to multiple centrosomes or the subsequent severe aneuploidy, which may explain the deviation in the expected mendelian ratios and the increased rates of still-born mice. This is consistent with the findings of Williams et al., (2008) who reported that cellular fitness of MEFs is decreased due to aneuploidy. Also, Vitre et al. (2015), Serçin et al., (2016) and Louro et al., (2021) indicated negative selection against centrosome amplification in MEFs derived from PLK4-overexpressing mice. Also, these findings are in line with data by Marthiens et al., (2013), who reported a negative selection against amplified centrosomes during neural system development in mice with neuron-specific PLK4 overexpression. They described that centrosome amplification leads to CNS degeneration rather than cancer formation and that PLK4 overexpression produced mitotic abnormalities with increased aneuploid cells, which led to TP53-induced apoptosis in the developing mouse brain. Brains of mice with PLK4 overexpression and TP53 inactivation showed accumulation of aneuploid cells that did not undergo apoptosis but differentiated and became incapable of proliferation, leading to neural progenitor cell depletion. This resulted in microcephaly and premature fetal death. Similarly, Vitre et al. (2015) found that the progeny of *Plk4*-transgenic mice

crossbred with Meox-2-Cre animals showed microcephaly with perinatal lethality, as the Meox-2-promoter is active in tissues derived from the epiblast, the progenitor of pluripotent stem and germ-line cells that will differentiate later into ectoderm, mesoderm and endoderm.

4. Conclusion: STIL-induced centrosome amplification causes a dose-dependent reduction in tumor formation

Our study is the first to demonstrate inhibition of both spontaneous and carcinogen-induced tumorigenesis by supernumerary centrosomes regardless TP53 activity, suggesting STIL overexpression as a new potential approach for cancer therapy.

More pronounced inhibition of proliferation, viability, and increased aneuploidy in homozygous as compared to heterozygous STIL-overexpressing MEFs suggests a dose-dependent effect.

V. SUMMARY

Centrosomes have an important role in mastering the microtubule system in mammalian cells. They regulate chromosome segregation during mitosis by forming the bipolar spindle. Centrosome duplication takes place during G1 and S phases while centrosome maturation occurs in G2 phase. Centrosome replication is controlled by a set of centrosomal proteins including CEP152, CEP192, PLK4, SAS6, CEP135, CPAP and STIL. Improper centrosome function, number or structure leads to chromosome missegregation and aneuploidy. Cancer cells from patients that harbor supernumerary centrosomes are characterized by chromosomal instability, clinical aggressiveness, and are associated with poor patient prognosis. However, the role of centrosome amplification in cancer development is still a matter of debate.

STIL is a structural centrosome protein without known roles outside the centrosome. Its overexpression *in vitro* induces supernumerary centrioles, chromosome missegregation, and aneuploidy. The consequences of STIL overexpression on centrosome amplification, chromosomal instability and cancer development *in vivo* are unknown. In this thesis, we generated a transgenic mouse model, B6-STIL, that overexpresses STIL when bred with a Cre-deleter line leading to STOP cassette excision. These mice have been used for (i) the generation and characterization of STIL overexpressing (STIL^{OE}) mice for the assessment of spontaneous tumor development; (ii) the generation and characterization of mouse embryonic fibroblasts derived from STIL^{OE} mice, and (iii) the generation and characterization of mice with tamoxifen-inducible epithelium-specific STIL overexpression with and without TP53 inactivation, which are used in a chemical skin carcinogenesis assay to assess the relative contribution of supernumerary centrosomes and chromosomal instability to tumor induction and progression in chemically induced skin tumors.

Our results indicate that STIL is overexpressed at both the mRNA and protein levels in STIL^{OE} MEFs and mouse tissues, leading to significant centrosome amplification and chromosomal missegregation via aberrant mitoses. Interestingly however, we found significantly decreased rates of both, spontaneous and chemically induced tumor formation in the STIL^{OE} transgenic mice as compared to control animals.

Conclusion: *In vivo* STIL overexpression leads to centrosome amplification, aberrant mitoses, and aneuploidy, which seem to inhibit tumor formation rather than enhancing it, in transgenic mice.

VI. ZUSAMMENFASSUNG

Zentrosomen spielen eine wichtige Rolle für die Organisation des Mikrotubulus-Systems in Säugerzellen. Sie regulieren die Chromosomensegregation während der Mitose, indem sie bipolare Spindeln bilden. Die Zentrosomenduplikation findet in der G1- und S-Phase statt, während die Zentrosomenreifung in der G2-Phase erfolgt. Die Zentrosomenreplikation wird durch eine Reihe von zentrosomalen Proteinen gesteuert, einschließlich CEP152, CEP192, PLK4, SAS6, CEP135, CPAP und STIL. Aberrante Zentrosomen-funktion, -anzahl oder -struktur führen zu mitotischer Chromosomenfehlverteilung und Aneuploidie. Tumorzellen mit überzähligen oder strukturell aberranten Zentrosomen zeichnen sich durch chromosomale Instabilität sowie klinische Aggressivität aus und sind mit einer schlechten Prognose vergesellschaftet. Ob Zentrosomenaberrationen an der Tumorentstehung beteiligt sind oder nur ein Epiphänomen darstellen ist jedoch noch nicht abschließend geklärt.

STIL ist ein Zentrosomen-Strukturprotein ohne weitere bisher bekannte Funktionen außerhalb der Zentrosomenreplikation. Seine Überexpression *in vitro* induziert überzähligen Zentriolen. Über die Konsequenzen einer STIL-Überexpression auf die Zentrosomenreplikation, chromosomale Instabilität und Tumorentwicklung *in vivo* ist noch nichts bekannt. In dieser Arbeit haben wir ein transgenes Mausmodell erzeugt, in dem STIL überexprimiert wird. Diese Mäuse wurden für (i) die Beurteilung der spontanen Tumorentwicklung nach STIL-Überexpression, (ii) die Erzeugung und Charakterisierung von embryonalen Fibroblasten von STIL^{OE}-Mäusen, und (iii) die Beurteilung der kutanen Tumorentwicklung nach tamoxifen-induzierbarer, epithel-spezifischer STIL-Überexpression mit und ohne TP53-Inaktivierung im chemischen Hautkarzinogenese-Assay verwendet.

Sowohl in MEFs als auch im Mausgewebe der transgenen Tiere konnte zunächst eine STIL-Überexpression auf mRNA- sowie auf Proteinebene nachgewiesen werden. STIL^{OE}-MEFs zeigten darüber hinaus eine Zentrosomenamplifikation mit chromosomaler Missegregation und aberranten Mitosen. Interessanterweise nahmen jedoch die Raten sowohl spontaner als auch chemisch induzierter Tumoren bei den transgenen STIL^{OE}-Mäusen im Vergleich zu den Kontrollen ab.

Schlussfolgerung: Die Überexpression des zentrosomalen Strukturproteins STIL

induziert in Mäusen Zentrosomenamplifikation und Aneuploidie, was allerdings die Entstehung von Tumoren im transgenen Mausmodell zu hemmen scheint.

VII. REFERENCES

- Abel, E.L., Angel, J.M., Kiguchi, K., and DiGiovanni, J. (2009). Multi-stage chemical carcinogenesis in mouse skin: Fundamentals and applications. *Nat Protoc* 4, 1350–1362.
- Aldaz, C.M., and Conti, C.J. (1989). The premalignant nature of mouse skin papillomas: histopathologic, cytogenetic, and biochemical evidence. *Carcinog Compr Surv* 11, 227–242.
- Aldaz, C.M., Trono, D., Larcher, F., Slaga, T.J., and Conti, C.J. (1989). Sequential trisomization of chromosomes 6 and 7 in mouse skin premalignant lesions. *Mol Carcinog* 2, 22–26.
- Amen, N., Mathow, D., Rabionet, M., Sandhoff, R., Langbein, L., Gretz, N., Jäckel, C., Gröne, H.-J., and Jennemann, R. (2013). Differentiation of epidermal keratinocytes is dependent on glucosylceramide:ceramide processing. *Hum Mol Gen* 22, 4164–4179.
- Anderhub, S.J., Krämer, A., and Maier, B. (2012). Centrosome amplification in tumorigenesis. *Can Lett* 322, 8–17.
- Andreassen, P.R., Lohez, O.D., Lacroix, F.B., and Margolis, R.L. (2001). Tetraploid state induces p53-dependent arrest of nontransformed mammalian cells in G1. *MBoC* 12, 1315–1328.
- Aplan, P., Lombardi, D., Ginsberg, A., Cossman, J., Bertness, V., and Kirsch, I. (1990). Disruption of the human SCL locus by “illegitimate” V-(D)-J recombinase activity. *Science* 250, 1426–1429.
- Aplan, P., Lombardi, D., Reaman, G., Sather, H., Hammond, G., and Kirsch, I. (1992). Involvement of the putative hematopoietic transcription factor SCL in T-cell acute lymphoblastic leukemia. *Blood* 79, 1327–1333.
- Aplan, P.D., Lombardi, D.P., and Kirsch, I.R. (1991). Structural characterization of SIL, a gene frequently disrupted in T-cell acute lymphoblastic leukemia. *Mol Cell Biol* 11, 5462–5469.
- Arquint, C., and Nigg, E.A. (2014). STIL Microcephaly Mutations Interfere with APC/C-Mediated Degradation and Cause Centriole Amplification. *Curr Bio* 24, 351–360.
- Arquint, C., and Nigg, E.A. (2016). The PLK4-STIL-SAS-6 module at the core of centriole duplication. *Biochem Soc Trans* 44, 1253–1263.
- Arquint, C., Sonnen, K.F., Stierhof, Y.-D., and Nigg, E.A. (2012). Cell-cycle-regulated expression of STIL controls centriole number in human cells. *Jour of Cell Sci* 125, 1342–1352.
- Arquint, C., Gabryjonczyk, A.-M., and Nigg, E.A. (2014). Centrosomes as signalling centres. *Philosophical Transactions of the Royal Society B: Biolog Sci* 369, 20130464.

- Balmain, A., Ramsden, M., Bowden, G.T., and Smith, J. (1984). Activation of the mouse cellular Harvey-ras gene in chemically induced benign skin papillomas. *Nature* *307*, 658–660.
- Basto, R., Brunk, K., Vinadogrova, T., Peel, N., Franz, A., Khodjakov, A., and Raff, J.W. (2008). Centrosome amplification can initiate tumorigenesis in flies. *Cell* *133*, 1032–1042.
- Bayani, J., Paderova, J., Murphy, J., Rosen, B., Zielenska, M., and Squire, J.A. (2008). Distinct patterns of structural and numerical chromosomal instability characterize sporadic ovarian cancer. *Neoplasia* *10*, 1057–1065.
- Bazzi, H., and Anderson, K.V. (2014). Acentriolar mitosis activates a p53-dependent apoptosis pathway in the mouse embryo. *PNAS* *111*, E1491–E1500.
- Blumberg, P.M. (1980). In vitro studies on the mode of action of the phorbol esters, potent tumor promoters: part 1. *Crit Rev Toxicol* *8*, 153–197.
- Boveri, T. (1902). Über mehrpolige Mitosen als Mittel zur Analyse des Zellkerns. *Verhandlungen Der Physikalisch-Medizinischen Gesellschaft Zu Würzburg* *35*, 67–90.
- Boveri, T. (2008). Concerning the Origin of Malignant Tumours by Theodor Boveri. Translated and annotated by Henry Harris. *Journal of Cell Science* *121*, 1–84.
- Brabletz, T., Jung, A., Spaderna, S., Hlubek, F., and Kirchner, T. (2005). Opinion: migrating cancer stem cells - an integrated concept of malignant tumour progression. *Nat Rev Cancer* *5*, 744–749.
- Branca, J.A., Low, B.E., Saxl, R.L., Sargent, J.K., Doty, R.A., Wiles, M.V., Dumont, B.L., and Hasham, M.G. (2020). Loss of TRP53 (p53) accelerates tumorigenesis and changes the tumor spectrum of SJL/J mice. *Genes Cancer* *11*, 83–94.
- Brayton, C.F., Treuting, P.M., and Ward, J.M. (2012). Pathobiology of Aging Mice and GEM: Background Strains and Experimental Design. *Vet Pathol* *49*, 85–105.
- Brown, K., Buchmann, A., and Balmain, A. (1990). Carcinogen-induced mutations in the mouse c-Ha-ras gene provide evidence of multiple pathways for tumor progression. *Proc Natl Acad Sci U S A* *87*, 538–542.
- Brown, N.J., Marjanović, M., Lüders, J., Stracker, T.H., and Costanzo, V. (2013). Cep63 and Cep152 Cooperate to Ensure Centriole Duplication. *PLOS ONE* *8*, e69986.
- Capecchi, M. (1989). Altering the genome by homologous recombination. *Science* *244*, 1288–1292.
- Carvalho-Santos, Z., Azimzadeh, J., Pereira-Leal, José.B., and Bettencourt-Dias, M. (2011). Tracing the origins of centrioles, cilia, and flagella. *Jour of Cell Biolog* *194*, 165–175.
- Castagna, M., Takai, Y., Kaibuchi, K., Sano, K., Kikkawa, U., and Nishizuka, Y.

(1982). Direct activation of calcium-activated, phospholipid-dependent protein kinase by tumor-promoting phorbol esters. *J Biol Chem* 257, 7847–7851.

Castiel, A., Danieli, M.M., David, A., Moshkovitz, S., Aplan, P.D., Kirsch, I.R., Brandeis, M., Krämer, A., and Izraeli, S. (2011). The Stil protein regulates centrosome integrity and mitosis through suppression of Chfr. *Jour of Cell Sci* 124, 532–539.

Cave, H., Suciu, S., Preudhomme, C., and Poppe, B. (2004). Clinical significance of HOX11L2 expression linked to t(5;14)(q35;q32), of HOX11 expression, and of SIL-TAL fusion in childhood T-cell malignancies: results of EORTC studies 58881 and 58951. *Blood* 103, 442–450.

Chan, J.Y. (2011). A Clinical Overview of Centrosome Amplification in Human Cancers. *Int. J. Biol. Sci.* 7, 1122–1144.

Chavali, P.L., Pütz, M., and Gergely, F. (2014). Small organelle, big responsibility: the role of centrosomes in development and disease. *Phil. Trans. R. Soc. B* 369, 20130468.

Chen, J., and Roop, D.R. (2008). Genetically engineered mouse models for skin research: taking the next step. *J Dermatol Sci* 52, 1–12.

Chen, C., Krohn, J., Bhattacharya, S., and Davies, B. (2011). A Comparison of Exogenous Promoter Activity at the ROSA26 Locus Using a PhiC31 Integrase Mediated Cassette Exchange Approach in Mouse ES Cells. *PLOS ONE* 6, e23376.

Chi, W., Wang, G., Xin, G., Jiang, Q., and Zhang, C. (2020). PLK4-phosphorylated NEDD1 facilitates cartwheel assembly and centriole biogenesis initiations. *Jour of Cell Biolog* 220.

Chng, W.J., Ahmann, G.J., Henderson, K., Santana-Davila, R., Greipp, P.R., Gertz, M.A., Lacy, M.Q., Dispenzieri, A., Kumar, S., Rajkumar, S.V., et al. (2006). Clinical implication of centrosome amplification in plasma cell neoplasm. *Blood* 107, 3669–3675.

Choudhry, Z., Rikani, A.A., Choudhry, A.M., Tariq, S., Zakaria, F., Asghar, M.W., Sarfraz, M.K., Haider, K., Shafiq, A.A., and Mobassarrah, N.J. (2014). Sonic hedgehog signalling pathway: a complex network. *Ann Neurosci* 21, 28–31.

Coelho, P.A., Bury, L., Sharif, B., Riparbelli, M.G., Fu, J., Callaini, G., Glover, D.M., and Zernicka-Goetz, M. (2013). Spindle Formation in the Mouse Embryo Requires Plk4 in the Absence of Centrioles. *Developmental Cell* 27, 586–597.

Coelho, P.A., Bury, L., Shahbazi, M.N., Liakath-Ali, K., Tate, P.H., Wormald, S., Hindley, C.J., Huch, M., Archer, J., Skarnes, W.C., et al. (2015). Over-expression of Plk4 induces centrosome amplification, loss of primary cilia and associated tissue hyperplasia in the mouse. *Open Biol.* 5, 150209.

Colaizzo-Anas, T., and Aplan, P.D. (2003). Cloning and characterization of the SIL promoter. *Biochim Biophys Acta* 1625, 207–213.

Collazo-Garcia, N., Scherer, P., and Aplan, P.D. (1995). Cloning and Characterization of a Murine SIL Gene. *Genomics* 30, 506–513.

- Conti, C.J., Aldaz, C.M., O'Connell, J., Klein-Szanto, A.J., and Slaga, T.J. (1986). Aneuploidy, an early event in mouse skin tumor development. *Carcinogenesis* 7, 1845–1848.
- Cosenza, M.R. (2015). Disruption of spindle pole symmetry by centriole overduplication induces chromosome instability in human malignancies.
- Cosenza, M.R., and Krämer, A. (2016). Centrosome amplification, chromosomal instability and cancer: mechanistic, clinical and therapeutic issues. *Chromosome Res* 24, 105–126.
- Cosenza, M.R., Cazzola, A., Rossberg, A., Schieber, N.L., Konotop, G., Bausch, E., Slynko, A., Holland-Letz, T., Raab, M.S., Dubash, T., et al. (2017). Asymmetric Centriole Numbers at Spindle Poles Cause Chromosome Missegregation in Cancer. *Cell Reports* 20, 1906–1920.
- Cottee, M.A., Muschalik, N., Wong, Y.L., Johnson, C.M., Johnson, S., Andreeva, A., Oegema, K., Lea, S.M., Raff, J.W., and van Breugel, M. (2013). Crystal structures of the CPAP/STIL complex reveal its role in centriole assembly and human microcephaly. *ELife* 2, e01071.
- Cottee, M.A., Muschalik, N., Johnson, S., Leveson, J., Raff, J.W., and Lea, S.M. (2015). The homo-oligomerisation of both Sas-6 and Ana2 is required for efficient centriole assembly in flies. *ELife* 4, e07236.
- Cristofoli, F., Keersmaecker, B.D., Catte, L.D., Vermeesch, J.R., and Esch, H.V. (2017). Novel STIL Compound Heterozygous Mutations Cause Severe Fetal Microcephaly and Centriolar Lengthening. *MSY* 8, 282–293.
- Cuomo, M.E., Knebel, A., Morrice, N., Paterson, H., Cohen, P., and Mittnacht, S. (2008). p53-Driven apoptosis limits centrosome amplification and genomic instability downstream of NPM1 phosphorylation. *Nat Cell Biol* 10, 723–730.
- Curry, J.D., and Smith, M.T. (2003). Measurement of SIL–TAL1 fusion gene transcripts associated with human T-cell lymphocytic leukemia by real-time reverse transcriptase-PCR. *Leukemia Research* 27, 575–582.
- D'Assoro, A.B., Lingle, W.L., and Salisbury, J.L. (2002). Centrosome amplification and the development of cancer. *Oncogene* 21, 6146–6153.
- Daughtry, B.L., and Chavez, S.L. (2016). Chromosomal instability in mammalian pre-implantation embryos: potential causes, detection methods, and clinical consequences. *Cell Tissue Res* 363, 201–225.
- David, A., Liu, F., Tibelius, A., Vulprecht, J., Wald, D., Rothermel, U., Ohana, R., Seitel, A., Metzger, J., Ashery-Padan, R., et al. (2014). Lack of centrioles and primary cilia in STIL^{-/-} mouse embryos. *Cell Cycle* 13, 2859–2868.
- David, A., Amartely, H., Rabinowicz, N., Shamir, M., Friedler, A., and Izraeli, S. (2016). Molecular basis of the STIL coiled coil oligomerization explains its requirement for de-novo formation of centrosomes in mammalian cells. *Sci Rep* 6, 24296.
- DiGiovanni, J. (1992). Multistage carcinogenesis in mouse skin. *Pharmacol Ther*

54, 63–128.

Donehower, L.A., Harvey, M., Slagle, B.L., McArthur, M.J., Montgomery, C.A., Butel, J.S., and Bradley, A. (1992). Mice deficient for p53 are developmentally normal but susceptible to spontaneous tumours. *Nature* 356, 215–221.

Donehower, L.A., Godley, L.A., Aldaz, C.M., Pyle, R., Shi, Y.P., Pinkel, D., Gray, J., Bradley, A., Medina, D., and Varmus, H.E. (1995). Deficiency of p53 accelerates mammary tumorigenesis in Wnt-1 transgenic mice and promotes chromosomal instability. *Genes Dev.* 9, 882–895.

Duensing, S., Duensing, A., Crum, C.P., and Münger, K. (2001). Human papillomavirus type 16 E7 oncoprotein-induced abnormal centrosome synthesis is an early event in the evolving malignant phenotype. *Cancer Res* 61, 2356–2360.

Duijf, P.H.G., Schultz, N., and Benezra, R. (2013). Cancer cells preferentially lose small chromosomes. *Int J Cancer* 132, 2316–2326.

Duncan, A.W., Taylor, M.H., Hickey, R.D., Hanlon Newell, A.E., Lenzi, M.L., Olson, S.B., Finegold, M.J., and Grompe, M. (2010). The ploidy conveyor of mature hepatocytes as a source of genetic variation. *Nature* 467, 707–710.

Erez, A., Perelman, M., Hewitt, S.M., Cojocar, G., Goldberg, I., Shahar, I., Yaron, P., Muler, I., Campaner, S., Amariglio, N., et al. (2004). Sil overexpression in lung cancer characterizes tumors with increased mitotic activity. *Oncogene* 23, 5371–5377.

Feil, R., Brocard, J., Mascrez, B., LeMeur, M., Metzger, D., and Chambon, P. (1996). Ligand-activated site-specific recombination in mice. *Proc Natl Acad Sci U S A* 93, 10887–10890.

FELASA working group on revision of guidelines for health monitoring of rodents and rabbits, Mähler (Convenor), M., Berard, M., Feinstein, R., Gallagher, A., Illgen-Wilcke, B., Pritchett-Corning, K., and Raspa, M. (2014). FELASA recommendations for the health monitoring of mouse, rat, hamster, guinea pig and rabbit colonies in breeding and experimental units. *Lab Anim* 48, 178–192.

Fırat-Karalar, E.N., and Stearns, T. (2014). The centriole duplication cycle. *Phil. Trans. R. Soc. B* 369, 20130460.

Florio, M., and Huttner, W.B. (2014). Neural progenitors, neurogenesis and the evolution of the neocortex. *Development* 141, 2182–2194.

Friedländer, M. (1982). Centrioles and centrospheres in giant cells of human gliomas. *J Submicrosc Cytol* 14, 401–406.

Fukasawa, K., Choi, T., Kuriyama, R., Rulong, S., and Vande Woude, G.F. (1996). Abnormal Centrosome Amplification in the Absence of p53. *Science* 271, 1744–1747.

Fukushima, K., Takahashi, K., Fukushima, N., Honoki, K., and Tsujiuchi, T. (2016). Different effects of GPR120 and GPR40 on cellular functions stimulated by 12-O-tetradecanoylphorbol-13-acetate in melanoma cells. *Biochemical and Biophysical Research Communications* 475, 25–30.

- Funk, L.C., Wan, J., Ryan, S.D., Kaur, C., Sullivan, R., Roopra, A., and Weaver, B.A. (2021). p53 Is Not Required for High CIN to Induce Tumor Suppression. *Mol Cancer Res* 19, 112–123.
- Fürstenberger, G., Berry, D.L., Sorg, B., and Marks, F. (1981). Skin tumor promotion by phorbol esters is a two-stage process. *Proc Natl Acad Sci U S A* 78, 7722–7726.
- Ganem, N.J., Godinho, S.A., and Pellman, D. (2009). A mechanism linking extra centrosomes to chromosomal instability. *Nature* 460, 278–282.
- Ghadimi, B.M., Sackett, D.L., Difilippantonio, M.J., Schröck, E., Neumann, T., Jauho, A., Auer, G., and Ried, T. (2000). Centrosome amplification and instability occurs exclusively in aneuploid, but not in diploid colorectal cancer cell lines, and correlates with numerical chromosomal aberrations. *Genes Chromosomes Cancer* 27, 183–190.
- Giam, M., Wong, C.K., Low, J.S., Sinelli, M., Dreesen, O., and Rancati, G. (2020). P53 induces senescence in the unstable progeny of aneuploid cells. *Cell Cycle* 19, 3508–3520.
- Gibbons, I.R., and Grimstone, A.V. (1960). On Flagellar Structure in Certain Flagellates. *The Journal of Biophysical and Biochemical Cytology* 7, 697–716.
- Godinho, S.A., and Pellman, D. (2014). Causes and consequences of centrosome abnormalities in cancer. *Phil. Trans. R. Soc. B* 369, 20130467.
- Gordon, S. (2016). Phagocytosis: An Immunobiologic Process. *Immunity* 44, 463–475.
- Greaves, M., and Maley, C.C. (2012). Clonal evolution in cancer. *Nature* 481, 306–313.
- Gruss, O.J. (2018). Animal Female Meiosis: The Challenges of Eliminating Centrosomes. *Cells* 7.
- Guichard, P., Chrétien, D., Marco, S., and Tassin, A.-M. (2010). Procentriole assembly revealed by cryo-electron tomography. *EMBO J* 29, 1565–1572.
- Gupta, H., Rajeev, R., Sasmal, R., Radhakrishnan, R.M., Anand, U., Chandran, H., Aparna, N.R., Agasti, S., and Manna, T.K. (2020). SAS-6 Association with γ -Tubulin Ring Complex Is Required for Centriole Duplication in Human Cells. *Current Biology* 30, 2395-2403.e4.
- Gustafson, L.M., Gleich, L.L., Fukasawa, K., Chadwell, J., Miller, M.A., Stambrook, P.J., and Gluckman, J.L. (2000). Centrosome hyperamplification in head and neck squamous cell carcinoma: a potential phenotypic marker of tumor aggressiveness. *Laryngoscope* 110, 1798–1801.
- Gustafsson, B.M., Mattsson, K., Bogdanovic, G., Leijonhufvud, G., Honkaniemi, E., Ramme, K., and Ford, A.M. (2018). Origins of STIL-TAL1 fusion genes in children who later developed paediatric T-cell acute lymphoblastic leukaemia: An investigation of neonatal blood spots. *Pediatr Blood Cancer* 65, e27310.

- Gyger, M., Berdoy, M., Dontas, I., Kolf-Clauw, M., Santos, A.I., and Sjöquist, M. (2019). FELASA accreditation of education and training courses in laboratory animal science according to the Directive 2010/63/EU. *Lab Anim* 53, 137–147.
- Hanahan, D., and Weinberg, R.A. (2000). The hallmarks of cancer. *Cell* 100, 57–70.
- Hennings, H., Michael, D., Lichti, U., and Yuspa, S.H. (1987). Response of carcinogen-altered mouse epidermal cells to phorbol ester tumor promoters and calcium. *J Invest Dermatol* 88, 60–65.
- Hennings, H., Glick, A.B., Lowry, D.T., Krsmanovic, L.S., Sly, L.M., and Yuspa, S.H. (1993). FVB/N mice: an inbred strain sensitive to the chemical induction of squamous cell carcinomas in the skin. *Carcinogenesis* 14, 2353–2358.
- Hirono, M. (2014). Cartwheel assembly. *Phil. Trans. R. Soc. B* 369, 20130458.
- Hoyer-Fender, S. (2010). Centriole maturation and transformation to basal body. *Seminars in Cell & Developmental Biology* 21, 142–147.
- Izraeli, S., Lowe, L.A., Bertness, V.L., Good, D.J., Dorward, D.W., Kirsch, I.R., and Kuehn, M.R. (1999). The SIL gene is required for mouse embryonic axial development and left–right specification. *Nature* 399, 691–694.
- Izraeli, S., Lowe, L.A., Bertness, V.L., Campaner, S., Hahn, H., Kirsch, I.R., and Kuehn, M.R. (2001). Genetic evidence that Sil is required for the sonic hedgehog response pathway. *Genesis* 31, 72–77.
- Janssen, A., Kops, G.J.P.L., and Medema, R.H. (2009). Elevating the frequency of chromosome mis-segregation as a strategy to kill tumor cells. *Proc Natl Acad Sci U S A* 106, 19108–19113.
- Jeganathan, K., Malureanu, L., Baker, D.J., Abraham, S.C., and van Deursen, J.M. (2007). Bub1 mediates cell death in response to chromosome missegregation and acts to suppress spontaneous tumorigenesis. *J Cell Biol* 179, 255–267.
- Jin, Y.-X., Cui, X.-S., Yu, X.-F., Lee, S.-H., Wang, Q.-L., Gao, W.-W., Xu, Y.-N., Sun, S.-C., Kong, I.-K., and Kim, N.-H. (2012). Cat fertilization by mouse sperm injection. *Zygote* 20, 371–378.
- Joukov, V., Walter, J.C., and De Nicolo, A. (2014). The Cep192-Organized Aurora A-Plk1 Cascade Is Essential for Centrosome Cycle and Bipolar Spindle Assembly. *Molecular Cell* 55, 578–591.
- Kaindl, A.M., Passemard, S., Kumar, P., Kraemer, N., Issa, L., Zwirner, A., Gerard, B., Verloes, A., Mani, S., and Gressens, P. (2010). Many roads lead to primary autosomal recessive microcephaly. *Progress in Neurobiology* 90, 363–383.
- Kakar, N., Ahmad, J., Morris-Rosendahl, D.J., Altmüller, J., Friedrich, K., Barbi, G., Nürnberg, P., Kubisch, C., Dobyns, W.B., and Borck, G. (2015). STIL mutation causes autosomal recessive microcephalic lobar holoprosencephaly. *Hum Genet* 134, 45–51.
- Kaneko, H., Ishikawa, S., Sumida, T., Sekiya, M., Toshima, M., Kobayashi, H., and

Naka, Y. (1980). Ultrastructural studies of a thymic carcinoid tumor. *Acta Pathol Jpn* 30, 651–658.

Kangsamaksin, T., Park, H.J., Trempus, C.S., and Morris, R.J. (2007). A perspective on murine keratinocyte stem cells as targets of chemically induced skin cancer. *Mol Carcinog* 46, 579–584.

Karkera, J.D., Izraeli, S., Roessler, E., Dutra, A., Kirsch, I., and Muenke, M. (2002). The genomic structure, chromosomal localization, and analysis of SIL as a candidate gene for holoprosencephaly. *Cytogenet Genome Res* 97, 62–67.

Kasai, K., Inaguma, S., Yoneyama, A., Yoshikawa, K., and Ikeda, H. (2008). SCL/TAL1 Interrupting Locus Derepresses GLI1 from the Negative Control of Suppressor-of-Fused in Pancreatic Cancer Cell. *Cancer Res* 68, 7723–7729.

Kazazian, K., Go, C., Wu, H., Brashavitskaya, O., Xu, R., Dennis, J.W., Gingras, A.-C., and Swallow, C.J. (2017). Plk4 Promotes Cancer Invasion and Metastasis through Arp2/3 Complex Regulation of the Actin Cytoskeleton. *Cancer Res* 77, 434–447.

Kemp, C.J. (2005). Multistep skin cancer in mice as a model to study the evolution of cancer cells. *Semin Cancer Biol* 15, 460–473.

Kitagawa, D., Kohlmaier, G., Keller, D., Strnad, P., Balestra, F.R., Fluckiger, I., and Gonczy, P. (2011). Spindle positioning in human cells relies on proper centriole formation and on the microcephaly proteins CPAP and STIL. *Journal of Cell Science* 124, 3884–3893.

Kollman, J.M., Merdes, A., Mourey, L., and Agard, D.A. (2011). Microtubule nucleation by γ -tubulin complexes. *Nat Rev Mol Cell Biol* 12, 709–721.

Kong, D., Farmer, V., Shukla, A., James, J., Gruskin, R., Kiriyama, S., and Loncarek, J. (2014). Centriole maturation requires regulated Plk1 activity during two consecutive cell cycles. *Journal of Cell Biology* 206, 855–865.

Krämer, A., Neben, K., and Ho, A.D. (2005). Centrosome aberrations in hematological malignancies. *Cell Biol Int* 29, 375–383.

Kulukian, A., Holland, A.J., Vitre, B., Naik, S., Cleveland, D.W., and Fuchs, E. (2015). Epidermal development, growth control, and homeostasis in the face of centrosome amplification. *PNAS* 112, E6311–E6320.

Kumar, A., Girimaji, S.C., Duvvari, M.R., and Blanton, S.H. (2009). Mutations in STIL, Encoding a Pericentriolar and Centrosomal Protein, Cause Primary Microcephaly. *The American Journal of Human Genetics* 84, 286–290.

Kuo, K.K., Sato, N., Mizumoto, K., Maehara, N., Yonemasu, H., Ker, C.G., Sheen, P.C., and Tanaka, M. (2000). Centrosome abnormalities in human carcinomas of the gallbladder and intrahepatic and extrahepatic bile ducts. *Hepatology* 31, 59–64.

Kwon, M., Leibowitz, M.L., and Lee, J.-H. (2020). Small but mighty: the causes and consequences of micronucleus rupture. *Exp Mol Med* 52, 1777–1786.

Lambrus, B.G., Uetake, Y., Clutario, K.M., Daggubati, V., Snyder, M., Sluder, G.,

and Holland, A.J. (2015). p53 protects against genome instability following centriole duplication failure. *Journal of Cell Biology* 210, 63–77.

LaMonica, B.E., Lui, J.H., Hansen, D.V., and Kriegstein, A.R. (2013). Mitotic spindle orientation predicts outer radial glial cell generation in human neocortex. *Nat Commun* 4, 1665.

Lancaster, M.A., and Knoblich, J.A. (2012). Spindle orientation in mammalian cerebral cortical development. *Curr Opin Neurobiol* 22, 737–746.

Lee, A.J.X., Endesfelder, D., Rowan, A.J., Walther, A., Birkbak, N.J., Futreal, P.A., Downward, J., Szallasi, Z., Tomlinson, I.P.M., Howell, M., et al. (2011). Chromosomal Instability Confers Intrinsic Multidrug Resistance. *Cancer Res* 71, 1858–1870.

Leedham, S.J., and Wright, N.A. (2008). Expansion of a mutated clone: from stem cell to tumour. *J Clin Pathol* 61, 164–171.

Lengauer, C., Kinzler, K.W., and Vogelstein, B. (1997). Genetic instability in colorectal cancers. *Nature* 386, 623–627.

Lepage, C.C., Thompson, L.L., Larson, B., and McManus, K.J. (2020). An Automated, Single Cell Quantitative Imaging Microscopy Approach to Assess Micronucleus Formation, Genotoxicity and Chromosome Instability. *Cells* 9, 344.

Levine, M.S., Bakker, B., Boeckx, B., Moyett, J., Lu, J., Vitre, B., Spierings, D.C., Lansdorp, P.M., Cleveland, D.W., Lambrechts, D., et al. (2017). Centrosome Amplification Is Sufficient to Promote Spontaneous Tumorigenesis in Mammals. *Developmental Cell* 40, 313-322.e5.

Li, J., Li, P., Carr, A., Wang, X., DeLaPaz, A., Sun, L., Lee, E., Tomei, E., and Li, L. (2013). Functional expression of SCL/TAL1 interrupting locus (Stil) protects retinal dopaminergic cells from neurotoxin-induced degeneration. *J Biol Chem* 288, 886–893.

Li, R., Sonik, A., Stindl, R., Rasnick, D., and Duesberg, P. (2000). Aneuploidy vs. gene mutation hypothesis of cancer: recent study claims mutation but is found to support aneuploidy. *Proc Natl Acad Sci U S A* 97, 3236–3241.

Liebelt, F., Jansen, N.S., Kumar, S., Gracheva, E., Claessens, L.A., Verlaan-de Vries, M., Willemstein, E., and Vertegaal, A.C.O. (2019). The poly-SUMO2/3 protease SENP6 enables assembly of the constitutive centromere-associated network by group deSUMOylation. *Nat Commun* 10, 3987.

Lii, C.-K., Chang, J.-W., Chen, J.-J., Chen, H.-W., Liu, K.-L., Yeh, S.-L., Wang, T.-S., Liu, S.-H., Tsai, C.-H., and Li, C.-C. (2016). Docosahexaenoic acid inhibits 12-O-tetradecanoylphorbol-13- acetate-induced fascin-1-dependent breast cancer cell migration by suppressing the PKC δ - and Wnt-1/ β -catenin-mediated pathways. *Oncotarget* 7, 25162–25179.

Lingle, W.L., and Salisbury, J.L. (1999). Altered centrosome structure is associated with abnormal mitoses in human breast tumors. *Am J Pathol* 155, 1941–1951.

Lingle, W.L., Lutz, W.H., Ingle, J.N., Maihle, N.J., and Salisbury, J.L. (1998).

Centrosome hypertrophy in human breast tumors: implications for genomic stability and cell polarity. *Proc Natl Acad Sci U S A* 95, 2950–2955.

Lingle, W.L., Barrett, S.L., Negron, V.C., D’Assoro, A.B., Boeneman, K., Liu, W., Whitehead, C.M., Reynolds, C., and Salisbury, J.L. (2002). Centrosome amplification drives chromosomal instability in breast tumor development. *Proceedings of the National Academy of Sciences* 99, 1978–1983.

Liu, Y., Gupta, G.D., Barnabas, D.D., Agircan, F.G., Mehmood, S., Wu, D., Coyaud, E., Johnson, C.M., McLaughlin, S.H., Andreeva, A., et al. (2018). Direct binding of CEP85 to STIL ensures robust PLK4 activation and efficient centriole assembly. *Nat Commun* 9, 1731.

Louro, M.A.D., Bettencourt-Dias, M., and Bank, C. (2021). Patterns of selection against centrosome amplification in human cell lines. *PLOS Computational Biology* 17, e1008765.

Lüders, J., and Stearns, T. (2007). Microtubule-organizing centres: a re-evaluation. *Nat Rev Mol Cell Biol* 8, 161–167.

Macmillan, J.C., Hudson, J.W., Bull, S., Dennis, J.W., and Swallow, C.J. (2001). Comparative Expression of the Mitotic Regulators SAK and PLK in Colorectal Cancer. *Ann Surg Oncol* 8, 729–740.

Marthiens, V., Rujano, M.A., Penetier, C., Tessier, S., Paul-Gilloteaux, P., and Basto, R. (2013). Centrosome amplification causes microcephaly. *Nat Cell Biol* 15, 731–740.

Martin, C.-A., Ahmad, I., Klingseisen, A., Hussain, M.S., Bicknell, L.S., Leitch, A., Nürnberg, G., Toliat, M.R., Murray, J.E., Hunt, D., et al. (2014). Mutations in PLK4, encoding a master regulator of centriole biogenesis, cause microcephaly, growth failure and retinopathy. *Nat Genet* 46, 1283–1292.

Martindill, D.M.J., Risebro, C.A., Smart, N., Franco-Viseras, M.D.M., Rosario, C.O., Swallow, C.J., Dennis, J.W., and Riley, P.R. (2007). Nucleolar release of Hand1 acts as a molecular switch to determine cell fate. *Nat Cell Biol* 9, 1131–1141.

McGranahan, N., Burrell, R.A., Endesfelder, D., Novelli, M.R., and Swanton, C. (2012). Cancer chromosomal instability: therapeutic and diagnostic challenges. *EMBO Rep* 13, 528–538.

Mikule, K., Delaval, B., Kaldis, P., Jurczyk, A., Hergert, P., and Doxsey, S. (2007). Loss of centrosome integrity induces p38—p53—p21-dependent G1—S arrest. *Nat Cell Biol* 9, 160–170.

Mittal, K., Kaur, J., Jaczko, M., Wei, G., Toss, M.S., Rakha, E.A., Janssen, E.A.M., Sjøiland, H., Kucuk, O., Reid, M.D., et al. (2021). Centrosome amplification: a quantifiable cancer cell trait with prognostic value in solid malignancies. *Cancer Metastasis Rev* 40, 319–339.

Miyoshi, Y., Iwao, K., Egawa, C., and Noguchi, S. (2001). Association of centrosomal kinase STK15/BTAK mRNA expression with chromosomal instability

in human breast cancers. *Int J Cancer* 92, 370–373.

Mogilner, A., and Keren, K. (2009). The Shape of Motile Cells. *Current Biology* 19, R762–R771.

Morris, R.J. (2004). A perspective on keratinocyte stem cells as targets for skin carcinogenesis. *Differentiation* 72, 381–386.

Moyer, T.C., Clutario, K.M., Lambrus, B.G., Daggubati, V., and Holland, A.J. (2015). Binding of STIL to Plk4 activates kinase activity to promote centriole assembly. *J Cell Biol* 209, 863–878.

Nelson, M.A., Futscher, B.W., Kinsella, T., Wymer, J., and Bowden, G.T. (1992). Detection of mutant Ha-ras genes in chemically initiated mouse skin epidermis before the development of benign tumors. *Proc Natl Acad Sci U S A* 89, 6398–6402.

Nievergelt, A.P., Banterle, N., Andany, S.H., Gönczy, P., and Fantner, G.E. (2018). High-speed photothermal off-resonance atomic force microscopy reveals assembly routes of centriolar scaffold protein SAS-6. *Nature Nanotech* 13, 696–701.

Nigg, E.A. (2002). Centrosome aberrations: cause or consequence of cancer progression? *Nat Rev Cancer* 2, 815–825.

Nigg, E.A. (2006). Origins and consequences of centrosome aberrations in human cancers. *International Journal of Cancer* 119, 2717–2723.

O’Connell, C.B., and Khodjakov, A.L. (2007). Cooperative mechanisms of mitotic spindle formation. *J Cell Sci* 120, 1717–1722.

Olive, K.P., Tuveson, D.A., Ruhe, Z.C., Yin, B., Willis, N.A., Bronson, R.T., Crowley, D., and Jacks, T. (2004). Mutant p53 Gain of Function in Two Mouse Models of Li-Fraumeni Syndrome. *Cell* 119, 847–860.

Papari, E., Bastami, M., Farhadi, A., Abedini, S., Hosseini, M., Bahman, I., Mohseni, M., Garshasbi, M., Moheb, L.A., Behjati, F., et al. (2013). Investigation of primary microcephaly in Bushehr province of Iran: novel *STIL* and *ASPM* mutations: Letter to the Editor. *Clin Genet* 83, 488–490.

Patwardhan, D., Mani, S., Passemard, S., Gressens, P., and El Ghouzzi, V. (2018). STIL balancing primary microcephaly and cancer. *Cell Death & Disease* 9, 1–11.

Peel, N., Stevens, N.R., Basto, R., and Raff, J.W. (2007). Overexpressing Centriole-Replication Proteins In Vivo Induces Centriole Overduplication and De Novo Formation. *Current Biology* 17, 834–843.

Pfaff, K.L., Straub, C.T., Chiang, K., Bear, D.M., Zhou, Y., and Zon, L.I. (2007). The zebra fish *cassiopeia* mutant reveals that SIL is required for mitotic spindle organization. *Mol Cell Biol* 27, 5887–5897.

Pihan, G.A. (2013). Centrosome Dysfunction Contributes to Chromosome Instability, Chromoanagenesis, and Genome Reprograming in Cancer. *Front. Oncol.* 3.

Pihan, G.A., Purohit, A., Wallace, J., Knecht, H., Woda, B., Quesenberry, P., and Doxsey, S.J. (1998). Centrosome defects and genetic instability in malignant tumors. *Cancer Res* 58, 3974–3985.

Pitot, H.C., and Dragan, Y.P. (1991). Facts and theories concerning the mechanisms of carcinogenesis. *FASEB J* 5, 2280–2286.

Quintyne, N.J., Reing, J.E., Hoffelder, D.R., Gollin, S.M., and Saunders, W.S. (2005). Spindle multipolarity is prevented by centrosomal clustering. *Science* 307, 127–129.

Rabinowicz, N., Mangala, L.S., Brown, K.R., Checa-Rodriguez, C., Castiel, A., Moskovich, O., Zarfati, G., Trakhtenbrot, L., Levy-Barda, A., Jiang, D., et al. (2017). Targeting the centriolar replication factor STIL synergizes with DNA damaging agents for treatment of ovarian cancer. *Oncotarget* 8, 27380–27392.

Ramaswamy, S., Ross, K.N., Lander, E.S., and Golub, T.R. (2003). A molecular signature of metastasis in primary solid tumors. *Nat Genet* 33, 49–54.

Rebois, R.V., and Patel, J. (1985). Phorbol ester causes desensitization of gonadotropin-responsive adenylate cyclase in a murine Leydig tumor cell line. *J Biol Chem* 260, 8026–8031.

Ribbert, H. (1914). Zur Frage der Entstehung maligner Tumoren. *Naturwissenschaften* 2, 676–679.

Rosario, C.O., Kazazian, K., Zih, F.S.W., Brashavitskaya, O., Haffani, Y., Xu, R.S.Z., George, A., Dennis, J.W., and Swallow, C.J. (2015). A novel role for Plk4 in regulating cell spreading and motility. *Oncogene* 34, 3441–3451.

Ruggeri, B., Caamano, J., Goodrow, T., DiRado, M., Bianchi, A., Trono, D., Conti, C.J., and Klein-Szanto, A.J. (1991). Alterations of the p53 tumor suppressor gene during mouse skin tumor progression. *Cancer Res* 51, 6615–6621.

Sabino, D., Gogendeau, D., Gambarotto, D., Nano, M., Penner, C., Dingli, F., Arras, G., Loew, D., and Basto, R. (2015). Moesin Is a Major Regulator of Centrosome Behavior in Epithelial Cells with Extra Centrosomes. *Current Biology* 25, 879–889.

Sander, K. (1993). Aneuploidy disrupts embryogenesis : Theodor Boveri's analysis of sea urchin dispermy. *Roux's Arch Dev Biol* 202, 247–247.

Schatten, H. (2008). The mammalian centrosome and its functional significance. *Histochem Cell Biol* 129, 667–686.

Schatten, H., Wiedemeier, A.M., Taylor, M., Lubahn, D.B., Greenberg, N.M., Besch-Williford, C., Rosenfeld, C.S., Day, J.K., and Ripple, M. (2000). Centrosome-centriole abnormalities are markers for abnormal cell divisions and cancer in the transgenic adenocarcinoma mouse prostate (TRAMP) model. *Biol Cell* 92, 331–340.

Scheer, U. (2014). Historical roots of centrosome research: discovery of Boveri's microscope slides in Würzburg. *Phil. Trans. R. Soc. B* 369, 20130469.

- Schliwa, M., Euteneuer, U., Gräf, R., and Ueda, M. (1999). Centrosomes, microtubules and cell migration. *Biochem Soc Symp* 65, 223–231.
- Schmidt, T.I., Kleylein-Sohn, J., Westendorf, J., Le Clech, M., Lavoie, S.B., Stierhof, Y.-D., and Nigg, E.A. (2009). Control of Centriole Length by CPAP and CP110. *Current Biology* 19, 1005–1011.
- Scholey, J.M., and Anderson, K.V. (2006). Intraflagellar Transport and Cilium-Based Signaling. *Cell* 125, 439–442.
- Schwenk, F., Baron, U., and Rajewsky, K. (1995). A cre-transgenic mouse strain for the ubiquitous deletion of loxP-flanked gene segments including deletion in germ cells. *Nucleic Acids Research* 23, 5080–5081.
- Segal, D.J., and McCoy, E.E. (1974). Studies on Down's syndrome in tissue culture. I. Growth rates and protein contents of fibroblast cultures. *J Cell Physiol* 83, 85–90.
- Seifert, H.W. (1978). [Electron microscopic investigation on cutaneous leiomyosarcoma (author's transl)]. *Arch Dermatol Res* 263, 159–169.
- Serçin, Ö., Larsimont, J.-C., Karambelas, A.E., Marthiens, V., Moers, V., Boeckx, B., Le Mercier, M., Lambrechts, D., Basto, R., and Blanpain, C. (2016). Transient PLK4 overexpression accelerates tumorigenesis in p53-deficient epidermis. *Nat Cell Biol* 18, 100–110.
- Shinmura, K., Kato, H., Kawanishi, Y., Nagura, K., Kamo, T., Okubo, Y., Inoue, Y., Kurabe, N., Du, C., Iwaizumi, M., et al. (2015). SASS6 overexpression is associated with mitotic chromosomal abnormalities and a poor prognosis in patients with colorectal cancer. *Oncology Reports* 34, 727–738.
- Shoshani, O., Bakker, B., de Haan, L., Tjhuis, A.E., Wang, Y., Kim, D.H., Maldonado, M., Demarest, M.A., Artates, J., Zhengyu, O., et al. (2021). Transient genomic instability drives tumorigenesis through accelerated clonal evolution. *Genes Dev* 35, 1093–1108.
- Silk, A.D., Zasadil, L.M., Holland, A.J., Vitre, B., Cleveland, D.W., and Weaver, B.A. (2013). Chromosome missegregation rate predicts whether aneuploidy will promote or suppress tumors. *Proc Natl Acad Sci U S A* 110, E4134–E4141.
- Silkworth, W.T., Nardi, I.K., Scholl, L.M., and Cimini, D. (2009). Multipolar Spindle Pole Coalescence Is a Major Source of Kinetochore Mis-Attachment and Chromosome Mis-Segregation in Cancer Cells. *PLOS ONE* 4, e6564.
- Sinha, D., Duijf, P.H.G., and Khanna, K.K. (2019). Mitotic slippage: an old tale with a new twist. *Cell Cycle* 18, 7–15.
- Siskos, N., Stylianopoulou, E., Skavdis, G., and Grigoriou, M.E. (2021). Molecular Genetics of Microcephaly Primary Hereditary: An Overview. *Brain Sciences* 11, 581.
- Smithies, O., Gregg, R.G., Boggs, S.S., Koralewski, M.A., and Kucherlapati, R.S. (1985). Insertion of DNA sequences into the human chromosomal β -globin locus by homologous recombination. *Nature* 317, 230–234.

- Sonnen, K.F., Gabryjonczyk, A.-M., Anselm, E., Stierhof, Y.-D., and Nigg, E.A. (2013). Human Cep192 and Cep152 cooperate in Plk4 recruitment and centriole duplication. *J Cell Sci* *126*, 3223–3233.
- Spektor, A., Tsang, W.Y., Khoo, D., and Dynlacht, B.D. (2007). Cep97 and CP110 Suppress a Cilia Assembly Program. *Cell* *130*, 678–690.
- Stingele, S., Stoehr, G., Peplowska, K., Cox, J., Mann, M., and Storchova, Z. (2012). Global analysis of genome, transcriptome and proteome reveals the response to aneuploidy in human cells. *Mol Syst Biol* *8*, 608.
- Sullenberger, C., Vasquez-Limeta, A., Kong, D., and Loncarek, J. (2020). With Age Comes Maturity: Biochemical and Structural Transformation of a Human Centriole in the Making. *Cells* *9*, 1429.
- Sun, L., Carr, A.L., Li, P., Lee, J., McGregor, M., and Li, L. (2014). Characterization of the human oncogene SCL/TAL1 interrupting locus (Stil) mediated Sonic hedgehog (Shh) signaling transduction in proliferating mammalian dopaminergic neurons. *Biochem Biophys Res Commun* *449*, 444–448.
- Sung, Y.M., He, G., and Fischer, S.M. (2005). Lack of Expression of the EP2 but not EP3 Receptor for Prostaglandin E2 Results in Suppression of Skin Tumor Development. *Cancer Res* *65*, 9304–9311.
- Tang, C.-J.C., Lin, S.-Y., Hsu, W.-B., Lin, Y.-N., Wu, C.-T., Lin, Y.-C., Chang, C.-W., Wu, K.-S., and Tang, T.K. (2011). The human microcephaly protein STIL interacts with CPAP and is required for procentriole formation: STIL is required for procentriole formation. *The EMBO Journal* *30*, 4790–4804.
- Tarapore, P., and Fukasawa, K. (2002). Loss of p53 and centrosome hyperamplification. *Oncogene* *21*, 6234–6240.
- Terradas, M., Martín, M., Hernández, L., Tusell, L., and Genescà, A. (2012). Nuclear envelope defects impede a proper response to micronuclear DNA lesions. *Mutation Research/Fundamental and Molecular Mechanisms of Mutagenesis* *729*, 35–40.
- Thomas, J.O., and Kornberg, R.D. (1975). An octamer of histones in chromatin and free in solution. *Proceedings of the National Academy of Sciences* *72*, 2626–2630.
- Torres, E.M., Sokolsky, T., Tucker, C.M., Chan, L.Y., Boselli, M., Dunham, M.J., and Amon, A. (2007). Effects of aneuploidy on cellular physiology and cell division in haploid yeast. *Science* *317*, 916–924.
- Trachana, V., Wely, K.H.M. van, Guerrero, A.A., Fütterer, A., and Martínez-A, C. (2007). Dido disruption leads to centrosome amplification and mitotic checkpoint defects compromising chromosome stability. *PNAS* *104*, 2691–2696.
- Trempeus, C.S., Morris, R.J., Ehinger, M., Elmore, A., Bortner, C.D., Ito, M., Cotsarelis, G., Nijhof, J.G.W., Peckham, J., Flagler, N., et al. (2007). CD34 expression by hair follicle stem cells is required for skin tumor development in mice. *Cancer Res* *67*, 4173–4181.
- Tsou, M.-F.B., Wang, W.-J., George, K.A., Uryu, K., Stearns, T., and Jallepalli,

P.V. (2009). Polo Kinase and Separase Regulate the Mitotic Licensing of Centriole Duplication in Human Cells. *Developmental Cell* 17, 344–354.

Uetake, Y., and Sluder, G. (2004). Cell cycle progression after cleavage failure : mammalian somatic cells do not possess a “tetraploidy checkpoint.” *Journal of Cell Biology* 165, 609–615.

Uzbekov, R., and Alieva, I. (2018). Who are you, subdistal appendages of centriole? *Open Biol.* 8, 180062.

Vassar, R., Rosenberg, M., Ross, S., Tyner, A., and Fuchs, E. (1989). Tissue-specific and differentiation-specific expression of a human K14 keratin gene in transgenic mice. *Proc. Natl. Acad. Sci. U.S.A.* 86, 1563–1567.

Vertii, A., Hung, H.-F., Hehnlly, H., and Doxsey, S. (2016). Human basal body basics. *Cilia* 5.

Vitre, B., Holland, A.J., Kulukian, A., Shoshani, O., Hirai, M., Wang, Y., Maldonado, M., Cho, T., Boubaker, J., Swing, D.A., et al. (2015a). Chronic centrosome amplification without tumorigenesis. *Proc Natl Acad Sci USA* 112, E6321–E6330.

Vitre, B., Holland, A.J., Kulukian, A., Shoshani, O., Hirai, M., Wang, Y., Maldonado, M., Cho, T., Boubaker, J., Swing, D.A., et al. (2015b). Chronic centrosome amplification without tumorigenesis. *Proc Natl Acad Sci USA* 112, E6321–E6330.

Vulprecht, J., David, A., Tibelius, A., Castiel, A., Konotop, G., Liu, F., Bestvater, F., Raab, M.S., Zentgraf, H., Izraeli, S., et al. (2012). STIL is required for centriole duplication in human cells. *Journal of Cell Science* 125, 1353–1362.

Wakida, N.M., Botvinick, E.L., Lin, J., and Berns, M.W. (2010). An Intact Centrosome Is Required for the Maintenance of Polarization during Directional Cell Migration. *PLOS ONE* 5, e15462.

Wang, J., Zuo, J., Wang, M., Ma, X., Gao, K., Bai, X., Wang, N., Xie, W., and Liu, H. (2019). Polo-like kinase 4 promotes tumorigenesis and induces resistance to radiotherapy in glioblastoma. *Oncol Rep* 41, 2159–2167.

Wang, J.T., Kong, D., Hoerner, C.R., Loncarek, J., and Stearns, T. (2017). Centriole triplet microtubules are required for stable centriole formation and inheritance in human cells. *ELife* 6.

Wang, W.-J., Soni, R.K., Uryu, K., and Bryan Tsou, M.-F. (2011). The conversion of centrioles to centrosomes: essential coupling of duplication with segregation. *Journal of Cell Biology* 193, 727–739.

Wang, X., Tsai, J.-W., Imai, J.H., Lian, W.-N., Vallee, R.B., and Shi, S.-H. (2009). Asymmetric centrosome inheritance maintains neural progenitors in the neocortex. *Nature* 461, 947–955.

Werner, S., Pimenta-Marques, A., and Bettencourt-Dias, M. (2017). Maintaining centrosomes and cilia. *Journal of Cell Science* 130, 3789–3800.

Wilker, E., Lu, J., Rho, O., Carbajal, S., Beltrán, L., and DiGiovanni, J. (2005). Role of PI3K/Akt signaling in insulin-like growth factor-1 (IGF-1) skin tumor promotion. *Mol Carcinog* *44*, 137–145.

Williams, B.R., Prabhu, V.R., Hunter, K.E., Glazier, C.M., Whittaker, C.A., Housman, D.E., and Amon, A. (2008). Aneuploidy Affects Proliferation and Spontaneous Immortalization in Mammalian Cells. *Science* *322*, 703–709.

Willis, A., Jung, E.J., Wakefield, T., and Chen, X. (2004). Mutant p53 exerts a dominant negative effect by preventing wild-type p53 from binding to the promoter of its target genes. *Oncogene* *23*, 2330–2338.

Wong, C., and Stearns, T. (2005). Mammalian cells lack checkpoints for tetraploidy, aberrant centrosome number, and cytokinesis failure. *BMC Cell Biology* *6*, 6.

Woodruff, J.B., Wueseke, O., and Hyman, A.A. (2014). Pericentriolar material structure and dynamics. *Philos Trans R Soc Lond B Biol Sci* *369*.

Wu, Q., Li, B., Liu, L., Sun, S., and Sun, S. (2020). Centrosome dysfunction: a link between senescence and tumor immunity. *Sig Transduct Target Ther* *5*, 1–9.

Xia, Y., Huang, N., Chen, Z., Li, F., Fan, G., Ma, D., Chen, J., and Teng, J. (2018). CCDC102B functions in centrosome linker assembly and centrosome cohesion. *Journal of Cell Science* jcs.222901.

Yuspa, S.H., Ben, T., Hennings, H., and Lichti, U. (1982). Divergent responses in epidermal basal cells exposed to the tumor promoter 12-O-tetradecanoylphorbol-13-acetate. *Cancer Res* *42*, 2344–2349.

Zasadil, L.M., Britigan, E.M.C., and Weaver, B.A. (2013). 2n or not 2n: Aneuploidy, polyploidy and chromosomal instability in primary and tumor cells. *Semin Cell Dev Biol* *24*, 370–379.

Zasadil, L.M., Britigan, E.M.C., Ryan, S.D., Kaur, C., Guckenberger, D.J., Beebe, D.J., Moser, A.R., and Weaver, B.A. (2016). High rates of chromosome missegregation suppress tumor progression but do not inhibit tumor initiation. *Mol Biol Cell* *27*, 1981–1989.

Zhang, X., Harrington, N., Moraes, R.C., Wu, M.-F., Hilsenbeck, S.G., and Lewis, M.T. (2009). Cyclopamine inhibition of human breast cancer cell growth independent of Smoothed (Smo). *Breast Cancer Res Treat* *115*, 505–521.

Zitouni, S., Francia, M.E., Leal, F., Gouveia, S.M., Nabais, C., Duarte, P., Gilberto, S., Brito, D., Moyer, T., Kandels-Lewis, S., et al. (2016). CDK1 prevents unscheduled PLK4-STIL complex assembly in centriole biogenesis. *Curr Biol* *26*, 1127–1137.

Zyss, D., and Gergely, F. (2009). Centrosome function in cancer: guilty or innocent? *Trends in Cell Biology* *19*, 334–346.

Complex Portal - CPX-1159.

SCL-interrupting locus protein (IPR026123) - InterPro entry - InterPro.

VIII. APPENDIX

Parts of the presented work have been published as posters in two conferences, while currently a publication is still in progress:

Amira-Talaat Moussa, Marco R. Cosenza, Tim Holland-Letz, Karin Müller-Decker, Alwin Krämer: Impact of STIL overexpression on supernumerary centriole formation, chromosomal instability, and cancer development in mice. Poster abstract (No. 64) in **Creating is understanding - EMBO - Heidelberg EMBL 2019**.

Amira-Talaat Moussa, Marco R. Cosenza, Katharina Brobeil, Timothy Wohlfromm, Tim Holland-Letz, Anna Jauch, Karin Müller-Decker, Alwin Krämer: STIL overexpression reduces tumor formation in mice. Poster abstract (No. 92) in **Centrosomes and spindle pole bodies - EMBO - Copenhagen, Denmark I Hybrid 2021**.

IX. ACKNOWLEDGMENT

I'm greatly indebted in all my work to God, Most Gracious, Most Merciful.

First and foremost, I want to sincerely thank my supervisor and my mentor Prof. Dr. Alwin Krämer for giving me the chance to work on this project and for his support, encouragement, guidance, insightful discussions, and supervision to develop an understanding of the topic. My words cannot express my deepest gratitude to him, he has been a turning point in my life and career through being an influencing scientist and understanding leader directing and inspiring me all the time.

All thanks to Prof. Dr. Bernhard Aigner for being my supervisor at LMU München and for his continuous help, and supportive tips.

I would like to acknowledge Prof. Dr. Kurt Reifenberg for his advice, being a member in the thesis advisory committee and for final thesis revision.

I would like to greatly thank Dr. Karin Müller-Decker and her co-workers for the skin carcinogenesis assay collaboration, advice, and continuous help. I cannot express my appreciation to all your support.

I would like to sincerely acknowledge Prof. Dr. Anna Jauch and Ms. Brigitte Schoell in Human Genetics Institute, Heidelberg University Hospital for M-FISH analysis of MEFs. I greatly appreciate all your efforts.

Great thanks to Prof. Dr. Stefan Duensing for being in the thesis advisory committee and his valuable advice.

Further, I want to acknowledge the DAAD-GERLS and DFG for financially supporting my residency in Germany.

My sincere gratitude to Dr. Marco R. Cosenza for his molecular biology and immunofluorescence microscopy guidance at the first half of my work in the lab. This project would have not been possible without the helpful contribution of Jana Schairer.

Special thanks to Katharina Sack, who sincerely helped in finalizing the experiments. You have really made the work easier to be completed and created a friendly atmosphere in hard days.

This work would not have been possible without the support of Dr. Kerstin Dell, the animal Facilities, ATV109 and Barrier B at DKFZ. Great appreciation to you all.

Sincere thanks to all members of the A360 department, the Clinical Cooperation Unit Molecular Hematology/Oncology of the German Cancer Research Center (DKFZ), especially to Dr. Bianca Kraft and Mr. Michael Kirsch for being supportive all the time and for the priceless help in teaching me a lot of experimental techniques.

Great thanks to Agnes Hotz-Wagenblatt, Dennis Friedel, Daniel Schrimpf, Damian Stichel and Timothy Wohlfromm for CNV analysis.

I'd like to greatly thank Dr. Tim Holland-Letz for the statistical tips, Dr. Daniel Sanzio Gimenes da Cruz for FACS instruction, and Dr. Ramon Lopez Perez for FlowJo analysis guidance.

Special thanks to my friend Dr. Manar Abdelmageed for the compassionate support, the technical advice and for initial thesis revision.

Sincere thanks to all members of the Veterinary Pathology department headed by Prof. Dr. Nahla A.G.A. Refat in Faculty of Veterinary Medicine, Zagazig University in Egypt for encouraging my study in Germany.

I'm forever grateful to all the friends and family who support me all the time and along my PhD, my mom, my sisters, my husband and my son, my godfather, and my uncle Dr. Abdelmoneem Soliman.

Lastly, I dedicate this work to my father who left the earth but not my name and soul.

